Development of a Completely Biological Tissue Engineered Heart Valve

A DISSERTATION
SUBMITTED TO THE FACULTY OF THE GRADUATE SCHOOL
OF THE UNIVERSITY OF MINNESOTA
BY

Zeeshan Hayder Syedain

IN PARTIAL FULFILLMENT OF THE REQUIREMENTS
FOR THE DEGREE OF
DOCTOR OF PHILOSOPHY

Robert T. Tranquillo, Advisor

April, 2009

Acknowledgements

This dissertation would not have culminated without tremendous support from mentors, colleagues, friends and family. My advisor, Bob Tranquillo's name is on top of the list for his generous support, advising, and guidance over the years. I want to thank you first for giving me the opportunity to work on this exciting project. I admire your vision and encouragement you have given me over the years. I hope I learned some of those qualities from you.

To Tranquillo lab members (former and current), hats off to you. Thank you to former members, especially Choon-sik Jhun and Paul Robinson for mentoring me in my younger days. Choon-sik, thank you for being so patient with my never ending questions and teaching me tissue mechanics. Paul, I am glad to take this project from you, without your strong foundation, I wouldn't be able to build this structure. I hope we will continue to share more stories, whether it is next generation of medical device, a trip to orchestra hall or the fast bicycle racing.

To Justin and Sandy, thank you for excellent collaborative work and making me truly appreciate 'biology'. As an engineer, I learned a lot more biology from you two than in any classes I took.

To Naomi, the guardian angle of our lab, thank you for keeping us in compliance with the safety protocols, keeping the supplies stocked, casting all those countless number of valve batches and almost 7 sets of so called 'last valve batch'.

To Katie Ahmann, I truly value your friendship; it was a fun journey all the way from two-way ANOVA on fondue, editing my writings, bioreactor meltdowns, and all the GAPSA events in which you couldn't win raffle. I wish you the very best in life and you keep collecting those 'shot glasses'.

To Cary, Ricky and Stephen, thank you for your technical help, your support has helped great length to develop the finer details in this dissertation.

To all my friends (too many to write all the names, beside you know who you are) thank you for being there and creating some of the most memorable time in graduate school for me.

To my loving family, I am truly blessed to have you all. My Aunt and Uncle (Amir mamu and Bushra momani) here in Minnesota. It was always a wonderful break from school to visit and enjoy home-cooked meals with you. To my siblings Asad, Qurat, Jawad, and Noori, you have been amazing. To our family's 'bundle of joy', my niece Areej 'Zoya', it's been wonderful first 3 years of life. Finally, to my parents, Abu (Dad in 'Urdu') and Ami (Mom in 'Urdu'), there are no words to thank you for your support, understanding, teaching, and love. You have been my inspiration and strength to finish this dissertation. I dedicate this dissertation to you.

I prayers to God Almight for your blessings, may your guidance always shine in my future path.

Abstract

In the United States alone, over 100,000 heart valve replacement procedures are performed each year, with approximately 45% of patients below age 65. While current mechanical and bioprosthetic heart valves are viable options, they have several limitations. The most significant limitation is for pediatric patients, since neither of these valve types grow and remodel with the patient. Tissue engineering provides a methodology to create functional heart valves that can grow and remodel similar to native tissue once implanted. Several tissue engineering approaches have been proposed using decellularized native scaffolds, synthetic biopolymers, and biological polymers seeded with cells. Fibrin provides a scaffold to create tissue-engineered heart valves (TEHV) that are completely biological with an environment permissive for extracellular matrix (ECM) deposition. Previous research in our lab has demonstrated the feasibility of creating a fibrin-based TEHV with neonatal human dermal fibroblast (nHDF) that yields valve leaflets with structural and mechanical anisotropy similar to native leaflets. However, the TEHV had sub-optimal tensile mechanical properties and was thus unable to withstand physiological forces. The development of tissue can be accelerated by both chemical and mechanical stimulus. Previously, fibrin based TEHV were cultured with chemical stimulus in the form of growth factors supplemented in the culture medium resulting in improved ECM deposition by the cells; however, no mechanical stimulation was applied.

Prior research in both our lab and by other researchers has shown cyclic stretching with constant strain amplitude is a method to stimulate remodeling of biological scaffolds seeded with cells. Initial experiments were conducted to evaluate the effect of cyclic stretching on fibrin-based tubular constructs seeded with porcine valve interstitial cells (PVIC) and nHDF. Cyclic stretching with 10% constant strain amplitude applied for 3 weeks led to modest improvement in tensile properties of the tubular constructs. We hypothesized that long-term cyclic stretching, as was used in this study, could induce cellular adaptation, minimizing the benefits of cyclic stretching. This hypothesis was tested in subsequent experiments using tubular constructs cultured with incremental strain amplitude cyclic stretching, with an average strain of 10% for 3 weeks. Both PVIC and nHDF seeded constructs exhibited a 2-fold improvement in ultimate tensile strength (UTS) and collagen density over samples conditioned with constant strain amplitude strteching. To verify that this was the result of a cellular response, phosphorylation of extracellular signal-regulated kinase (ERK) was measured by western blot. At 5 weeks, the phosphorylated ERK was 255% higher in incremental cyclic strained samples compared to constant strain samples.

nHDF-seeded tubular constructs were also used to optimize the use of transforming growth factor beta (TGF-β). Studies showed that under cyclic stretching conditions, TGF-β has detrimental effects on total collagen deposition and collagen maturation. Western blot analysis showed a decrease in p-ERK signaling in TGF-β treated samples. However, TGF-β use demonstrated a benefit by increasing the elastin content of the tissue constructs. In subsequent experiments, a sequence of cyclic

stretching and TGF-β supplementation was used to optimize tensile mechanical properties and elastin content of the engineered tissue.

Based on the results with tubular constructs, a novel bioreactor was designed to apply controlled cyclic stretching to the fibrin-based TEHV. Briefly, the valve was mounted on two plastic end-pieces with elastic latex tube placed around TEHV. Using a reciprocating syringe pump, culture medium was cyclically pumped into the bioreactor. The root distension, which was determined by the stiffer latex was used as a control parameter, and in turn stretched the leaflets. A separate flowloop (connected to the bioreactor end-pieces) was used to control nutrient transport to the TEHV. Using an incremental strain amplitude stretching regime, fibrin-based TEHV were conditioned in the bioreactor for 3 weeks. Cyclically stretched valves (CS valve) had improved tensile properties and collagen deposition compared to statically-cultured valves. The mechanical stiffness (modulus) and anisotropy (measured as ratio of leaflet modulus in circumferential to radial directions) in the leaflets was comparable to native sheep pulmonary valve leaflets. Collagen organization/ maturation also improved in CS valves over statically-cultured valves as observed by picrosirius red staining of tissue cross-sections. In addition, the CS valve root could withstand pressures of up to 150 mmHg and its compliance was comparable to that of the sheep pulmonary artery at physiological pressures.

To assess *in vivo* remodeling TEHV were implanted in the pulmonary artery of two sheep for 4.5 weeks with the pulmonary valve either left intact or rendered incompetent by leaflet excision. Echocardiography immediately after implantation showed functional coapting leaflets, with normal right heart function. It was also performed just prior to explantation, revealing functional leaflets although with moderate regurgitation in both cases and a partial detachment of one leaflet from the root in one case. The explanted leaflets had thickness and tensile properties comparable the implanted leaflets. There was endothelialization on the lumenal surface of the TEHV root. These preliminary results are unprecedented for a TEHV developed from a biological scaffold; however, many issues remain to be surmounted.

In further development of the TEHV with a fibrin scaffold, photo-cross linking of the fibrin gel was utilized as a method to stiffen the matrix, thereby inhibiting excessive cell-induced compaction. Preliminary studies with tubular constructs demonstrated reduced compaction of cross-linked fibrin gel during cyclic stretching with no effect on nHDF proliferation or deposited collagen. In addition, a preliminary investigation using blood outgrowth endothelial cells (BOEC) has been conducted to assess their adhesion to the remodeled TEHV surface. Studies showed BOEC adhesion and proliferation on remodeled fibrin surface creating a confluent layer after 4 days of culture. Successful seeding of sheep BOEC on the TEHV surface prior to implantation would reduce the risk of clotting.

Overall, the studies presented in this dissertation advance the development of a completely biological tissue-engineered heart valve. These studies improve our understanding of the role of cyclic stretching in tissue remodeling and have furthered the science of mechnotransduction and tissue remodeling.

Table of Contents

ABSTRACT II

CHAPTER 1: INTRODUCTION AND BACKGROUND 1

1.1: Introduction 2

1.2: Heart Valve Diseases and Treatment 2
1.2.1: Human Heart Valves 2
1.2.1.1: Anatomy 2
1.2.1.2: Mechanical properties 5
1.2.2: Disease of the Heart Valves 6
1.2.3: Current prosthesis 8

1.3: Tissue Engineered Heart Valve 9
1.3.1: Scaffold for heart valve 9
1.3.2: Cell sources for tissue engineering 12
1.3.3: Fibrin as a scaffold 14
1.3.4: Mechanical requirements for tissue engineered valve equivalents 16
1.3.5: Role of mechanical conditioning in tissue engineering 18
1.3.6: Relevance of strain conditioning in engineered valve leaflets 23
1.3.7: Mechno-transduction in tissue engineering 24

1.4: References 28

CHAPTER 2: CYCLIC DISTENSION OF FIBRIN-BASED TISSUE CONSTRUCTS: EVIDENCE OF ADAPTATION DURING GROWTH OF ENGINEERED CONNECTIVE TISSUE 32

2.1: Summary 33

2.2: Introduction 34

2.3: Results 37
2.3.1: CD and ICD results in different construct dimensions but not different volumes 37
2.3.2: CD improves construct mechanical properties 38
2.3.3: Incremental CD further improves construct mechanical properties and correlates with increased net collagen deposition per cell 38
2.3.4: Incremental CD yields similar results for HDF-populated constructs 39
2.3.5: CD-mediated improvement in tissue growth requires 2-3 weeks of CD 39
2.3.6: CD results in collagen maturation in constructs 40
2.3.7: Incremental CD results in elevated ERK 1/2 signaling 40

2.4: Discussion 41

2.5: Materials and Methods 45

2.6: References 52

CHAPTER 3: TGF-β LEADS TO DIMINISHED COLLAGEN PRODUCTION VIA DECREASED PERK DURING LONG-TERM CYCLIC STRETCHING OF ENGINEERED CONNECTIVE TISSUE 62

3.1: Summary 63

3.2: Introduction 65

3.3: Results 67
3.3.1: TGF-β supplemented samples possessed inferior mechanical properties 67
3.3.2: Improvement in mechanical properties of -TGF-β samples correlated with increased collagen deposition and organization. 68
3.3.3: TGF-β increased elastin deposition by the nHDF 69
3.3.4: TGF-β increased αSMA expression and phosphorylation of SMAD-2 69
3.3.5: TGF-β decreased phosphorylation of ERK1/2 69
3.3.6: Sequential cyclic stretching and TGF-β supplementation leads to both improved mechanical properties and increased elastin deposition 70

3.4: Discussion 71

3.5: Materials and Methods 74

3.6: References 80

3.7: Figures 82

CHAPTER 4: A NOVEL BIOREACTOR FOR TISSUE ENGINEERED HEART VALVES BASED ON CONTROLLED CYCLIC STRETCHING 88

4.1: Summary 89

4.2: Introduction 90

4.4: Results 92
4.4.1: Controlled cyclic stretching leads to improved TEHV leaflet properties and anisotropy in stiffness comparable to native leaflet. 92
4.4.2: Cyclic stretching improves ECM organization and collagen maturation of TEHV leaflet and root 93
4.4.3: VE root tensile properties improve with cyclic stretching and VE withstands cyclic pulmonary pressures 94

4.5: Discussion 95

4.3: Materials and Methods 100

4.6: References 105

4.7: Figures 107

CHAPTER 5: *IN VIVO* ASSESSMENT OF A COMPLETELY BIOLOGICAL TISSUE ENGINEERED HEART VALVE 113

5.1: Summary **114**

5.2: Introduction **115**

5.3: Material and Methods **115**

5.4: Results **120**
5.4.1: Leaflet functionality post implant and after 4.5 weeks *in vivo* 120
5.4.2: Explanted VE leaflets had unaltered tensile mechanical properties 121
5.4.3: Explanted VE leaflets had increased collagen and elastin concentrations 121
5.4.4: VE root tissue was compliant and remodeled with evidence of endothelium formation 122

5.5: Discussion **122**

5.6: References **127**

5.7: Figures **128**

CHAPTER 6: CONTROLLED COMPACTION OF CELL SEEDED FIBRIN CONSTRUCTS **138**

6.1: Summary **139**

6.2: Introduction **141**

6.3: Blebbistatin and Y-27632 effects on compaction of fibrin gel **143**
6.3.1: Material and Methods 143
6.3.2: Results 146
6.3.2.1: Cell morphology and migration assay of Blebbistatin and Y-27632 treated nHDF 146
6.3.2.2: Blebbistatin and Y-27632 reduce TC compaction 146
6.3.2.3: Blebbistatin and Y-27632 inhibit cell proliferation with Blebbistatin reducing collagen deposition 147
6.3.2: Discussion 147
6.3.4: Figures 150

6.4: Ruthenium cross-linking of fibroblast-seeded fibrin gel for tissue engineering **155**
6.4.1: Material and Methods 155
6.4.2: Results 160
6.4.2.1: Ruthenium cross-linking kinetics 160
6.4.2.2: Ruthenium cross-linking increased the fibrin gel stiffness without affecting cell viability 161
6.4.2.3: Ruthenium cross-linking of TC leads to reduced compaction 161
6.4.2.4: Cross-linked TC had increased cell proliferation and comparable collagen density 162
6.4.2.6: Ruthenium cross-linked TC require a longer incubation to achieve desired tensile properties 163
6.4.3: Discussion 163
6.4.4: Figures 167

6.5: References **176**

CHAPTER 7: ONGOING WORK, FUTURE DIRECTION AND CONCLUSIONS **177**

7.1: Introduction **178**

7.2: Ongoing and Future Studies **179**
7.2.1: Endothelialization of valve surface 179
7.2.2: Hypoxia induced remodeling of nHDF seeded fibrin constructs 182
7.2.3: Optimizing mechno-chemical environment to manipulate protein signaling 183
7.2.4: Hybrid root for the fibrin TEHV 186

7.3: Towards clinical trial of TEHV **186**

7.4: Conclusions **188**

7.5: References **191**

BIBLIOGRAPHY **192**

APPENDIX **202**

Appendix A: Tubular tissue construct and valve equivalent fabrication protocols **203**

Appendix A: Tubular tissue construct and valve equivalent fabrication protocols **203**
A1: Tubular Constructs 203
A2: Valve Equivalent 204

Appendix B: Protocols for mechanical and biochemical analysis of tissue properties **205**
B1: Mechanical testing of strips 205
B2: Picrosirius red staining of collagen 206
B3: Pepsin Acid digestion of Collagen in Fibrin construct 207
B4: Western blotting protocol 208
B5: Endothelial cells staining protocol 209
B6: Photo-chemical crosslinking of thrombin-crosslinked fibrin gels 210

Appendix C: VE mold and bioreactor designs and schematics **211**
C1: Bi-leaflet VE drawing 211
C2: VE mold dimensions and specs 212
C3: CD bioreactor schematics 213
C4: Valve bioreactor (CS Bioreactor) design 213
C5: Valve bioreactor end-piece design I 214
C6: Valve bioreactor end-piece design II 215

List of Figures

Chapter 1

Figure 1-1: Cross-sectional view of human heart 3
Figure 1-2: Diagram of aortic leaflets with valve ring (annulus) 4
Figure 1-3: Illustration of developing TEHV from autologous cell and scaffolding polymer along with *in vitro* developmental steps. 11
Figure 1-4: A: Fibrin based tissue engineered heart valve. B: VE mold made from Teflon, left image has the outer casing on it. 15
Figure 1-5: A basic SMAD pathway and cross-talk with mitogen activated protein kinase (MAPK) signaling proteins. 26
Figure 1-6: A conceptual illustration of several cellular mechanotransduction mechanisms (taken from Wang *et al* (71)) 27

Chapter 2

Figure 2-1: Tensile Mechanical Properties of Constructs Following CD. (a) Normalized UTS and (b) Normalized modulus (E). Values are normalized to paired static controls. In all cases where error bars are not overlapping, the means are significantly different ($p<0.05$); for groups with overlapping error bars, a significant difference ($p<0.05$) between means is shown with paired symbols. Inset shows schematic of CD and ICD regimens: CD, shown for 10% strain amplitude, ICD with 2 steps (ICD-2), the amplitude changed from 5% → 10% → 15%, and ICD with 4 steps (ICD-4), the amplitude changed from 5% → 7.5% → 10% → 12.5% → 15%. 55
Figure 2-2: Composition of PVIC Constructs Following CD. (a) Normalized collagen concentration, (b) Normalized cell concentration, and (c) Normalized collagen concentration/cell concentration. See Fig. 1 regarding statistical significance. 56
Figure 2-3: Time course of HDF Constructs During CD. (a) UTS and, (b) Collagen concentration. See Fig. 1 regarding statistical significance. 57
Figure 2-4: Histology of Constructs Following CD. Lillie's Trichrome-stained sections of static control samples (a-d,m) for corresponding CD samples (e,f,n-p). Picrosirius red-stained sections for static control samples (g-j,r) for corresponding CD samples (k,l,s-u). For comparison, stained sections of porcine carotid artery, Trichrome (q) and Picrosirius red (v) are also shown. All images were acquired at the same magnification with 100 μm scale bar shown in (a) and (m). 58
Figure 2-5: Western Blot for ERK 1/2 Activation Following CD. 59

Chapter 3

Figure 3-1: Time course of fibrin-based TC with and without TGF-β supplementation during incremental cyclic stretching a: UTS, b: Modulus, c: Collagen concentration, d: Elastin concentration, e: Cell concentration and f: Collagen/Cell concentrations after 2, 5 & 7 weeks of incubation. In all cases where error bars are not overlapping, the means are different ($p<0.05$); for groups with overlapping error bars, difference ($p<0.05$) between means is shown with paired symbols. 82
Figure 3-2: Trichrome and picrosirius red staining of TC after 2, 5 and 7 weeks. In trichrome stained section, collagen stains green and fibrin (and other proteins) stain red. In picrosirius red stained sections, brighter intensity of red color indicate more mature collagen. All images

were taken at same magnification with 200μm scale bar (black line) shown in 2 weeks trichrome images. The lumen of TC is on the left side of all sections. 83

Figure 3-3: a: Western blot of αSMA expression by nHDF in TC constructs at week 5. β-actin bands indicate the same protein loading in all lanes, implying TGF-β induced expression of αSMA. b: TC in PBS at week 5 after removal from latex tube of the cyclic stretch bioreactor shows curling of TGF-β samples. 84

Figure 3-4: a: Western blotting for ERK 1/2 and SMAD activation of nHDF in TC (n=3) with and without TGF-β supplementation at 5 weeks. 85

Figure 3-5: Elastin concentration comparison of –TGF-β samples at weeks 5 and 7 with the ∗TGF-β treated group and native tissue control. Statistical significance at $p<0.05$ is shown by paired symbols. 86

Figure 3-6: Trichrome, picrosirius red, Verhoeff, and elastin immunostaining for –TGF-β samples and ∗TGF-β samples at week 7 with native tissue control.
Inset of Verhoeff stain shows magnified image of elastin fiber strands in native control and ∗TGF-β treated TC. All images were taken at same magnification with 200μm scale bar (black line) shown in native trichrome images. The lumen of TC and ventricular side of native leaflet is on the left side of all sections. 87

Chapter 4

Figure 4-1: (a) (a) Schematic of controlled cyclic stretching TEHV bioreactor, showing the reciprocating syringe pump for cyclic pressurization and stretching of the VE mounted within the latex tube, (b) Image of the bioreactor with the latex housing slit to reveal the VE mounted within and its tie-down to both endpieces, and (c) End-on view of the VE through the glass window of the bioreactor during a stretching cycle, showing the leaflets coapting when the lumen is not pressurized, and separated when the lumen is pressurized and the root and leaflets are stretched. 107

Figure 4-2: Average strain amplitude in circumferential and radial directions in the VE leaflets during cyclic stretching. 108

Figure 4-3: Tensile mechanical properties of ICS VE leaflets. (a) Ultimate tensile stress (UTS), (b) Modulus (E), (c) Thickness, (d) Maximum tension, and (e) Membrane stiffness, showing comparison of static control VE, ICS VE, and sheep pulmonary valve leaflets. Differences between groups ($p < 0.05$) are indicated by paired symbols (n=8). 109

Figure 4-4: Structural comparison of VE and native valve leaflets: (from left to right) polarized light image of a whole leaflet, picrosirius red stain of a cross-section under polarized light, and trichrome stain of a cross-section. The orientations of the yellow segments in the polarized light images correspond to the local average fiber direction, and their lengths are proportional to the local average retardation, a measure of the fiber alignment strength. The pixel gray level is mapped from isotropic (black) to maximally aligned (white). A 200 μm scale bar is shown in trichrome image of a control VE, with all images acquired at the same magnification. 110

Figure 4-5: Comparison of tensile mechanical properties in the circumferential direction of static and ICS VE root with native pulmonary artery. (a) UTS and modulus, (b) maximum tension and membrane stiffness, and (c) pressure-strain curve of ICS VE *vs.* sheep pulmonary artery (PA). 111

Figure 4-6: Trichrome and picrosirius red staining comparison of VE root with sheep pulmonary artery on cross-section in the circumferential direction. A 200 μm scale bar is shown in trichrome of the control VE, with all images acquired at the same magnification. 112

Chapter 5

Figure 5-1: Post implant echocardiogram images of NAVT 9 showing leaflets in open (a&c) and close (b&d) positions from side (a&b) and end-on view (c&d). i. Doppler flow profile. 128
Figure 5-2: Echocardiogram images at 4.5 week of NAVT 7. a. valve leaflets in open and close position, b. Doppler flow profile. 129
Figure 5-3: Gross image of explanted VE, a. Surface view of intact bi-leaflet VE, b. proximal end of VE root with native pulmonary artery. 130
Figure 5-4: Stress-strain profile comparison of explanted VE leaflet with native pulmonary valve leaflet. 131
Figure 5-5: Tensile mechanical properties of explanted VE in comparison to *in vitro* VE and native pulmonary leaflet. a. Thickness, b. UTS and c. Modulus. 132
Figure 5-6: Biochemical analysis of explanted VE with *in vitro* VE. a. Collagen concentration, b. Elastin concentration and c. cell concentration. 133
Figure 5-7: Trichrome and Picrosirius red stained cross-section of in vitro VE (a&d), explanted VE at 4.5 weeks from sheep with intact native leaflets (b&e) and sheep without native leaflets intact (c&f). 134
Figure 5-8: Lumen surface of explanted VE root at 4.5 week, a. Trichrome stain, b. vWF immuno staining (red) with DAPI cell nuclei (blue) and c. Trichrome and picrosirius red stain of collagen fibers aligned in circumferential direction inside the wall of VE root. 135
Figure 5-9: Vasculature lumen inside the wall of a. VE root and b. native pulmonary artery stained with vWF (red) and DAPI cell nuclei (blue). 136

Chapter 6

Figure 6-1: Time-lapse image of nHDF on tissue culture plastic treated with 20μM Blebbistatin, 10 μM Y-27632, or both (B+Y), compared to un-treated control. 150
Figure 6-2: Calceim A staining (for live cell) of Blebbistatin, Y-27632 and B+Y treated cells after 72hrs of drug treatment. 151
Figure 6-3: Total cell number after 72 hrs treatment with Blebbistatin, Y-27632 and B+Y. Paired symbols show statistically significant difference at *P<0.05* 152
Figure 6-4: a. Time lapse axial length of nHDF seeded TC treated with Blebbistatin and Y-27632 (n=4-5). b. Images of nHDF TC control over time 153
Figure 6-5: Tensile mechanical and biochemical properties of TC after 10 days of Blebbistatin (B) and Y-27632 (Y) or both (B+Y) treatment (n = 4 to 5). 154
Figure 6-6: Photochemical cross-linking of fibrinogen solution at 10 mg/ml using Ru(II) as a catalyst, a. Evaluation of Ru(II) concentration effect on fibrinogen cross-linking at concentrations of Ru(II) at 0.02, 0.2, 0.5, 1 and 2mM. b. Evaluation of blue light exposure time on Ru(II) cross-linking with time of 1, 5, 10 and 20 seconds at 10mW/cm^2. The first lane on the left side of each gel has a protein ladder (L) followed by untreated fibrinogen solution loaded at 10μg (F). 167
Figure 6-7:a. Live-dead comparison of an nhDF-seeded fibrin HC photo cross-linked with Ruthenium catalyst and a control HC, b. Visual comparison of HC compaction after detachment from surface c. Comparison of compression stiffness (* significantly different at p<0.05). 168
Figure 6-8: Process of Ruthenium cross-linking. Bottom right shows Live/Dead image of TC cross-linked (x-linked) compared to untreated control. 169
Figure 6-9: a. Time-course of axial length of the TC, b. Image of the TC at 3 week (from left to right: 1 day, 7 day, and control) 170
Figure 6-10: a. Cell number, b. total collagen and c. collagen/cell for TC after 3 weeks of culture in CD bioreactor. In a. horizontal line represents the initial cell number. 171

Figure 6-11: **a. UTS, b. modulus, c. collagen density and d. cell concentration in TC after 3 weeks** **172**

Figure 6-12: Collagen density versus modulus of TC after 3 week of incubation, linear regression had R^2=0.97 (line on the plot) **173**

Figure 6-13: **Comparison of compaction and tensile mechanical properties of non cross-linked TC control after 3 weeks of culture to photo cross-linked TC after 3 and 5 weeks of culture. All samples were statically cultured on mandrel for 1 week followed by 2-4 weeks in the CD bioreactor. a. Overall length compaction as % of initial length, b. thickness, c. UTS, d. modulus, and e. Collagen density.** **174**

Figure 6-14: Trichrome and Picrosirius Red Stain of the TC control (a&c) and photo cross-linked TC after 3 (b&d) and 5 (c&f) weeks of culture. **175**

List of Tables

Chapter 3

Table 2.1: UTS and Modulus (E) of fibrin constructs subjected to CD paired static controls. (*) indicate significant difference ($p<0.05$) between CD and paired static controls. 60

Table 2.2: Collagen concentration, cell concentration and collagen per cell in fibrin constructs subjected to CD with paired static controls. (*) indicate significant difference ($p<0.05$) between CD and paired static controls. 61

Chapter 5

Table 5.1: Summary of VE implant attempts to date in sheep pulmonary artery of TEHV 137

Chapter 1: Introduction and Background

1.1: Introduction

In the United States, every year approximately 106,000 inpatient valve surgeries on adults are performed with over 20,000 deaths due to valve disorder (1). In pediatric patient, several thousand patients require replacement/repair of the pulmonary valve (1, 2). While currently used replacement valves are efficacious and function to both improve and prolong life, they are far from ideal and have some significant limitations. Current replacement valves significantly lack the true valvular function and require prolonged medical treatment. Hence a need exists for a fully functional biological valve that would prevent immune reactions and would have the ability to grow, repair and remodel *in vivo*. The need is even greater for pediatric patients who require a replacement valve that can accommodate to their growing size. The tissue engineering technology provides an excellent means to create heart valve replacement by seeding cells onto a scaffold, which degrades as tissue is developed by the cells. The following chapter provides the background on the anatomy and diseases of the heart valves, the current prosthesis and the tissue engineering technology for the heart valve.

1.2: Heart Valve Diseases and Treatment

1.2.1: Human Heart Valves

1.2.1.1: Anatomy

The heart consist of four valves, two of which control flow between chambers of the heart and other two control the flow into main pulmonary artery and aorta. Approximately 60% of the replacement surgeries in adults are performed for diseased

aortic valve. The aortic valve is located at the outlet of the left ventricle (Fig 1). The aortic valve has the important role of guiding flow of blood from the heart to rest of the body, while preventing back flow. The aortic valve consists of three leaflets. The line of attachment of the leaflets to the aortic wall is the valve annulus (Fig 2). The free-side of the leaflets extends into the aortic lumen with all three leaflets overlapping each other. This overlap or coaptation closes the valve and prevents backflow, medically described as regurgitation.

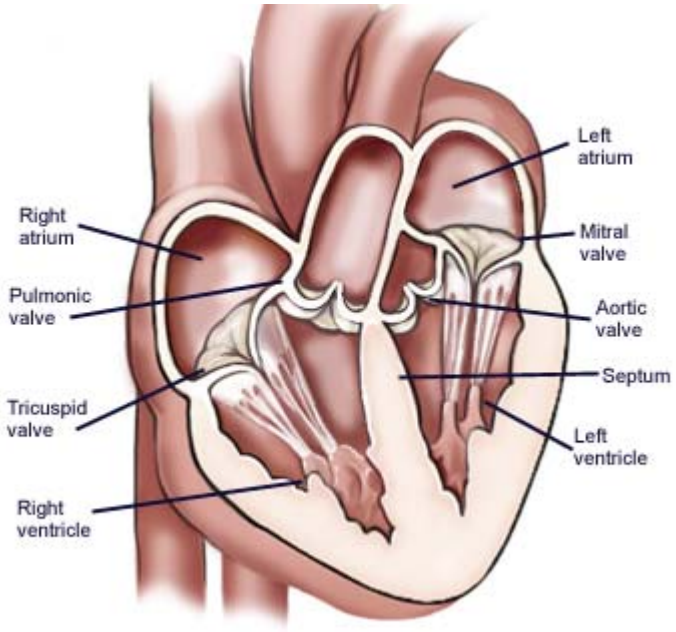

Figure 1-1: Cross-sectional view of human heart
(copyright 2006, Cleveland Clinic)

The leaflets provide the mechanical function of the valve and regulate about 3.7 billion cycles in a lifetime (3). The leaflets are composed of three layers namely Ventricularis, Spongiosa and Fibrosa. The ventricularis – the layer at the inflow surface – is composed of radially aligned elastin fibers. The middle layer, spongiosa consists of

loosely arranged collagen and an abundant amount of proteoglycans. The outer layer, fibrosa is comprised mainly of circumferentially aligned collagen fibers (4). The fibrosa is considered to be the main load bearing layer and prevents excessive stretch (5). Research has also shown that collagen layer help in smooth opening and closing of leaflet during valve cycle (6). Study by Vesely *et al* showed elastic modulus of 23MPa in the circumferential direction and 3.71MPa in the radial direction for fibrosa layer (7). Similarly, the researchers showed the ventricularis layer has crcumferential modulus of 9.55MPa and 3.7MPa in the radial direction. Even though individual layers of leaflets show different mechanical characteristics due to the difference in composition, the overall mechanical response of the leaflet is a summation of the mechanics of the individual layers (8-10).

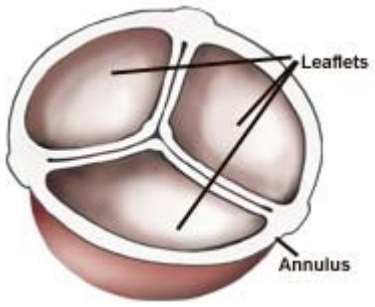

Figure 1-2: Diagram of aortic leaflets with valve ring (annulus)
(copyright 2006, Cleveland Clinic)

The pulmonary valve control flow between right ventricular and pulmonary artery which leads blood to lungs for oxygenation. Pulmonary valve has similar structure as the aortic valve, however has distinctive mechanical properties. In Ross procedure, the pulmonary valve is used as replacement for diseased aortic valve, hence shown that pulmonary valve is capable of withstanding aortic pressures and flow. The

comparison of tensile properties for human aortic and pulmonary valve by Stradin et al showed no significant difference (11). The diseases of the pulmonary valve are more common in pediatric patient who are born with right heart abnormalities and require replacement/repair of pulmonary valve leaflets.

The other two valves in heart are mitral valve and tricuspid valve, which separates the left and right atrium from ventricular, respectively. Mitral valve is prone to disease with age and most common mode is repair rather than replacement in the case of non-calcification disease.

1.2.1.2: Mechanical properties

As discussed earlier, the overall mechanical response of the leaflet depends on the compositions of all layers. Lo and Vesely (12) measured a maximal extensibility of porcine aortic valve leaflets of 24% in the radial direction and 11% in the circumferential direction using biaxial testing. During the test, a natural biaxial loading environment can be mimicked. In the circumferential direction, the mechanical properties exhibit the properties of collagen bundles whereas in the radial direction elastin mesh is the predominant factor. Even though elastin is found in small quantity 13% versus 50-60% collagen by dry weight, it is an important element of the leaflet (4, 13, 14). Using uniaxial tensile testing of circumferential and radial leaflet strips with and without digestion of elastin has shown considerable difference in overall stiffness and stress-strain curves (15).

Study by Stradin *et al* comparing mechanical properties of the aortic valve leaflet versus the pulmonary valve leaflet showed smaller modulus in radial direction at

stress level of 1.0 MPa: 1.32 MPa vs. 1.98 MPa (11). The researcher also found modulus to be similar in circumferential direction with values of 16.05 MPa and 15.34 MPa. The ultimate tensile strength (UTS) measured in the study showed similar values in both the circumferential and radial directions. In another study, Grant *et al* looked at the biaxial behavior of pulmonary valve versus aortic valve (14). In their study, the researchers found higher stretch values in the radial direction for pulmonary valve compared to aortic valve. However, in circumferential direction there was no significant difference between the two valves indicating compositional difference in only radial direction. In both studies, authors concluded that pulmonary valve have more elasticity in radial direction. Several other studies have been published with wide range of numbers for modulus and ultimate tensile strength for aortic valve (7, 11, 15, 16). The typical values for modulus in circumferential direction vary from 3MPa to 20 MPa. In radial direction the range is much smaller with variation from 1MPa to 3MPa.

Schoen *et al* summarized the biomechanics of the aortic valve as follows. Aortic cups open against the aortic wall during systole and close rapidly under minimal pressure change. When the valve is closed, the collagen bundles in fibrosa are fully unfolded, enabling a stress increase while preventing a prolapse of the leaflets. The elastin in ventricularis expands when the cups are closed to enlarge the coaptation area, but recoil to make smaller cups during systole (17).

1.2.2: Disease of the Heart Valves

Though tissue engineering technology can be used to replace any diseased valve in the heart, the major advantage would be to use in patient where current prosthesis are

not viable. Congenital valvular disease is a prime example where tissue engineering technology is front runner for the next valve replacement graft. In US, about 36,000 children are born with congenital disease of which about 22% have a pulmonary valve defect (1). Another common disease which often doesn't require immediate intervention is a bicuspid aortic valve. Congenital aortic valve disease get problematic as patient grow to adulthood (18).

The defects in pulmonary valve are often associated with other congenital defects like tetralogy of fallot, pulmonary atresia, pulmonary stenosis, atrioventricular spetal defects, and VSD (2, 19). In most cases, surgical intervention is required with subsequent multiple surgeries throughout the growing period of patient's life. In a recent publication of congenital heart disease in Belgium, 11% of the defects (921 in 1 year of ~111,000 births in Belgium) were associated with pulmonary valve (20). For the patients with valve defect, 36% required interventional surgery. Trans-catheter approach was used in majority of the patients with advantage of avoiding open heart surgery at young age. Other patient with more complex defect had open heart surgery performed at the mean age of 1.7 years. The mortality rate was around 4% for congenital heart defect after a year of live-birth. The current trans-catheter approach described in above study is approved by European regulatory body; however, it still has not been approved by FDA for use in the United States.

According to most recent AHA statistics, more than 50% of aortic valve replacement surgeries are performed in patient of age 65 or younger. All current valve replacement options have limited life in the range of 10-20 years. Though in many cases, a second or even third surgery can be performed, all subsequent intervention

increases the risk to patients life and in many cases creates other complications. In Adults, the most common reason for valve failure is calcification of the leaflet, which leads to reduced functionality of the leaflets. Other defects can be due to pre-existing conditions, for example bileaflet aortic valve or congenital heart disease.

1.2.3: Current prosthesis

For adult patients, three options exist for aortic valve replacement: mechanical, bioprosthetic and allograft. Mechanical heart valves are made entirely of artificial materials, which mainly consist of metals, rubber material and polymers. Mechanical valves display good structural durability however lacks substantially in mimicking valve anatomy and biological functions. Bioprosthetic valves composed of synthetic and biological material better mimic the structure of natural valve giving its recipient the advantage of low rates of thromboembolism. Allograft valves rely on the replacement of a valve from human organ donor including using pulmonary valve from the same patient as a homograft.

Each type of prosthetics has significant limitation and hence treatment option depends on several factors like patient's age, other diseases, life-style etc. Mechanical valves generally have durability of 10-15 yrs, however due to the design of these valves, high shear rate on blood cells causes thrombosis formation (21). Hence all mechanical heart valve recipients need to be chronically treated with an anticoagulant for long durations, which can have other health implications (22). Bioprosthetic and allograft valves do not require long-term anticoagulation. However, progressive tissue

deterioration and subsequent structural dysfunction due to both calcification and non-calcific mechanisms, decrease their long term durability (23).

1.3: Tissue Engineered Heart Valve

Considering the short coming of the current design, there is a need for an innovative design to create a biologically active valve with the ability to grow, repair and remodel. Tissue engineering technology provides an approach to develop fully functional biological prosthetic valve. The approach generally involves seeding cells from a donor onto an appropriate scaffold, in the shape of heart. Subsequent stimulation, in the form of culture media (chemical stimuli) or via 'conditioning' of the tissue in a bioreactor (mechanical stimuli), promotes cells to remodel the scaffold into functional tissue, comparable to native heart valve tissue.

1.3.1: Scaffold for heart valve

For TEHV, scaffold can be characterized in three categories 1: synthetic biodegradable (24-27), 2: biopolymer (28-32) and 3: decellularized valve graft (33-36). TEHV made from all three type of scaffold have been successfully used in animal model. The synthetic and biological polymers have the advantage of creating any desired size scaffold from raw polymer compared to decell valve, which is of a fixed dimension.

Animal implant studies have been performed with synthetic scaffold made from polyglycolic acid and polyhydroxyalkanoate. The synthetic polymer can have

comparable or higher tensile properties to native tissue (24, 25). The scaffold stiffness gives the advantage of early implant, since scaffold can provide significant durability to the TEHV. However, this also allows for subsequent degradation and weakening of properties during *in vivo*. Other disadvantageous of synthetic polymer include when polymer degrade *in vivo,* it can have an inflammatory response and reactive by-product accumulations.

The decellularized valve has the advantage of retaining gross anatomy of the valve and in some cases the extracellular matrix structure. By re-seeding the valve with autologous cells, a decell valve can be easily used for the implant. Knight *et al*. published results of decellularizing porcine aortic valve and reseeding with human mesenchymal progenitor cells. Results showed good penetration of cells with about 2% cell density compared to homograft (36). It is yet to be determined, to what extent detergents used for removing the cells damage the matrix and if seeded cells would have the ability to remodel the original matrix. The major concern with the synthetic and decell valve scaffold is inability to homogeneously disperse cells in the scaffold.

Biopolymer provides the advantage of forming a homogeneously cell seeded gel. In the case of fibrin, a completely autologous valve can be made by using fibrin and cells from the same patients. Figure 3 illustrates how blood from the patient can be used to extract fibrin for the scaffold. Cells like dermal fibroblast can be extracted to embed in the fibrin gel and blood derived endothelial cells can be used to coat the luminal surface prior to the implant. Figure 3 shows the mechanism like mechanical and chemical growth stimulus in bioreactor to mature the valve grafts (this is discussed in more details in the following chapters). Since biopolymer gels are fairly weak, they

require significant in vitro development before desirable mechanical properties can be achieved. Collagen and hularonic acid have also been proposed as biopolymer for tissue engineering, however remodeling in these scaffold is yet to be proven. The fibrin scaffold is discussed in details below.

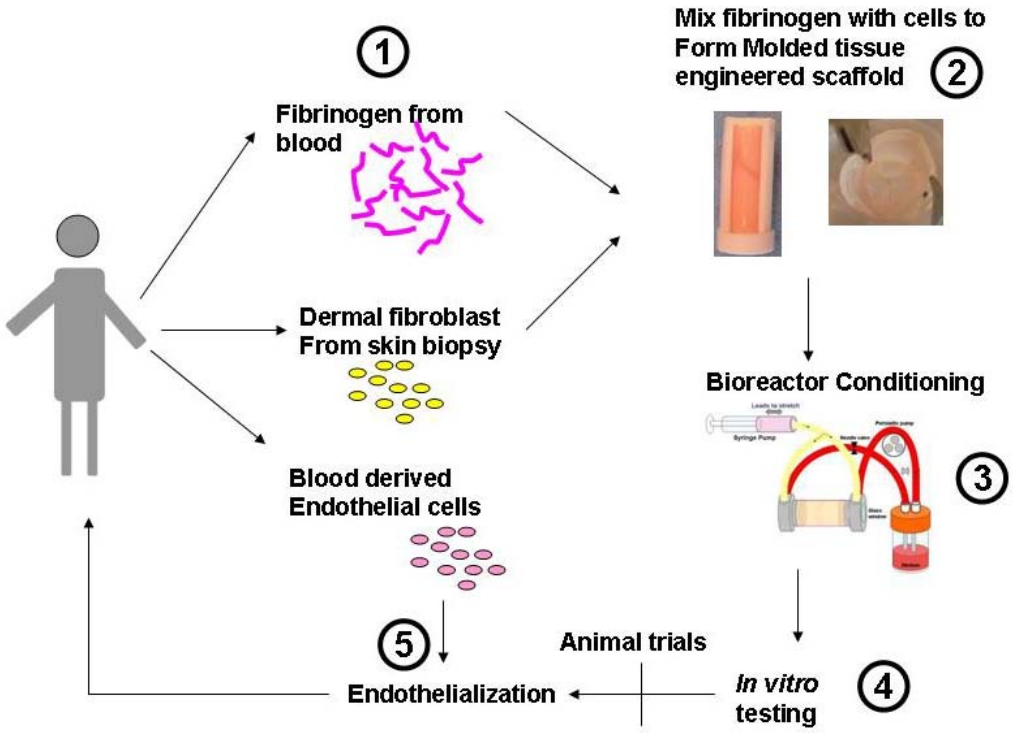

Figure 1-3: Illustration of developing a TEHV from autologous cell and scaffolding polymer along with *in vitro* developmental steps.

The cell types that have been studied in these scaffolds include bone-marrow derived stromal cells (37), human valve interstitial cells (24, 25, 38, 39), fibroblast cells (30) and endothelial cells (40). All of these combinations have shown some promise *in vitro*, with success in short term *in vivo* experiments (24, 25, 34).

1.3.2: Cell sources for tissue engineering

Successful, cost-effective, and large-scale production of engineered tissue requires an adequate source of healthy cells which can be passage several times before seeding into a scaffold (41). Cell sources for tissue engineering fall into three categories: autologous cells (from the patient); allogeneic cells (from a human donor, but not immunologically identical); and xenogeneic cells (donor from different species). Each category can be further delineated in terms of stem cells (adult or embryonic) or differentiated cells. With respect to current research in tissue engineering, most work is done with cells derived from animal models.

Poh *et al.* has worked with human smooth muscle cells (SMCs) derived from the saphenous vein seeded on polyglycolic acid (PGA) mesh (42). The study showed that the cells from older donors (age 55-67yr) had poor vascular graft durability and structure compared to younger donors (47 yrs). The study further looked at the telomerase extension with gene therapy which showed promising results. In other studies by Solan *et al.*, vascular SMCs from swine were used for strained testing of vascular grafts (43). Other studies with SMCs in engineered tissue have been conducted by Isenberg and Tranquillo (44), Cummings *et al.* (45) and Seliktar *et al.* (46).

Seliktar *et al*. compared the tissue properties of samples seeded with rat aortic SMC, human aortic SMC and human dermal fibroblast (HDF) (46). The researcher found more dominant effects of straining on rat SMC-based tissue compared to human cells. The mechanical properties were similar for both human cell types, while much higher for rat SMCs. The study concluded that species-dependent differences in tissue properties exist; however, there was no major difference within the species.

Another major cell source for tissue engineering is fibroblast cells. Balestrini *et al.* (47) and Berry *et al.* (48) have published work with fibroblast cells where scaffold were mechanically conditioned. Balestini used fibrin based discs to apply biaxial strain on tissue and found significant increases in collagen production. Similarly, Berry *et al* also showed enhanced collagen production in the strained tissue.

The studies published to date on cell sources have shown promising results with several cell types. In our lab, we have studies tissue constructs with rat SMC, neonatal HDF (NHDF) and porcine aortic valve cells (PAVC). In cyclic distension experiments (work presented in chapter 2) in the fibrin tubular constructs were performed with both NHDF and PAVC. All VE studies were performed with NHDF cells. Previously, published data from our lab with cyclic distension studies had used SMC in collagen constructs (44). Other optimization studies with cells types discussed above in our lab have been published by Long *et al.* (49), Neidart *et al.* (50), Ross *et al.* (51) and Grassel *et al.* (52). Long *et al.* compared the fibrin and collagen based constructs seeded with SMC and NHDF. They showed enhanced elastin production in fibrin constructs. Neidart *et al.* compared the effects of culture media supplements on tissue properties using NHDF in the fibrin gel. Ross *et al.* compared RNA expression for SMC seeded fibrin construct along with biochemical and tensile mechanical properties, while Grassel *et al.* studied the fibrin based constructs using SMC. Studies in our lab and by others have demonstrated several cell types as potential sources for tissue engineering of heart valve.

1.3.3: Fibrin as a scaffold

On the similar principle as discussed in section 1 regarding scaffolds, our current approach to tissue engineering a heart valve is via fibrin gel for creating a valve equivalent (VE). This approach is based upon previous research with both collagen and fibrin cell-embedded gels (49, 50, 52, 53). Gels with entrapped cells can be cast on mold of any geometry. With time, traction by cells on surrounding fibers causes compaction of the fibrillar network. The design of the mold can constrain gel compaction and hence lead to the alignment of fibers in a desired orientation.

Previous studies comparing collagen and fibrin gels have shown better remodeling of the ECM with the fibrin gel (49, 53). It has been shown that cells embedded in fibrin gel are more active in ECM synthesis. The advantages of natural ECM synthesis are many including the ability to remodel artificial tissue and provide mechanical strength to withhold large stresses as in the leaflets of a valve. Studies have also shown that fibrin based tissue equivalents (TE) (gel strips or hemispheres) have similar mechanical properties to collagen gels, however with the ability of cells to produce ECM in the fibrin gel, overtime these TEs can have enhanced mechanical properties (53). It has been shown that fibrin TEs can synthesize more elastin which is an important structural protein in the valve leaflets (49). Further, the studies with fibrin have shown that ECM production can also be enhanced with supplements like fetal bovine serum (FBS), transforming growth factor beta (TGF-β) (50), fibroblast growth factor (FGF) (54), vascular endothelial growth factor (VEGF) (55), insulin, and Vitamin C (50, 55).

Our laboratory is currently working with a bi-leaflet valve design. The fibrin based cell solution consisting of neonatal human dermal fibroblast has been primarily researched as the construct for a tissue engineered heart valve (Fig 3A). The fibrin solution mixed with cells is injected into a custom designed mold (Fig 3B).

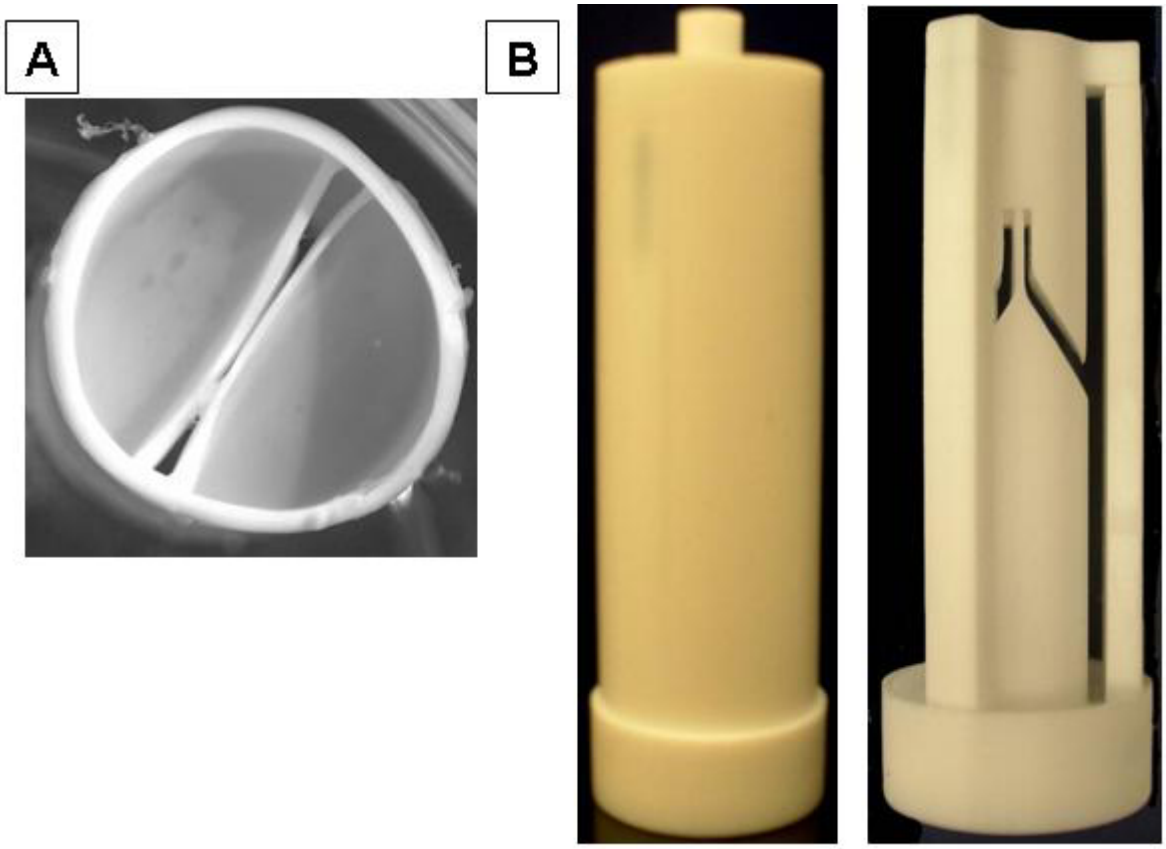

Figure 1-4: A: Fibrin based tissue engineered heart valve. B: VE mold made from Teflon, left image has the outer casing on it.

1.3.4: Mechanical requirements for tissue engineered valve equivalents

The human aortic valve opens and closes approximately 103,000 times each day and about 3.7 billion times in a lifetime (3). One of the primary reasons for failure of the current prosthetics is their inability to withstand such long fatigue life. Tissue engineering technology promises growth and remodeling of the implanted tissue. For this reason, tissue engineering heart valve equivalents assure longer life once implanted. However, a bigger issue for current tissue engineered valve equivalents made from biopolymer is their initial mechanical properties, which are sub-par compared to natural tissue. *In vivo* studies with PGA based valve in the pulmonary position have shown remodeling of the construct over the duration of implantation with tissue development comparable to the native valve tissue (24, 25, 56). However, PGA polymer mesh has much higher mechanical properties (maximal tensile strength 3.2 MPa) compared to the fibrin based valve equivalents (maximal tensile strength ~0.25 MPa). In previous studies, although initial mechanical properties of the PGA were high, explanted tissue after 17 weeks showed ultimate tensile strength of 0.65 MPa (24). The researcher found no abnormalities in the valvular function using echocardiography. Hence, a more important question is: what are the minimum mechanical requirements for a tissue engineered valve?

During each cycle, valves experience tensile, bending and compressive stresses. In diastole phase, when leaflet are closed, the average trans-valvular pressure on aortic valve is around 80 mmHg, inducing primarily tensile stresses. During systole, when the valve is in an open state, all three stresses mentioned earlier are experienced by the leaflet tissue. The stress analysis of the aortic valves *in vivo* has been conducted by

Thubrikar *et al.* (5, 57-59) and Kalath *et al.* (60). Thubrikar *et al.* used a canine model to study *in vivo* stress-strain behavior using fluoroscopy (5, 59). The analysis was done with markers measuring displacement in the radial direction of the leaflets. The researchers calculated the mean modulus of elasticity during diastole to be 2.44 MPa (1.16 MPa *in vitro* under similar strains) and 0.05 MPa (0.075 MPa *in vitro* under similar strains) for systole. In the circumferential direction, studies by Thubrikar *et al.* have shown membrane stresses to be 2.4 MPa during diastole and 0.17 MPa during systole (59). In the same study, the researchers also looked at bending stresses and concluded that bending stresses are compressive on the aortic side during diastole and tensile on the ventricular side. This results in total stresses being variable throughout the thickness of the leaflets. In another study with bioprosthetic aortic valves, Thubrikar *et al.* calculated membrane stresses during diastole in the circumferential direction to be 0.33 MPa and 0.17 MPa in the radial direction (58). In the same study, the researchers also studied bending and compressive stresses during systole. The tensile stress due to bending was found to be 0.36 MPa and compressive stress due to bending on ventricular side of the leaflet to be 0.09 MPa. The techniques used by Thubrikar *et al.* to measure displacement in the leaflets were not the most precise technique but, as claimed by authors, it was simplified and robust. Other *in vivo* studies in humans have been conducted by Kalath *et al.* using echocardiography and sphymomanometry (60). The researchers found average circumferential elastic modulus over the entire cardiac cycle to be 0.3 MPa in young patients and 0.47 MPa in old patients.

Using computer modeling with smoothed geometry for aortic valves, Cataloglu *et al.* calculated the stress field in a leaflet during diastole (61). The researchers

calculated stresses using 73 mmHg (1 g/mm^2 force) trans-membrane pressure. In calculation of stresses, the researchers also took into account the variable thickness of the leaflet (0.25 mm to 1.33 mm). The reported maximum principle stresses were from 0.33 to 0.56 MPa.

To date, no major study has been published with rigorous analysis of the stresses in leaflet during the cardiac cycle, especially during the transition period between end diastole and end systole. The limited current data indicates that any tissue engineered valve in an aortic position should be able to tolerate tensile stresses of at least 0.5 MPa. Another option for *in vivo* studies is to study valves in the pulmonary position as described earlier. In the pulmonary position, diastole pressure varies form 5-30 mmHg compared to 80-100 mmHg in the aortic position (14).

1.3.5: Role of mechanical conditioning in tissue engineering

In cardiovascular tissue engineering, stimulation of tissue formation by mechanical conditioning has proven to be a useful tool in enhancing mechanical properties and allowing the tissue to grow, remodel and repair. Various bioreactor systems have been developed to apply mechanical stimulation to engineered tissue. Most bioreactors developed for tissue engineered heart valve mimic the opening and closing of the natural heart valve (62-64). Recently, a new focus has been given to strain-controlled conditioning of the engineered valves, with less emphasis on mimicking *in vivo* flow conditions (27). For development of the tissue engineered blood vessels and tissue strips, several bioreactors have been designed to control straining of the tissue. Some of the most relevant work to this project is discussed here.

Studies with collagen-based cylindrical constructs by Berry *et al.* showed significantly higher mechanical properties of 10% strained gel constructs compared to static preloaded constructs (48). The researchers used collagen gels seeded with fibroblast cells. The constructs were preloaded at 2mN or 10mN and then subjected to 10% cyclic strain at 1 Hz. The researchers found higher cell proliferation, collagen synthesis and stiffness in 10% stained tissue after 24hr in culture. Similarly, Seliktar *et al.* compared collagen gels seeded with human aortic smooth muscle cells (HASM), rat aortic smooth muscle cells (RASM) and human dermal fibroblast cells (HDF) (46). The researchers applied 10% strain to constructs for 4-8 days and compared mechanical properties. They found increased mechanical properties with all cell types when mechanically strained. The previous studies focused on very short periods of time (maximum of 8 days) during which even enhanced mechanical properties are suboptimal. Studies by Isenberg and Tranquillo focused on the long term effect of strain on the mechanical properties of collagen gels seeded with rat smooth muscle cells (44). Tissue constructs at conditions varying from 2.5% to 10% strain were cultured for up to 11 weeks. The results showed increased mechanical properties for 5% and 10% straining compared to static culture. The study further analyzed the effects of stretch and relaxation time during a cycle on the properties of tissue constructs.

Salon *et al.* studied biodegradable polyglycolic acid (PGA) mesh based vascular constructs for the effect of mechanical conditioning on tissue properties (43). The tissue constructs were developed by seeding vascular SMC onto the scaffold and mechanically conditioned on a silicon tube. The researchers conditioned vascular constructs at 1.5% strain at a frequency of 0 Hz, 1.5 Hz and 2.75 Hz representing static, human heart rate

and fetal heart rate frequencies. The results showed higher collagen contents in vessels grown at 1.5Hz and 2.75 Hz compared to static culture. More recently, researchers have focused on fibrin based tissue constructs. Cummings *et al.* applied 10% strain to collagen-fibrin mixed gel constructs with rat SMC (45). After 4 days of culture, researchers showed increased mechanical properties for strained tissue with similar cell counts and decreased gel compaction. Balestrini *et al.* studies biaxial straining of pure fibrin gel constructs (47). The researchers applied biaxial stretch to fibrin gel disks seeded with human dermal fibroblast cells. About 16% uniform strain was applied to fibrin disks stretched at 0.2 Hz for 8 days with the FlexCell® system. The researchers found 7 fold decreases in thickness of stretched samples (106 μm) compared to static samples (764 μm). The ultimate tensile stress was ten fold higher (119 kPa) in stretched samples compared to static samples (12 kPa). Collagen content was also found to be higher in stretched samples, leading to ten fold higher collagen density in stretched disc (1047 $\mu g/cm^3$ in stretched samples compared to 132 $\mu m/cm^3$ in static samples).

In the field of heart valve tissue engineering, most work to date has been done with mechanical conditioning of bio-polymer based engineered tissue. Flow controlled bioreactors mimicking physiological opening and closing of valve leaflets have been designed by Dumont *et al* (62), Warnock *et al* (65), Hoerstrup *et al* (63) and Hildebrand *et al* (64). The bioreactor designed by Hoerstrup *et al* has been used for *in vitro* culture of PGA based trileaflet heart valves. The valve was manufactured with non-woven PGA mesh seeded with ovine myofibroblast cells and coated with endothelial cells. After 4 days of static incubation, the valves were conditioned in the bioreactor for 14 days with progressive increases in flow (125 mL/min to 750 mL/min) and pressure (30 mmHg to

55 mmHg). After conditioning, the valves were tested for 60 minutes at high pressure (>150 mmHg) and implanted in the pulmonary position of lambs. The researchers described collagen, DNA, GAG and elastin content as a percent of native valve tissue. The valves that were incubated in the bioreactor had 80% collagen (relative to native valves) at 28 days of incubation compared to ~10% in statically incubated valves. Similarly, DNA and GAG content were also higher in mechanically conditioned valves. The modulus was 1 MPa for engineered tissue versus 1.6 MPa for native tissue. The ultimate tensile strength was ~0.7 MPa for engineered tissue compared to ~0.8 MPa for native pulmonary valves. The researchers also conducted *in vivo* trials by replacing the pulmonary valves of lambs with tissue engineered valves (25). The implanted valves were harvested at different time points up to 20 weeks with no thrombosis formation.

In recent publication researchers have independently studied the effect of cyclic tensile strain and cyclic flexure of PGA based heart valve tissue (27, 66). Mol *et al* designed a bioreactor system that induces cyclic pressure gradients on leaflets, giving strain values as high as 20% (27). The study found a 71% increase in collagen content after three weeks of strain compared to non-strained samples. However there was also 112% increase in DNA content, suggesting a collagen increase due to cell proliferation. The mechanical properties of strained tissue was found to be 3 times higher for dynamically strained tissue (UTS 0.25 MPa, Modulus 0.78 MPa) compared to the non-loaded case (UTS 0.07 MPa, Modulus 0.18 MPa) after three weeks. Engelmayr Jr *et al* conducted their study in bioreactor system designed to bend PGA tissue strips seeded with SMCs (66). In this study, the tissue strip was placed between four stainless steel stationary posts (two on each corner of the tissue strip) and two flexure pins in the

center connected to a linear actuator. The actuator was moved at a 1 Hz frequency to produce a bending angle of 62 degrees, representing physiological bending of heart leaflets. The study was motivated to independently evaluate the effects of flexure on tissue remodeling. The effective stiffness (defined as flexure rigidity/ moment of inertia) was 17.6% higher in flexed tissue strips compared to static strips. There was also a 62% increase in collagen with no change in DNA or GAG content, indicating increased collagen production by flexed SMCs.

Comparing the studies done by Hoerstrup *et al*, Mol *et al* and Engelmayr Jr *et al*, the largest increase in collagen content was found in the study by Hoerstrup *et al*. Hoerstrup *et al* found a 1075% increase in collagen in mechanically conditioned constructs compared to those in static culture. The conditioned constructs also had a 261% increase in DNA content, indicating a much higher collagen output on a per cell basis (~409%). Compared to this, Engelmayr Jr *et al* calculated about ~62% increase in collagen on per cell basis, while Mol *et al* showed no change (even possibly a decrease) in the collagen content on per cell basis in mechanically conditioned tissue.

Based on the published data so far, very little is known about the effects of mechanical conditioning on fibrin based tissue. Early work in our lab and by others has shown the ability of fibrin constructs to produce mechanically enhanced tissue in response to mechanical stimulation. For tissue engineered valves to date, no collagen or fibrin based system has been published where mechanical conditioning, whether tensile, flexural or both have been studied. Hence, this research proposal focuses on a project that would evaluate strain controlled conditioning of fibrin based tissue engineered heart valve (TEHV).

1.3.6: Relevance of strain conditioning in engineered valve leaflets

Tissue engineering provides an excellent approach for creating heart valve replacements by seeding cells onto a scaffold which degrades as the ECM is deposited by cells. The developing tissue provides the predominant biomechanical function necessary in engineered tissue like valve leaflets. Despite the success of this approach, problems arise concerning the mechanical properties of engineered tissue. Increasing evidence suggest that mechanical conditioning as a valuable method to improve mechanical properties of engineered tissue prior to implant (67). Mechanical conditioning of engineered tissue involves the application of various mechanical stimuli inside a bioreactor, such as flow induced shear stress (25) and strain (27), being either dynamic or static in nature.

For tissue engineered heart valves, the most commonly used bioreactor is a pulse duplicator system, which drives flow through the leaflets to mimic the opening and closing behavior of natural valves. Some of the newer versions of these bioreactors are capable of simulating physiological conditions like pressure and flow profiles and compliance of heart chambers (62, 68). However little research has been done with strain-controlled conditioning of tissue engineered heart valves even though a substantial amount of data has shown enhanced properties of strained engineered tissue. Most of the work on strain-controlled systems has been done with cylindrical samples (representing arterial graft). Work with minimum flow rate and cyclic strain on leaflets of tissue engineered valves has shown enhancement of properties like modulus and ultimate tensile strength (UTS) (27). However the researchers in the previous study

used polyglycolic acid mesh (PGA) as the scaffold, which is a very different system than the fibrin scaffold.

1.3.7: Mechno-transduction in tissue engineering

Functional tissue engineered construct requires tensile mechanical properties to withstand physiological stress and strains. Since fibrin gel is incapable of tolerating physiological conditions, *in vitro* remodeling of the fibrin based construct is essential. Cells in fibrin gel can be manipulated to increase collagen and elastin deposition (two major ECM proteins), organization of ECM and cell proliferation by inducing chemical or mechanical stimulus. Growth factor like TGF-β can be added to culture medium in which fibrin based construct is incubated to induce these effects. The growth factor can diffuse through fibrin matrix and bind to cellular membrane receptors. Similarly, a mechanical stimulus like stretch can be applied to the entire fibrin tissue construct, and global stretch would lead to potential stretch in the fibers attach directly to cells and induce a stretch on the cell membrane.

Integrins are transmembrane protein that couple in intracellular and extracellular structural protein network for a cell. Several good reviews are available on structure of integrins (for a recent review on integrin biochemistry see (69)). From a mechanical stimulus, the stretch to ECM fiber could induce conformational changes in the integrin leading to intercellular protein cascade (70). In side the cells, the integrins connect to cell-matrix adhesion complex. A large array of proteins are thought to be part of the focal adhesions under various conditions, and still more molecules apparently interact with adhesion complex proteins to transducer signals or alter function of the cell/ECM

coupling, including notably focal adhesion kinase (FAK), the G-protein Rho, and MAPK signaling proteins like extracellular signal-regulated kinase (ERK) (70-72). ERK is one of the major signaling proteins discussed in chapter 2 and 3 and relevance to cyclic strain. The signaling proteins can activate key transcription factors (e.g. AP-1 and NF-kB) and gene expression (71). The mechanical stimulus can also induce production and stabilization of growth factors like TGF-β (73).

Chemical stimulus like TGF-β can bind to TGF-β specific receptor on cell surface and induce phosphorylation of the intracellular signal proteins like SMAD, p38 and Akt. phosphoSMAD can bind with its co-factor, migrate through nuclear pore complex and activate gene transcription by binding to DNA-cofactor (74). Specific gene expression is regulated by affinity of SMAD complex to DNA-binding cofactor. The proteins in TGF-β pathway can cross-talk with mitogen activated protein kinase pathway (74). This can lead to complex cell signaling pathways and responses. An illustration of the TGF-β pathway and cross-talk with MAPK is shown in Figure 5 (taken from Massague (74)). A brief experimental study of TGF-β effect in presence of mechanical stretching is presented in chapter 3.

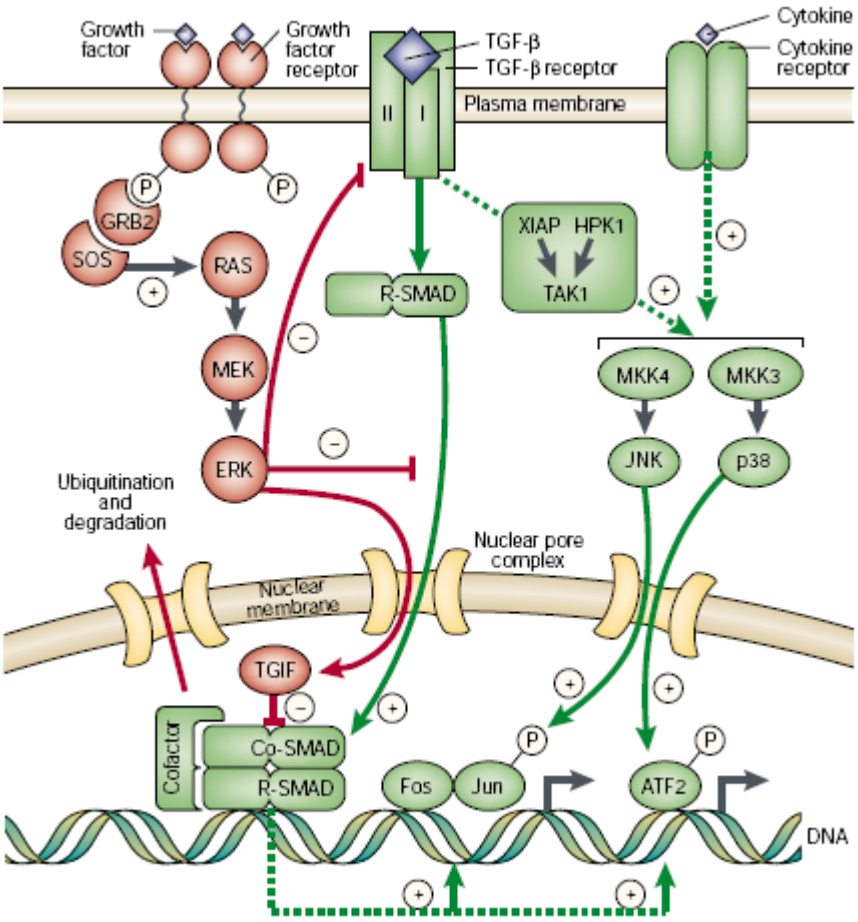

Figure 1-5: A basic SMAD pathway and cross-talk with mitogen activated protein kinase (MAPK) signaling proteins (Taken from Massague (74)).

Both mechanical and chemical stimulus can activate mechano/chemi-sensitive ion channels and trigger ions entry into cells (72). For example influx of Ca^{2+} can activate proteases such as calpain which is associated with FAs. Their putative targets include structural and regulatory components such as paxillin and Rho (71).

In brief, a summary of external signals that can influence ECM transcription genes and eventually regulate ECM environment are summarized in Figure 6 (taken from Wang *et al* (71)).

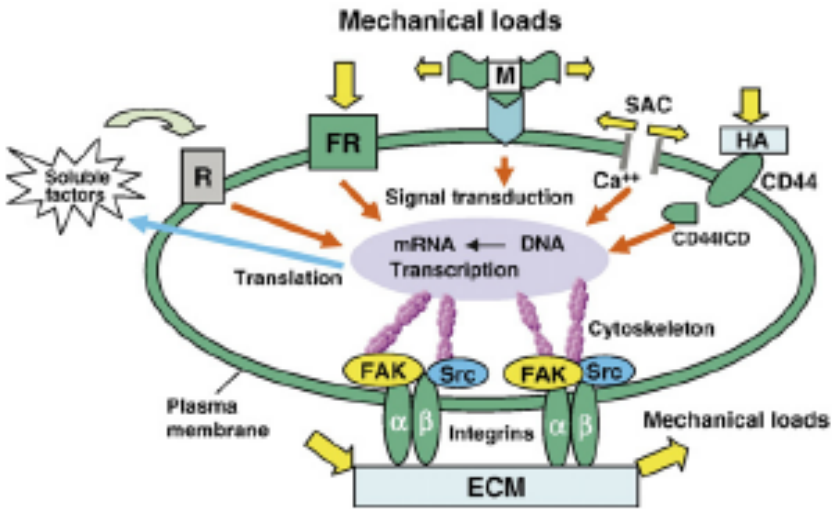

Figure 1-6: A conceptual illustration of several cellular mechanotransduction mechanisms (taken from Wang *et al* (71))

1.4: References

1. Rosamond, W., *et al.* (2008) Heart disease and stroke statistics--2008 update: a report from the American Heart Association Statistics Committee and Stroke Statistics Subcommittee. *Circulation* **117,** e25-146.
2. Allen, H. D., *et al.* (2008) *Moss and Adams' Heart Disease in Infants, Children, and Adolescents* (Lippincott Williams & Wilkins, Philadelphia).
3. Thubrikar M (1990) *The Aortic Valve* (CRC Press, Boca Raton).
4. Vesely, I. (1998) The role of elastin in aortic valve mechanics. *J Biomech* **31,** 115-123.
5. Thubrikar, M. J., *et al.* (1986) Comparison of the in vivo and in vitro mechanical properties of aortic valve leaflets. *J Thorac Cardiovasc Surg* **92,** 29-36.
6. De Hart, J., *et al.* (2004) Collagen fibers reduce stresses and stabilize motion of aortic valve leaflets during systole. *J Biomech* **37,** 303-311.
7. Vesely, I., Lozon, A. (1993) Natural preload of aortic valve leaflet components during glutaraldehyde fixation: effects on tissue mechanics. *J Biomech* **26,** 121-131.
8. Vesely, I., Noseworthy, R. (1992) Micromechanics of the fibrosa and the ventricularis in aortic valve leaflets. *J Biomech* **25,** 101-113.
9. Scott, M., Vesely, I. (1995) Aortic valve cusp microstructure: the role of elastin. *Ann Thorac Surg* **60,** S391-394.
10. Scott, M. J., Vesely, I. (1996) Morphology of porcine aortic valve cusp elastin. *J Heart Valve Dis* **5,** 464-471.
11. Stradins, P., *et al.* (2004) Comparison of biomechanical and structural properties between human aortic and pulmonary valve. *Eur J Cardiothorac Surg* **26,** 634-639.
12. Lo, D., Vesely, I. (1995) Biaxial strain analysis of the porcine aortic valve. *Ann Thorac Surg* **60,** S374-378.
13. Lee, T. C., *et al.* (2001) The effect of elastin damage on the mechanics of the aortic valve. *J Biomech* **34,** 203-210.
14. Christie, G. W., Barratt-Boyes, B. G. (1995) Mechanical properties of porcine pulmonary valve leaflets: how do they differ from aortic leaflets? *Ann Thorac Surg* **60,** S195-199.
15. Sauren, A. A., *et al.* (1983) The mechanical properties of porcine aortic valve tissues. *J Biomech* **16,** 327-337.
16. Purinya, B., *et al.* (1994) Biomechanical and structural properties of the explanted bioprosthetic valve leaflets. *J Biomech* **27,** 1-11.
17. Schoen, F. J., Levy, R. J. (1999) Founder's Award, 25th Annual Meeting of the Society for Biomaterials, perspectives. Providence, RI, April 28-May 2, 1999. Tissue heart valves: current challenges and future research perspectives. *J Biomed Mater Res* **47,** 439-465.
18. Webb, G. D. (2002) *Advances in adult congenital heart disease* (W.B. Saunders Co, , Philadelphia).

19. Solomon, N. A., *et al.* (2006) In search of a pediatric cardiac surgeon's 'Holy Grail': the ideal pulmonary conduit. *Expert Rev Cardiovasc Ther* **4,** 861-870.
20. Moons, P., *et al.* (2009) Congenital heart disease in 111 225 births in Belgium: birth prevalence, treatment and survival in the 21st century. *Acta Paediatr* **98,** 472-477.
21. Cobanoglu, A., *et al.* (1988) Aortic valve replacement with the Starr-Edwards prosthesis: a comparison of the first and second decades of follow-up. *Ann Thorac Surg* **45,** 248-252.
22. Senthilnathan, V., *et al.* (1999) Heart valves: which is the best choice? *Cardiovasc Surg* **7,** 393-397.
23. Huang-Lee, L. L., *et al.* (1990) Biochemical changes and cytotoxicity associated with the degradation of polymeric glutaraldehyde derived crosslinks. *J Biomed Mater Res* **24,** 1185-1201.
24. Sodian, R., *et al.* (2000) Tissue engineering of heart valves: in vitro experiences. *Ann Thorac Surg* **70,** 140-144.
25. Hoerstrup, S. P., *et al.* (2000) Functional living trileaflet heart valves grown in vitro. *Circulation* **102,** III44-49.
26. Baaijens, F., *et al.* (2005) Functional tissue engineering of the aortic heart valve. *Clin Hemorheol Microcirc* **33,** 197-199.
27. Mol, A., *et al.* (2005) Tissue engineering of human heart valve leaflets: a novel bioreactor for a strain-based conditioning approach. *Ann Biomed Eng* **33,** 1778-1788.
28. Rothenburger, M., *et al.* (2001) In vitro modelling of tissue using isolated vascular cells on a synthetic collagen matrix as a substitute for heart valves. *Thorac Cardiovasc Surg* **49,** 204-209.
29. Ye, Q., *et al.* (2000) Fibrin gel as a three dimensional matrix in cardiovascular tissue engineering. *Eur J Cardiothorac Surg* **17,** 587-591.
30. Mol, A., *et al.* (2005) Fibrin as a cell carrier in cardiovascular tissue engineering applications. *Biomaterials* **26,** 3113-3121.
31. Robinson, P. S., *et al.* (2008) Functional tissue-engineered valves from cell-remodeled fibrin with commissural alignment of cell-produced collagen. *Tissue Eng Part A* **14,** 83-95.
32. Flanagan, T. C., *et al.* (2007) The in vitro development of autologous fibrin-based tissue-engineered heart valves through optimised dynamic conditioning. *Biomaterials* **28,** 3388-3397.
33. Samouillan, V., *et al.* (1999) Thermal analysis characterization of aortic tissues for cardiac valve bioprostheses. *J Biomed Mater Res* **46,** 531-538.
34. Elkins, R. C., *et al.* (2001) Decellularized human valve allografts. *Ann Thorac Surg* **71,** S428-432.
35. Tudorache, I., *et al.* (2007) Tissue engineering of heart valves: biomechanical and morphological properties of decellularized heart valves. *J Heart Valve Dis* **16,** 567-573; discussion 574.
36. Knight, R. L., *et al.* (2005) Tissue engineering of cardiac valves: re-seeding of acellular porcine aortic valve matrices with human mesenchymal progenitor cells. *J Heart Valve Dis* **14,** 806-813.

37. Hoerstrup SP, S. R., Daebritz S, Wang J, Bacha EA, Martin DP, Moran AM, Guleserian KJ, Sperling JS, Kaushal S, Vacanti JP, Schoen FJ, Mayer JE Jr, (2000) Functional living trileaflet heart valves grown in vitro. *Circulation* **102,** III44-49.
38. Masters, K. S.*, et al.* (2004) Designing scaffolds for valvular interstitial cells: cell adhesion and function on naturally derived materials. *J Biomed Mater Res A* **71,** 172-180.
39. Taylor, P. M.*, et al.* (2002) Human cardiac valve interstitial cells in collagen sponge: a biological three-dimensional matrix for tissue engineering. *J Heart Valve Dis* **11,** 298-306; discussion 306-297.
40. Bader, A.*, et al.* (1998) Tissue engineering of heart valves--human endothelial cell seeding of detergent acellularized porcine valves. *Eur J Cardiothorac Surg* **14,** 279-284.
41. Naughton, G. K. (2002) From lab bench to market: critical issues in tissue engineering. *Ann N Y Acad Sci* **961,** 372-385.
42. Poh, M.*, et al.* (2005) Blood vessels engineered from human cells. *Lancet* **365,** 2122-2124.
43. Solan, A.*, et al.* (2003) Effect of pulse rate on collagen deposition in the tissue-engineered blood vessel. *Tissue Eng* **9,** 579-586.
44. Isenberg, B. C., Tranquillo, R. T. (2003) Long-term cyclic distention enhances the mechanical properties of collagen-based media-equivalents. *Ann Biomed Eng* **31,** 937-949.
45. Cummings, C. L.*, et al.* (2004) Properties of engineered vascular constructs made from collagen, fibrin, and collagen-fibrin mixtures. *Biomaterials* **25,** 3699-3706.
46. Seliktar, D.*, et al.* (2003) Mechanical strain-stimulated remodeling of tissue-engineered blood vessel constructs. *Tissue Eng* **9,** 657-666.
47. Balestrini, J. L., Billiar, K. L. (2006) Equibiaxial cyclic stretch stimulates fibroblasts to rapidly remodel fibrin. *J Biomech* **39,** 2983-2990.
48. Berry, C. C.*, et al.* (2003) Influence of external uniaxial cyclic strain on oriented fibroblast-seeded collagen gels. *Tissue Eng* **9,** 613-624.
49. Long, J. L., Tranquillo, R. T. (2003) Elastic fiber production in cardiovascular tissue-equivalents. *Matrix Biol* **22,** 339-350.
50. Neidert, M. R.*, et al.* (2002) Enhanced fibrin remodeling in vitro with TGF-beta1, insulin and plasmin for improved tissue-equivalents. *Biomaterials* **23,** 3717-3731.
51. Ross, J. J., Tranquillo, R. T. (2003) ECM gene expression correlates with in vitro tissue growth and development in fibrin gel remodeled by neonatal smooth muscle cells. *Matrix Biol* **22,** 477-490.
52. Grassl, E. D.*, et al.* (2003) A fibrin-based arterial media equivalent. *J Biomed Mater Res A* **66,** 550-561.
53. Grassl, E. D.*, et al.* (2002) Fibrin as an alternative biopolymer to type-I collagen for the fabrication of a media equivalent. *J Biomed Mater Res* **60,** 607-612.
54. Takehara, K. (2000) Growth regulation of skin fibroblasts. *J Dermatol Sci* **24 Suppl 1,** S70-77.

55. Yao, L., *et al.* (2005) Fibrin-based tissue-engineered blood vessels: differential effects of biomaterial and culture parameters on mechanical strength and vascular reactivity. *Tissue Eng* **11,** 991-1003.
56. Shinoka, T., *et al.* (1996) Tissue-engineered heart valves. Autologous valve leaflet replacement study in a lamb model. *Circulation* **94,** II164-168.
57. Thubrikar, M., *et al.* (1980) Stresses of natural versus prosthetic aortic valve leaflets in vivo. *Ann Thorac Surg* **30,** 230-239.
58. Thubrikar, M. J., *et al.* (1982) Stress analysis of porcine bioprosthetic heart valves in vivo. *J Biomed Mater Res* **16,** 811-826.
59. Thubrikar, M., *et al.* (1980) The elastic modulus of canine aortic valve leaflets in vivo and in vitro. *Circ Res* **47,** 792-800.
60. Kalath, S., *et al.* (1986) Non-invasive assessment of aortic mechanical properties. *Ann Biomed Eng* **14,** 513-524.
61. Cataloglu, A., *et al.* (1977) Stress analysis of aortic valve leaflets with smoothed geometrical data. *J Biomech* **10,** 153-158.
62. Dumont, K., *et al.* (2002) Design of a new pulsatile bioreactor for tissue engineered aortic heart valve formation. *Artif Organs* **26,** 710-714.
63. Hoerstrup, S. P., *et al.* (2000) New pulsatile bioreactor for in vitro formation of tissue engineered heart valves. *Tissue Eng* **6,** 75-79.
64. Hildebrand, D. K., *et al.* (2004) Design and hydrodynamic evaluation of a novel pulsatile bioreactor for biologically active heart valves. *Ann Biomed Eng* **32,** 1039-1049.
65. Warnock, J. N., *et al.* (2005) Design of a sterile organ culture system for the ex vivo study of aortic heart valves. *J Biomech Eng* **127,** 857-861.
66. Engelmayr, G. C., Jr., *et al.* (2005) The independent role of cyclic flexure in the early in vitro development of an engineered heart valve tissue. *Biomaterials* **26,** 175-187.
67. Butler, D. L., *et al.* (2000) Functional tissue engineering: the role of biomechanics. *J Biomech Eng* **122,** 570-575.
68. Ruel, J., Lachance, G. (2009) A New Bioreactor for the Development of Tissue-Engineered Heart Valves. *Ann Biomed Eng*.
69. Arnaout, M. A., *et al.* (2002) Coming to grips with integrin binding to ligands. *Curr Opin Cell Biol* **14,** 641-651.
70. Pedersen, J. A., Swartz, M. A. (2005) Mechanobiology in the third dimension. *Ann Biomed Eng* **33,** 1469-1490.
71. Wang, J. H., *et al.* (2007) Mechanoregulation of gene expression in fibroblasts. *Gene* **391,** 1-15.
72. Silver, F. H., *et al.* (2003) Mechanobiology of force transduction in dermal tissue. *Skin Res Technol* **9,** 3-23.
73. Nakatani, T., *et al.* (2002) Mechanical stretching force promotes collagen synthesis by cultured cells from human ligamentum flavum via transforming growth factor-beta1. *J Orthop Res* **20,** 1380-1386.
74. Massague, J. (2000) How cells read TGF-beta signals. *Nat Rev Mol Cell Biol* **1,** 169-178.

Chapter 2: Cyclic distension of fibrin-based tissue constructs: Evidence of adaptation during growth of engineered connective tissue

Published in *the Proceeding of the National Academy of Science*, USA. 2008

2.1: Summary

Tissue engineering provides a means to create functional living tissue replacements. Here we examined the effects of 3 weeks of cyclic distention (CD) on fibrin-based tubular tissue constructs seeded with porcine valve interstitial cells. CD with circumferential strain amplitude ranging 2.5% to 20% was applied to evaluate the effects of CD on fibrin remodeling into tissue. We hypothesized that during long-term CD cells adapt to cyclic strain of constant strain amplitude ("constant CD"), diminishing tissue growth. We thus also subjected constructs to CD with strain amplitude that was incremented from 5-15% over the 3 weeks of CD ("incremental CD"). For constant CD, improvement occurred in construct mechanical properties and composition, peaking at 15% strain: ultimate tensile strength and tensile modulus increased 47% and 45% over statically incubated controls (to 1.1 and 4.7 MPa, respectively); collagen density increased 29% compared to controls (to 27 mg/ml). Incremental CD further improved outcomes. Ultimate tensile strength increased 98% and modulus increased 62% compared to the largest values with constant CD, and collagen density increased 34%. Only in the case of incremental CD was the ratio of collagen content to cell number greater (70%) than controls, consistent with increased collagen deposition per cell. Studies with human dermal fibroblasts showed similar improvements, generalizing the findings, and revealed a 255% increase in extracellular signal-regulated kinase signaling for incremental CD *vs.* constant CD. These results suggest cell adaptation may limit conventional strategies of stretching with constant strain amplitude and that new approaches might optimize bioreactor operation.

2.2: Introduction

The vast majority of approaches to cardiovascular tissue engineering involve seeding matrix-producing cells, typically smooth muscle cells, fibroblasts, and/or myofibroblasts, onto a synthetic polymer or entrapping the cells within a forming biopolymer gel cast in a mold. In either case, there is typically an *in vitro* culture stage with the goal of having the cells transform the starting polymer into tissue that confers the required properties of the tissue-engineered construct. Essential criteria for a successful construct in many applications include requisite mechanical properties such as sufficient tensile and/or burst strength, physiological modulus/compliance, and elastic recoil. This endeavor has been coined "functional tissue engineering" (1). Achieving these properties has motivated several strategies and bioreactor concepts, including the use of chemical stimulation (e.g. growth factor supplementation to the construct incubation medium) and mechanical stimulation (e.g. stretching, compressing, or bending the construct). Mechanical stimulation has become a primary strategy for inducing tissue growth *in vitro* (2).

In vascular tissue engineering, cyclic distension (CD) of constructs via pulsatile flow of medium through the lumen (3-5) or inflation of an elastic tube placed through the lumen (6-9) are the primary bioreactor configurations. In particular, mechanical properties of tissue constructs have been shown to improve when stretching constructs prepared by seeding cells on synthetic polymers (10, 11) and entrapping cells in collagen (7, 9). A recent review of related research is available (12).

In heart valve tissue engineering, cyclic distension/stretching of constructs has been accomplished by pulsatile flow of medium through the valve (13, 14) or pulsatile

back-pressure on the valve (15). The cell types primarily investigated in these studies have been dermal and adventitial fibroblasts and valve interstitial cells (VIC), which are predominantly a myofibroblast phenotype (16). As with vessel constructs, mechanical properties of valve constructs have been shown to improve with cyclic stretching and correlate with ECM deposition and cell proliferation (15, 17).

We use fibrin gel as the scaffold for fabrication of bioartificial arteries and heart valves because it is conducive to collagen deposition under static culture conditions (18). However, we have not yet assessed the outcome of using fibrin in a bioreactor designed to impart mechanical stretching. In this study we assessed the outcome of CD during culture of tubular fibrin constructs with entrapped tissue cells, which has relevance to the design and operation of bioreactors to cyclically stretch fibrin-based valve constructs (19), as well as fibrin-based artery constructs (20). We have previously shown that fibroblasts and VICs remodel fibrin disk-shaped constructs adherent to tissue culture plastic (21). Although a static tension develops in these constructs, which is likely an important stimulatory signal (22), it is not a cyclic tension as occurs during cyclic stretching.

The vast majority of studies that have examined the effects of CD on tubular constructs have restricted their conditions to CD with constant parameters, specifically strain amplitude, stretch time, and relaxation time (the last two being equivalent to frequency and duty cycle). However, it is well known that cells adapt their behavior to constant environmental stimuli; that is, cells initially respond but return to a baseline level following sustained stimulation (23-25). A well known and relevant example of adaptation exhibited by mammalian cells is the response of osteoblasts to mechanical

loading (25-27). Schriefer *et al.* studied this in rat ulnar bone (26) and found significantly higher bone mineral content with an applied cyclic loading, but with the mineralization diminishing over time. Kim *et al.* observed significant trabecular bone formation occurring in response to loading within the first week, with significantly less during weeks 2-4 of loading (27).

To understand how bone tissue responds to changing environment, Tang *et al.* examined the effects of step-wise increasing strain amplitude on cyclic stretch of osteoblasts cultured on a distensible substratum (28). In that study, the higher strain amplitude steps were correlated with diminishing collagen production by the cells; hence, no overall significant benefit of using step-wise incremental strain amplitude during cyclic stretching was found. (The incubation times used in that study were at most 24 hr compared to the weeks needed to achieve significant tissue growth *in vitro*. Also, the applied strain levels used were physiologically relevant for osteoblasts but an order of magnitude below those typically used in cardiovascular tissue engineering, and the cells were not entrapped in a 3D polymeric scaffold.)

Thus, in this study, we also examined the effect of periodically step-wise incrementing the CD strain amplitude in addition to using constant strain amplitude, the latter being the conventional approach, to assess whether adaptation may play a role in the success of using long-term CD to achieve tissue growth. Samples were characterized in terms of mechanical properties, collagen content, cellularity, and histology in order to elucidate the basis for any improvement in mechanical properties due to CD. Selected samples were also assayed for activation of the extracellular signal-regulated kinase (ERK) signaling pathway, which has been correlated to collagen

expression during mechanical stretching of fibroblasts on a distensible membrane (29), in order to establish a mechanistic basis for any adaptation.

2.3: Results

Tubular constructs were cultured for 3 weeks on a distensible latex mandrel in the CD bioreactor, during which time no downward movement was observed. Upon harvest, all constructs slid off the mandrel, indicating there was insignificant adhesion to the latex mandrel and that construct elasticity maintained it in contact with the latex mandrel during CD. Unless indicated, all results were derived from constructs prepared with porcine VIC (PVIC). For brevity, constant strain amplitude CD and step-wise incremental strain amplitude CD experiments are referred to as simply "CD" and "ICD", respectively, and paired statically-incubated controls are referred to as "controls".

2.3.1: CD and ICD results in different construct dimensions but not different volumes

As seen in Supporting Information, the final length and thickness inversely varied with some conditions; however, all constructs were less than 1% of their initial volume, with no difference between the final volumes of the CD and ICD constructs and their controls.

2.3.2: CD improves construct mechanical properties

Fig. 1 shows there was no improvement in mechanical properties for 2.5% and 5% CD, but improvement in ultimate tensile strength (UTS) and tensile modulus (E) were observed for 10% and 15% CD. At 10%, the UTS increased 29% compared to controls and E increased 59% compared to controls. At 15% CD, UTS increased 47% compared to controls, and E increased 45% compared to controls. Absolute values of UTS and E are presented in Table 1. Further studies were conducted at 20% CD; however, the majority of the constructs either tore during the first week of CD or permanently deformed (slid down the mandrel) indicating a strain amplitude between 15% and 20% causes damage to the growing tissue in this system.

Fig. 2a shows there was no increase in collagen concentration at 2.5%, 5%, or 10% CD. At 15%, the collagen concentration increased 29% compared to controls. There was no difference in the cell concentration at 2.5%, 5%, or 10% (Fig 2b); however, at 15% it increased by 47% compared to controls. For the collagen concentration normalized by the cell concentration, a measure of the collagen deposited in the ECM per cell, there was no difference between CD constructs and controls (Fig 2c). Absolute values of cell and collagen concentrations and their ratios are presented in Table 2.

2.3.3: Incremental CD further improves construct mechanical properties and correlates with increased net collagen deposition per cell

Constructs were subjected to ICD from 5% to 15% in 2 (ICD-2) and 4 (ICD-4) equal time steps over 3 weeks (Fig. 1). For ICD-2, UTS increased by 84% and E

increased by 85% compared to controls. ICD-4 further improved the mechanical properties, with UTS increased by 191% and E increased by 158% compared to controls. Comparing to the highest UTS and E achieved with CD, the UTS was 98% higher with ICD-4 in comparison to 15% CD, and E was 61% higher with ICD-4 in comparison to 10% CD.

Collagen concentration increased 55% for ICD-2 and 73% for ICD-4 compared to controls as shown in Fig 2a. The collagen concentration was 34% higher with ICD-4 in comparison to 15% CD, which had the highest value among all CD groups. There was no difference in cell concentration for ICD-2 or ICD-4 compared to controls. However, the collagen concentration normalized by the cell concentration was greater than controls for both ICD-2 by 37% and ICD-4 by 70%.

2.3.4: Incremental CD yields similar results for HDF-populated constructs

Similar to PVIC constructs, constructs prepared from neonatal human dermal fibroblasts (HDF) showed improved mechanical properties and collagen concentration with both CD and ICD compared to controls. With 10% CD, UTS increased 85% compared to controls (903±126 kPa *vs.* 489±50 kPa) and E increased 127% compared to controls (3160±416 kPa *vs.*1392±138 kPa). With ICD-4, UTS increased 61% (to 1453±102 kPa) and E increased 36% (to 4306±189 kPa) compared to 10% CD. In comparison to controls, UTS increased 197% and E increased 209%. The collagen concentration increased 84% (to 24±3 mg/cm^3) with 10% CD and 178% (to 36±1 mg/cm^3) with ICD-4 compared to controls.

2.3.5: CD-mediated improvement in tissue growth requires 2-3 weeks of CD

In order to elucidate whether a critical period for tissue development existed, HDF constructs were characterized just prior to CD at week 2 and then weekly for the 3 week CD period. The time course data for HDF constructs shown in Fig. 3 reveals the increases in UTS (Fig. 3a) and collagen content (Fig. 3b) due to 10% CD and ICD-4 occurred largely during the third week of CD. For the ICD-4 case, the UTS increased 52% during week 2 and 197% during week 3.

2.3.6: CD results in collagen maturation in constructs

Using Picrosirius red staining, we examined collagen maturation in histological cross-sections of constructs. As shown in Fig. 4, there was stronger staining in CD and ICD constructs (k,l,s-u) compared to controls (j,r), suggesting that CD and ICD induces collagen maturation, which contributed to the improved mechanical properties. It can be further observed that staining was brighter in ICD constructs (l,t,u) compared to CD constructs (k,s). Based on the Trichrome-stained sections, the cells appear more strongly aligned in the circumferential direction in CD and ICD constructs (e,f,n-p) compared to controls (d,m), indicating that CD and ICD induced stronger cell alignment as well as stronger collagen alignment.

2.3.7: Incremental CD results in elevated ERK 1/2 signaling

To investigate the mechanism for improved tissue growth with ICD and develop evidence to test the adaptation hypothesis, we measured the activation of ERK (Fig. 5). In the case of ICD-4, this measurement corresponded to 4 days following the final increment in strain amplitude. While total ERK was similar for 10% CD, ICD-4, and

controls, the fraction of ERK that was phosphorylated ERK (pERK) following 3 weeks of CD was 255% greater for ICD *vs.* CD.

2.4: Discussion

This study showed that CD can be used to improve the mechanical properties of cell-seeded fibrin-based tubular constructs. The study also revealed an apparent adaptation of the cells to long-term CD. With incremental CD, the UTS increased almost 300% compared to static culture, as compared to a modest 50% increase for constant CD. pERK also was elevated for ICD relative to CD, consistent with ICD overcoming a tendency of cells to adapt to CD. Histological analysis showed maximal alignment and maturation of collagen in the case of ICD.

Several studies have investigated the effect of CD on tissue-engineered tubular constructs (5, 9, 11). However, most studies have been limited to a single distension condition or short durations. In short durations, cell induced gel compaction alone, causing a structural remodeling of the gel, can have a significant influence on the mechanical properties of collagen and fibrin gels before any significant compositional remodeling occurs. Furthermore, in the case of fibrin, rapid fibrinolysis can occur over short durations, if not controlled as done in this study using the inhibitor aminocaproic acid with PVIC constructs; the "compaction" may thus reflect fibril degradation as well as consolidation. To isolate the effects of CD on construct properties without the influence of extensive fibrin compaction, we incubated fibrin-based tubular constructs for 2 weeks on their mandrels in static culture before mounting them in the CD bioreactor. This allowed almost all of the volume reduction (exceeding 95%) to occur

prior to the CD initiated at week 2, in comparison to that occurring over the 3-week CD period (an additional 4%, to 99% total). In the 5% CD constructs, more axial shortening occurred than in controls, but there was no improvement in mechanical properties, indicating that any effect of CD on length or thickness occurring in these experiments had no correlation with construct mechanical properties; moreover, these variations in length and thickness were offsetting in that there were no differences in volume reduction between CD constructs and controls.

Several studies using both cells on membranes and cells in 3-D scaffolds have shown increased cell-produced ECM when cells are subjected to cyclic stretching. *In vivo,* VIC are subject to large strain values during each cardiac valve cycle; Lo *et al.* reported a maximum stretch of 24% in the radial direction and 11% in the circumferential direction (30). *In vitro*, using PVIC cultured on a flexible membrane, Ku *et al.* have shown improved incorporation of [^{3}H]-proline (indicative of higher collagen production) when subjected to 10%, 14% and 20% CD (31). In the current study, using PVIC in fibrin-based tubular constructs subjected to CD, we found no improvement in either mechanical properties or collagen concentration at low strain amplitudes (2.5% and 5%). This suggests that there is a strain threshold below which cells have no apparent response to CD. Similar effects were observed by Ku *et al.* (31) with an apparent strain threshold of 7%. We observed increases in UTS and E of constructs at 10% and 15% CD, with no differences between values at 10% and 15% CD.

In contrast, the collagen concentration was found to be greater than controls only at 15% CD, indicating that there is some difference in the cell response to 10% *vs.*

15% CD. This suggested that CD might also improve tensile mechanical properties by improving the functional quality of ECM. Picrosirius red stains for mature collagen fibers, which have been defined as thicker (32), more aligned (33) and more cross-linked (34). We found that CD and ICD constructs stained brighter, indicating more collagen maturation, compared to controls (Fig. 4), which likely contributed to their improved mechanical properties. Balguid *et al.* correlated the modulus of tissue-engineered valve leaflets and native pig valve leaflets with collagen cross-linking (34), showing via Picrosirius red staining that constructs with higher modulus had stronger staining. Similarly in our case, the maturation observed in CD and ICD constructs by Picrosirius red staining also correlates with higher UTS and E than controls (Fig. 1). The Trichrome-stained sections also revealed that CD and ICD constructs exhibited stronger cell alignment in the circumferential direction compared to static controls. Qualitatively, the cell alignment correlates with maturation of the cell-produced collagen, also exhibiting strong circumferential alignment, as implied by the Picrosirius red stain. This is consistent with the cells exhibiting a contact guidance response to the aligned cell-produced collagen fibers, a phenomenon characterized in statically incubated constructs (35), but not in CD constructs.

We hypothesized that long-term CD may induce an adaptation response of the cells. Such an adaptive response to CD has been reported with osteoblasts (25, 26). However, analogous studies have not been reported in cardiovascular tissue engineering. To test this hypothesis, we conducted experiments with a time-averaged CD strain amplitude of 10% by incrementing it from 5% to 15% in 2 or 4 equal time steps during 3 weeks of CD (Fig. 1 inset). UTS and E improved greatly with ICD-4

beyond what was achieved with CD (98% and 61% higher), attaining the values of 2.30 MPa and 11.4 MPa, respectively. These values compare favorably to those of native cardiovascular tissues (30). UTS and E also differed among the 15% CD, ICD-2 and ICD-4 groups. These results are consistent with an adaptive behavior at CD that was partially overcome with ICD-2 and further overcome with the more frequent stimulus perturbation of ICD-4. It can be concluded that the adaptation time for the cell response leading to improvement in mechanical properties is smaller than 3-4 days, which was the duration of each strain amplitude in ICD-4.

A trend similar to the effect of CD on mechanical properties was found for collagen concentration. Moreover, the collagen concentration normalized by the cell concentration increased only in the case of ICD, consistent with ICD acting to mitigate a reduction in the rate of collagen deposited per cell due resulting from adaptation to constant CD.

Experiments with HDF constructs showed results similar to PVIC constructs: ICD-4 again showed improvement in mechanical properties and collagen concentration beyond what was achieved with CD. These results demonstrate that the apparent adaptation response to CD is not restricted to a particular tissue cell type. A time course study with HDF constructs also revealed that while the UTS and collagen content of controls progressively increased over 3 weeks, they dramatically increased during week 3 for the ICD constructs.

Consistent with the hypothesis that ICD mitigates adaptation to the stimulus presented by CD, a 255% increase in pERK was observed in ICD-4 *vs.* 10% CD constructs after 3 weeks of CD. Papakrivopoulou *et al.* have shown that pERK

elevation correlated with collagen expression in cardiac fibroblasts adhered to distensible membranes when subjected to CD (29); this is consistent with our results showing elevated pERK and increased collagen deposition per cell for HDF constructs subjected to ICD-4. While our results are consistent with adaptation to CD, which is mitigated with ICD, it is recognized that there are other possible explanations for these results besides invoking adaptation. For example, if the collagen produced by the cells becomes increasingly less susceptible to degradation when stretched (36), the collagen concentration in the ICD constructs should be greater than the 10% CD constructs, as is the case. Even if the beneficial effect of constant CD and incremental CD is directly connected to cell metabolism via ERK signaling, it is still unknown whether the mechanism is due to cyclic mechanical strain of the cells or altered transport of biomolecules through the tissue during its transient compression (37). Regardless of the mechanism, the application of CD generally and incremental CD specifically can be used to improve mechanical and biochemical properties and structural organization of tissue-engineered tubular constructs, which has direct relevance to the fabrication of vascular and heart valve constructs using bioreactors that apply controlled stretching.

2.5: Materials and Methods

2.5.1: Cell culture

Porcine valve interstitial cells (PVIC) were isolated from porcine aortic valve leaflets (generously donated by experimental surgical services (ESS) at the University of Minnesota) by a 30 min enzymatic digestion with 1 mg/mL collagenase and 0.5 mg/mL elastase. PVIC were cultured in DMEM/F12 culture medium (Gibco)

supplemented with 10% fetal bovine serum (FBS, Hyclone), 100 U/ml penicillin, and 100 μg/ml streptomycin. Cells were incubated at 37ºC in 100% humidity and 5% CO_2. Cells were passaged at 80-90% confluency and harvested for use from passage 5-8.

Neonatal human dermal fibroblasts (HDFs, Clonetics) were maintained in DMEM/F12 supplemented with 10% FBS,100 U/ml penicillin, 100 μg/ml streptomycin, and 2.5 μg/ml amphotericin-β. Cells were passaged at 100% confluency and harvested for use from passage 7-9.

2.5.2: Tubular construct preparation and culture

A cell-seeded fibrin gel was molded by mixing cells suspended in DMEM into a solution of bovine fibrinogen (Sigma) in 20mM HEPES-buffered saline. A mixture of bovine thrombin (Sigma) and calcium chloride in DMEM was then added to the suspension. All components were at room temperature. For PVIC constructs, final concentrations were 3.3 mg/ml fibrinogen, 0.2 U/ml thrombin, 1.8 mM Ca^{++}, and 500,000 cells/ml. For HDF constructs, final concentrations were 6.6 mg/ml fibrinogen, 0.4 U/ml thrombin, 3.6mM Ca^{++}, and 500,000 cells/ml. Suspensions were mixed well by trituration and injected into tubular molds comprised of a Teflon mandrel centered in a polypropylene casing.

The molds were then placed vertically in an incubator for 30 min. After gelation, the casing was removed and the constructs were placed horizontally in culture medium. PVIC constructs were cultured in 50:50 DMEM/F12 supplemented with 10% FBS, 100 U/ml penicillin, 100 μg/ml streptomycin, 1 ng/ml TGF-β, 2 μg/ml insulin, 50 μg/ml ascorbic acid and 2 mg/ml ε-aminocaproic acid. HDF constructs were cultured in DMEM supplemented with 10% FBS, 100 U/ml penicillin, 100 μg/ml streptomycin, 2

μg/ml insulin, 50 μg/ml ascorbic acid and 2.5 μg/ml amphotericin-β. Initially, the constructs had an internal diameter of 8 mm, a thickness of 3.8 mm, and a length of 12.5 mm. Constructs were cultured for 2 weeks after which they were transferred to the CD bioreactor. This allowed for cell-mediated fibrin compaction and initial ECM deposition so that the constructs could withstand transfer to the bioreactor.

2.5.3: CD Bioreactor

Constructs were transferred onto a distensible mandrel in a custom built bioreactor described previously (7). In brief, the distensible mandrel was a thin latex tube (Kent Elastomer). One end of the tube was closed with a polycarbonate stopper using epoxy sealant, while the other end was connected to an in-house air line regulated by a pressure regulator. The frequency and duty of the air cycle were controlled by a solenoid valve connected downstream of the pressure regulator. Digital images were taken of the latex tube at different inlet air pressures and a pressure-diameter correlation was recorded, which was used to set the maximum strain for each experiment. For all studies, a frequency of 0.5 Hz with 12.5% duty cycle was used, corresponding to a 0.25 sec stretch time in a 2 sec cycle period. For CD experiments, a strain amplitude of 2.5%, 5%, 10%, 15% or 20% was applied to constructs for 3 weeks. For ICD experiments, the strain amplitude was incremented from 5% to 15% in 2 and 4 equal time steps over the 3 week (Fig. 1). 70% of the medium in the CD bioreactor was changed 3 times per week.

After harvest, each construct was divided into 3 equal length sections for tensile testing followed by biochemical analysis, DNA quantification, and histology or protein extraction.

2.5.4: Uniaxial Tensile Testing

One-third strip of a construct was tested for uniaxial properties in the circumferential direction. The thickness was measured using a 50 g-force probe attached to a displacement transducer. Tissue strips were then placed in compressive grips, attached to the actuator arm and load cell of a Microbionix (MTS Systems) and straightened with a load of 0.005 N. This position was used as the reference length of the strip. Following 6 cycles of 0-10% strain at 2 mm/min, constructs were stretched to failure. True strain was calculated based on the change in length of the tissue over time. The stress was calculated as force divided by the initial cross sectional area. Young's modulus (E) was determined by linear regression of the stress-strain curve.

2.5.5: Histology

Constructs for histology were fixed in 4% paraformaldehyde, infiltrated with a solution of 30% sucrose and 5% DMSO, frozen in OCT (Tissue-Tek), and sectioned into 9 μm cross-sections. Sections were stained with Lillie's Trichrome and Picrosirius red. Images were taken at 10x using a color CD camera. For Picrosirius red, images were taken with the samples placed between crossed plane polarizers.

2.5.6: Collagen and Cell quantification

Collagen content was quantified by the hydroxyproline assay (19). Sample volume was calculated using the measured length, width, and thickness of the strips. Collagen concentrations were calculated as the amount per unit volume in each sample assuming 7.7 mg collagen per mg hydroxyproline.

DNA content was quantified with a modified Hoechst assay (19). Cell numbers were obtained from DNA contents assuming 7.6 pg of DNA per cell . Cell concentrations were calculated as the number of cells per unit volume using the dimensions of the strip.

2.5.7: Protein Extraction

For each condition, tissue was pooled from two constructs and rinsed with phosphate buffered saline (PBS). The tissue was then disrupted by sonication in ice-cold lysis buffer (25 mM Tris pH 7.4, 225 mM NaCl, 25 mM NaF, 5% glycerol, 0.5% NP-40, 0.025% sodium deoxycholate, 1 mM EDTA, 2 mM $NaVO_4$, 1 μg/ml aprotinin, pepstatin, and leupeptin). The soluble lysate was isolated by centrifugation and the protein concentration was determined by BCA assay (Pierce).

2.5.8: Western Blot

For each sample, 20 μg of total protein was boiled in reducing sample buffer and separated by SDS-PAGE. Protein was transferred to nitrocellulose (Whatman) using wet transfer buffer (10% methanol, 2.2 g/L CAPS, pH 11). The blot was incubated in blocking solution (5% dry milk, 0.1% Tween-20 in PBS) for one hour and then incubated with primary rabbit polyclonal phospho-ERK antibody (p-Thr202/p-Tyr204,

Calbiochem, 1:2500) overnight at 4°C. The blot was then probed with HRP-conjugated secondary anti-rabbit IgG (Amersham) at a dilution of 1:10000 and developed using enhanced chemiluminescence. The blot was then stripped of antibodies using Restore Plus (Pierce) and re-probed using rabbit polyclonal ERK1/2 antibody (Calbiochem, 1:2500). The pERK to total ERK ratio was determined by densitometry of scanned autoradiograms.

2.5.9: Statistics

For each group of constructs, a subset was randomly chosen as the paired static controls, which were mounted in the bioreactor but not subjected to CD (n = 5-8). The remaining constructs were subjected to CD as described (n = 5-8). The mean of the measurements obtained from the static controls were used to normalize the paired CD constructs so that results could be compared from different experiments, where variability in the control values occurred. The controls value of 1 ± stdev in Figs. 1 and 2 represents the mean of all normalized control values from all experiments. Statistical difference between groups was determined using one-way ANOVA using SPSS software for Windows. Levene's test was used for homogeneity of population variances amongst groups. If the test was significant (p <0.05), post hoc analysis was done using Games-Howell procedure, which does not assume equal variance between groups. Otherwise the Schieffe method was used. In all cases where the error bars (plus or minus standard deviation) are non-overlapping, the differences are significant; hence, for clarity, no symbols are used. In cases where error bars are overlapping and the difference is statistically significant, paired symbols are used to indicate the difference.

Any reference to a difference in the Results and Discussion implies statistical significance at the level $p < 0.05$.

2.6: References

1. Butler, D. L., Goldstein, S. A., Guilak, F. (2000) Functional tissue engineering: the role of biomechanics. *J Biomech Eng* **122,** 570-575.
2. Freed, L. E.*, et al.* (2006) Advanced tools for tissue engineering: scaffolds, bioreactors, and signaling. *Tissue Eng* **12,** 3285-3305.
3. Jeong, S. I.*, et al.* (2005) Mechano-active tissue engineering of vascular smooth muscle using pulsatile perfusion bioreactors and elastic PLCL scaffolds. *Biomaterials* **26,** 1405-1411.
4. Solan, A., Mitchell, S., Moses, M., Niklason, L. (2003) Effect of pulse rate on collagen deposition in the tissue-engineered blood vessel. *Tissue Eng* **9,** 579-586.
5. Hahn, M. S.*, et al.* (2007) Physiologic pulsatile flow bioreactor conditioning of poly(ethylene glycol)-based tissue engineered vascular grafts. *Ann Biomed Eng* **35,** 190-200.
6. Seliktar, D., Nerem, R. M., Galis, Z. S. (2003) Mechanical strain-stimulated remodeling of tissue-engineered blood vessel constructs. *Tissue Eng* **9,** 657-666.
7. Isenberg, B. C., Tranquillo, R. T. (2003) Long-term cyclic distention enhances the mechanical properties of collagen-based media-equivalents. *Ann Biomed Eng* **31,** 937-949.
8. Cummings, C. L., Gawlitta, D., Nerem, R. M., Stegemann, J. P. (2004) Properties of engineered vascular constructs made from collagen, fibrin, and collagen-fibrin mixtures. *Biomaterials* **25,** 3699-3706.
9. Seliktar, D., Black, R. A., Vito, R. P., Nerem, R. M. (2000) Dynamic mechanical conditioning of collagen-gel blood vessel constructs induces remodeling in vitro. *Ann Biomed Eng* **28,** 351-362.
10. Niklason, L. E.*, et al.* (1999) Functional arteries grown in vitro. *Science* **284,** 489-493.
11. Kim, B. S., Nikolovski, J., Bonadio, J., Mooney, D. J. (1999) Cyclic mechanical strain regulates the development of engineered smooth muscle tissue. *Nat Biotechnol* **17,** 979-983.
12. Isenberg, B. C., Williams, C., Tranquillo, R. T. (2006) Small-diameter artificial arteries engineered in vitro. *Circ Res* **98,** 25-35.
13. Hoerstrup, S. P.*, et al.* (2000) New pulsatile bioreactor for in vitro formation of tissue engineered heart valves. *Tissue Eng* **6,** 75-79.
14. Hildebrand, D. K., Wu, Z. J., Mayer, J. E., Jr., Sacks, M. S. (2004) Design and hydrodynamic evaluation of a novel pulsatile bioreactor for biologically active heart valves. *Ann Biomed Eng* **32,** 1039-1049.
15. Mol, A.*, et al.* (2005) Tissue engineering of human heart valve leaflets: a novel bioreactor for a strain-based conditioning approach. *Ann Biomed Eng* **33,** 1778-1788.
16. Chester, A. H., Taylor, P. M. (2007) Molecular and functional characteristics of heart-valve interstitial cells. *Philos Trans R Soc Lond B Biol Sci* **362,** 1437-1443.

17. Hoerstrup, S. P., *et al.* (2000) Functional living trileaflet heart valves grown in vitro. *Circulation* **102,** III44-49.
18. Grassl, E. D., Oegema, T. R., Tranquillo, R. T. (2002) Fibrin as an alternative biopolymer to type-I collagen for the fabrication of a media equivalent. *J Biomed Mater Res* **60,** 607-612.
19. Robinson, P. S., *et al.* (2007) Functional Tissue-Engineered Valves from Cell-Remodeled Fibrin with Commissural Alignment of Cell-Produced Collagen. *Tissue Eng*.
20. Isenberg, B. C., Williams, C., Tranquillo, R. T. (2006) Endothelialization and Flow Conditioning of Fibrin-Based Media-Equivalents. *Ann Biomed Eng*.
21. Williams, C., Johnson, S. L., Robinson, P. S., Tranquillo, R. T. (2006) Cell sourcing and culture conditions for fibrin-based valve constructs. *Tissue Eng* **12,** 1489-1502.
22. Grinnell, F., Ho, C. H. (2002) Transforming growth factor beta stimulates fibroblast-collagen matrix contraction by different mechanisms in mechanically loaded and unloaded matrices. *Exp Cell Res* **273,** 248-255.
23. Turner, C. H., Robling, A. G., Duncan, R. L., Burr, D. B. (2002) Do bone cells behave like a neuronal network? *Calcified tissue international* **70,** 435-442.
24. Li, Y. S., Haga, J. H., Chien, S. (2005) Molecular basis of the effects of shear stress on vascular endothelial cells. *J Biomech* **38,** 1949-1971.
25. Turner, C. H. (1998) Three rules for bone adaptation to mechanical stimuli. *Bone* **23,** 399-407.
26. Schriefer, J. L., *et al.* (2005) Cellular accommodation and the response of bone to mechanical loading. *J Biomech* **38,** 1838-1845.
27. Kim, C. H., *et al.* (2003) Trabecular bone response to mechanical and parathyroid hormone stimulation: the role of mechanical microenvironment. *J Bone Miner Res* **18,** 2116-2125.
28. Tang, L. L., Wang, Y. L., Pan, J., Cai, S. X. (2004) The effect of step-wise increased stretching on rat calvarial osteoblast collagen production. *J Biomech* **37,** 157-161.
29. Papakrivopoulou, J., Lindahl, G. E., Bishop, J. E., Laurent, G. J. (2004) Differential roles of extracellular signal-regulated kinase 1/2 and p38MAPK in mechanical load-induced procollagen alpha1(I) gene expression in cardiac fibroblasts. *Cardiovasc Res* **61,** 736-744.
30. Lo, D., Vesely, I. (1995) Biaxial strain analysis of the porcine aortic valve. *Ann Thorac Surg* **60,** S374-378.
31. Ku, C. H., *et al.* (2006) Collagen synthesis by mesenchymal stem cells and aortic valve interstitial cells in response to mechanical stretch. *Cardiovasc Res* **71,** 548-556.
32. Dayan, D., *et al.* (1989) Are the polarization colors of picrosirius red-stained collagen determined only by the diameter of the fibers? *Histochemistry* **93,** 27-29.
33. Junqueira, L. C., Montes, G. S., Sanchez, E. M. (1982) The influence of tissue section thickness on the study of collagen by the Picrosirius-polarization method. *Histochemistry* **74,** 153-156.

34. Balguid, A., *et al.* (2007) The role of collagen cross-links in biomechanical behavior of human aortic heart valve leaflets--relevance for tissue engineering. *Tissue Eng* **13,** 1501-1511.
35. Grassl, E. D., Oegema, T. R., Tranquillo, R. T. (2003) A fibrin-based arterial media equivalent. *J Biomed Mater Res A* **66,** 550-561.
36. Ruberti, J. W., Hallab, N. J. (2005) Strain-controlled enzymatic cleavage of collagen in loaded matrix. *Biochem Biophys Res Commun* **336,** 483-489.
37. Chahine, N. O., *et al.* (2007) Effect of Dynamic Loading on the Transport of Solutes into Agarose Hydrogels. *Biophysical Journal* **inpress**.

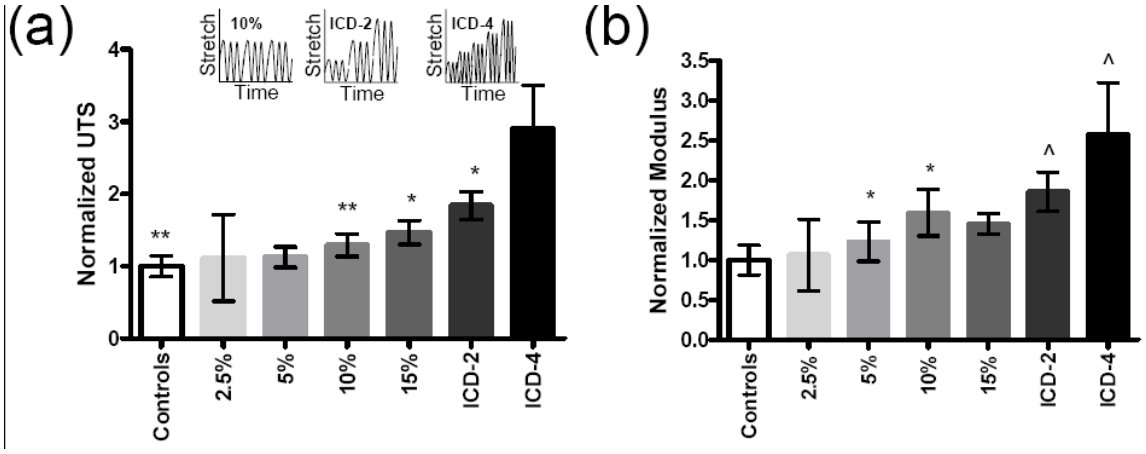

Figure 2-1: Tensile Mechanical Properties of Constructs Following CD. (a) Normalized UTS and (b) Normalized modulus (E). Values are normalized to paired static controls. In all cases where error bars are not overlapping, the means are significantly different ($p<0.05$); for groups with overlapping error bars, a significant difference ($p<0.05$) between means is shown with paired symbols. Inset shows schematic of CD and ICD regimens: CD, shown for 10% strain amplitude, ICD with 2 steps (ICD-2), the amplitude changed from 5% → 10% → 15%, and ICD with 4 steps (ICD-4), the amplitude changed from 5% → 7.5% → 10% → 12.5% → 15%.

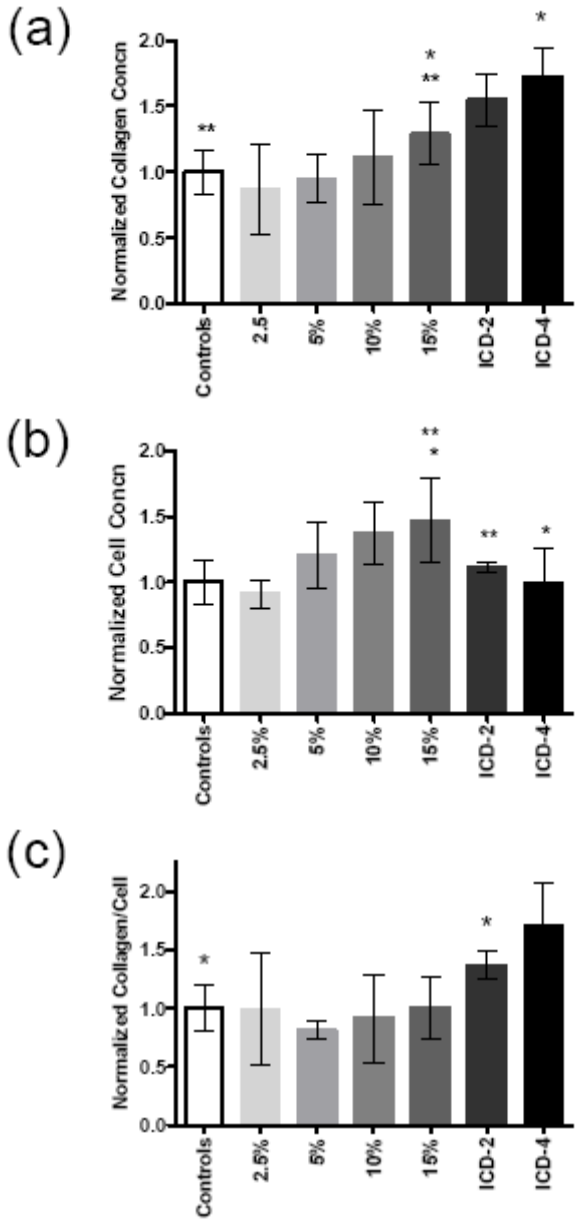

Figure 2-2: Composition of PVIC Constructs Following CD. (a) Normalized collagen concentration, (b) Normalized cell concentration, and (c) Normalized collagen concentration/cell concentration. See Fig. 1 regarding statistical significance.

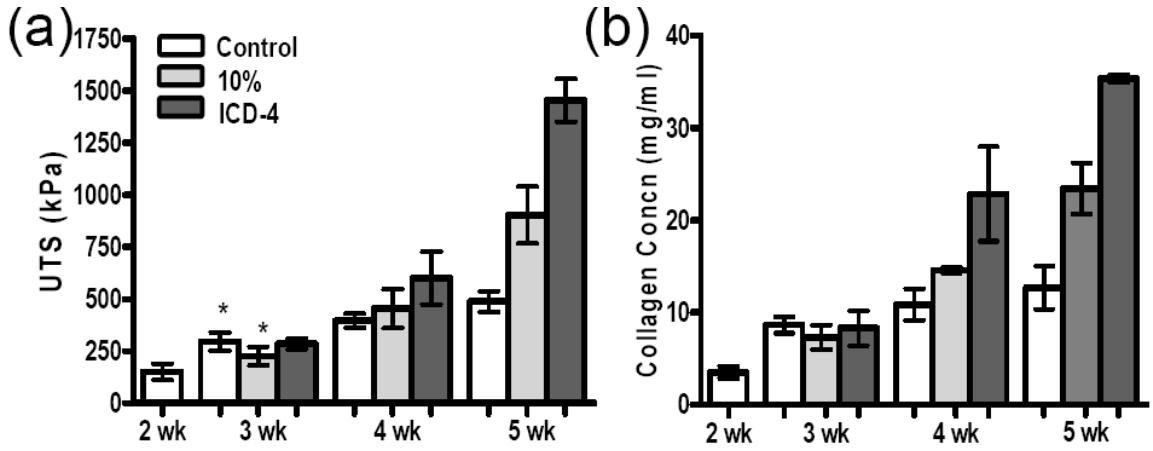

Figure 2-3: Time course of HDF Constructs During CD. (a) UTS and, (b) Collagen concentration. See Fig. 1 regarding statistical significance.

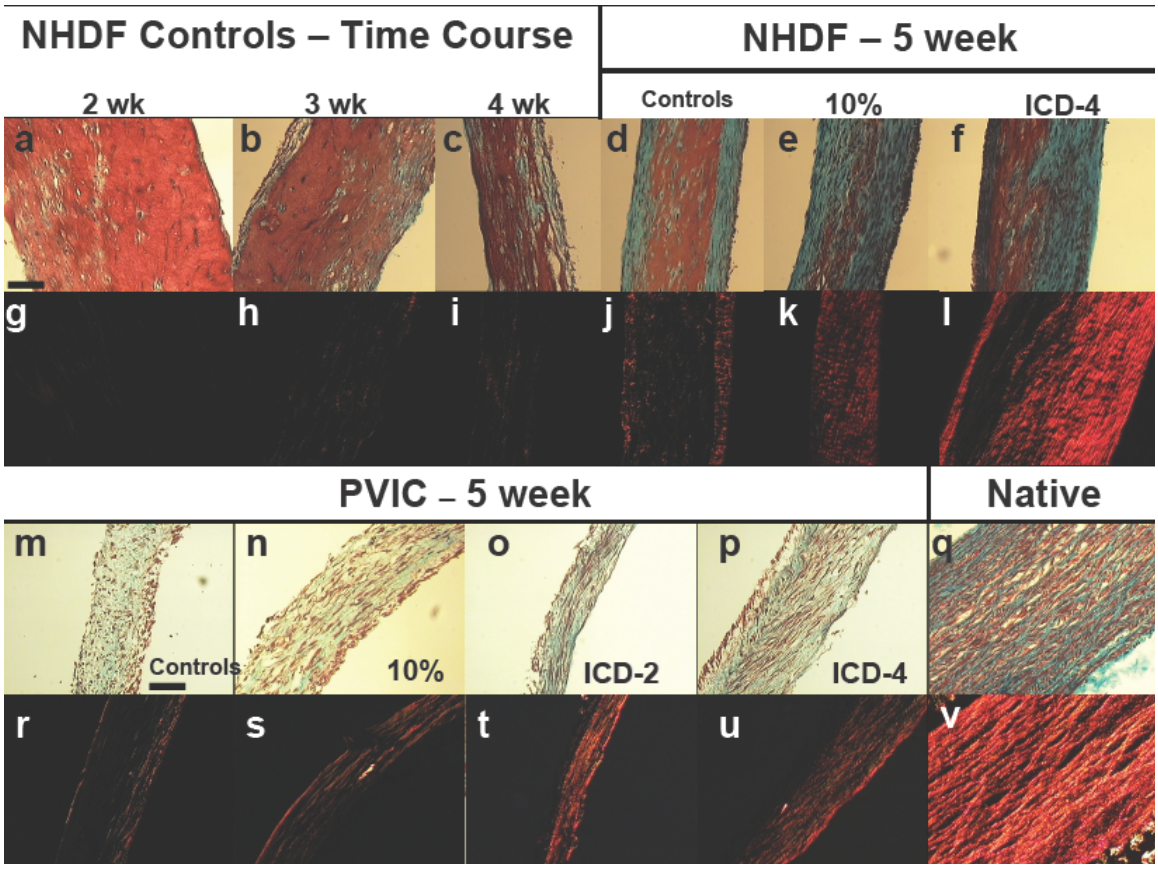

Figure 2-4: Histology of Constructs Following CD. Lillie's Trichrome-stained sections of static control samples (a-d,m) for corresponding CD samples (e,f,n-p). Picrosirius red-stained sections for static control samples (g-j,r) for corresponding CD samples (k,l,s-u). For comparison, stained sections of porcine carotid artery, Trichrome (q) and Picrosirius red (v) are also shown. All images were acquired at the same magnification with 100 μm scale bar shown in (a) and (m).

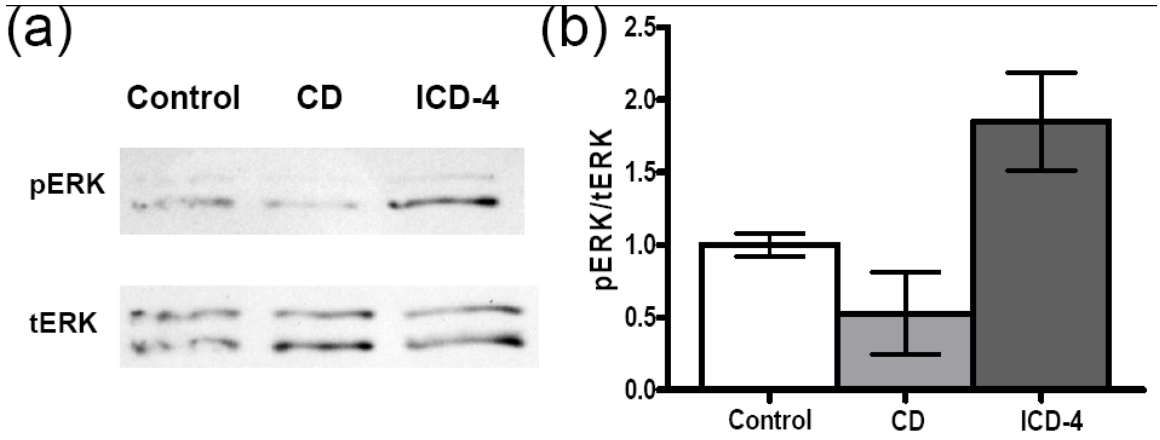

Figure 2-5: Western Blot for ERK 1/2 Activation Following CD.
(a) 20 µg protein was analyzed by Western Blot for levels of total (tERK) and threonine 202/tyrosine204 phosphorylated (pERK) ERK 1/2. Protein was isolated from control, 10% CD, and ICD-4 constructs following 3 weeks CD. Bands appear at 42/44 kD. (b) Band intensity was determined by densitometry and expressed as the ratio of pERK and tERK, normalized to the control value. Ranges for two blots are shown.

	UTS ± stdev (kPa)	Modulus ± stdev (kPa)
2.5% CD	1188 ± 637	5610 ± 2364
2.5% Controls	1064 ± 272	5280 ± 884
5% CD	758 ± 68	4478 ± 896
5% Controls	673 ± 103	3638 ± 541
10% CD	923 ± 113*	5267 ± 972*
10% Controls	714 ± 66	3302 ± 417
15% CD	1112 ± 126*	4706 ± 416*
15% Controls	758 ± 228	3235 ± 894
ICD-2	2500 ± 261*	12733 ± 1698*
ICD-2 Controls	1359 ± 190	6865 ± 906
ICD-4	2295 ± 467*	11407 ± 2867*
ICD-4 Controls	789 ± 408	4428 ± 2339

Table 2.1: UTS and Modulus (E) of fibrin constructs subjected to CD paired static controls. (*) indicate significant difference ($p<0.05$) between CD and paired static controls.

	Collagen ± stdev (mg/ml)	Cell ± stdev (million cells/ml)	Collagen/Cell ± stdev (ng/cell)
2.5% CD	22.2 ± 8.7	220 ± 65	0.11 ± 0.05
2.5% Controls	25.6 ± 1.8	243 ± 30	0.11 ± 0.02
5% CD	15.6 ± 3.0	131 ± 28	0.12 ± 0.01
5% Controls	16.4 ± 4.8	109 ± 21	0.15 ± 0.03
10% CD	18.2 ± 5.9	133 ± 21	0.14 ± 0.06
10% Controls	16.4 ± 4.8	102 ± 21	0.15 ± 0.03
15% CD	27.4 ± 5.0*	308 ± 66*	0.09 ± 0.02
15% Controls	21.3 ± 2.6	210 ± 77	0.11 ± 0.02
ICD-2	46.6 ± 5.9*	290 ± 21	0.16 ± 0.01*
ICD-2 Controls	30.1 ± 2.3	260 ± 47	0.12 ± 0.02
ICD-4	41.3 ± 5.3*	204 ± 70	0.21 ± 0.05*
ICD-4 Controls	23.9 ± 5.3	211 ± 39	0.12 ± 0.02

Table 2.2: Collagen concentration, cell concentration and collagen per cell in fibrin constructs subjected to CD with paired static controls. (*) indicate significant difference ($p<0.05$) between CD and paired static controls.

Chapter 3: TGF-β leads to diminished collagen production via decreased pERK during long-term cyclic stretching of engineered connective tissue

3.1: Summary

Completely biological tissue-engineered vascular and valve grafts would be ideal tissue replacements. Prior to implant, these grafts must have compliance comparable to native tissue for appropriate function as well as sufficient strength to withstand physiological forces. Growth factors like TGF-β and cyclic stretching have been used to enhance extracellular matrix (ECM) production by cells in engineered tissue. In this study, the effects of TGF-β were evaluated during long-term culture of fibrin-based tubular constructs (TC) seeded with neo-human dermal fibroblast (nHDF) under cyclic stretching. TC were evaluated at 2, 5 and 7 weeks for tensile mechanical properties and ECM deposition. At 2 weeks, +TGF-β samples had 101% higher collagen concentration but no difference in UTS/modulus compared to –TGF-β samples. At weeks 5 and 7, –TGF-β samples had higher UTS/modulus and collagen concentration, but lower elastin concentration compared to +TGF-β samples. The collagen was better organized in –TGF-β samples as seen with picrosirius red stain. Western blot analysis at week 5 showed increased phosphorylation of ERK in –TGF-β samples, which correlated with higher collagen deposition. We further hypothesized a role for down stream protein signals of TGF-β activation. The TGF-β effects were evaluated by western blot for αSMA and SMAD2/3 expression, which were 16-fold and 10-fold higher in +TGF-β samples. One advantage of TGF-β treatment was a 4-fold higher elastin deposition in TC at 7 weeks. Further cyclic stretching experiments were conducted with constructs cultured for 5 weeks without TGF-β to obtain improved tensile properties followed by TGF-β supplementation for two weeks to enhance elastin content. This study shows that

the short-term benefits of TGF-β in nHDF-seeded engineered tissue do not translate with long-term cyclic stretching. However, an optimized approach can be used to engineer tissue with desirable tensile and elastic properties.

3.2: Introduction

Cardiovascular disease is the leading cause of death in Western countries with over 450,000 coronary bypass and 95,000 valvular replacement surgeries performed annually in the United States alone (1). Tissue-engineered vascular and valvular grafts have been proposed as a promising solution for replacement surgery (2, 3). Under physiological cyclic loading, both tensile and elastic properties are important for *in vivo* success of engineered tissue constructs. Mechanical conditioning (primarily stretching) has been studied both for vascular and valvular graft as a mean to improve tensile properties of engineered tissue prior to implantation (4). Growth factors like TGF-β have also been shown to improve collagen (5-7) and elastin (8-10) deposition, which are major components that provide tensile and elastic properties, respectively.

To date, most studies on the effects of TGF-β, whether with native or engineered tissue or a 2D culture of cells, have been limited to short duration (several days up to 3 weeks). These studies are meaningful to understand the short-term response of cells to growth factors. However, tissue engineering requires long-term culture (often greater than 5 weeks) with additional mechanical stimulus like cyclic stretching to develop the desired tissue mechanical and organizational properties. To date, no studies have investigated the translation of the short-term effects of TGF-β into long-term tissue development.

TGF-β treatment of fibroblasts generally leads to transformation of the cells into alpha-smooth muscle actin (αSMA)-expressing myofibroblasts, with enhanced collagen production. In both native and engineered tissue, higher αSMA expression and collagen synthesis have been reported after 2-3 weeks (5, 11). For a tissue-engineered construct,

the organization of the deposited collagen is equally important in order to attain the desired tensile properties. Several studies have looked at the effects of transformation of fibroblasts to myofibroblasts on collagen cross-linking and organization (12, 13)

In our previous study, we showed that incremental strain amplitude cyclic stretching (ICS) of fibrin-based engineered tissue with neonatal human dermal fibroblast (nHDF) led to significantly higher UTS and modulus compared to traditional constant strain amplitude cyclic stretching (14). We also demonstrated that higher collagen deposition in the ICS samples correlated with enhanced phosphorylation of ERK1/2. Regulation of other signaling proteins like SMAD-2 (15, 16), Akt (17, 18) and p38 (18, 19) have also been shown to be important for collagen and elastin expression by fibroblasts. Hence, in this study we also investigated the activation of ERK1/2 and SMAD-2 to understand their role in the remodeling of fibroblast-seeded fibrin gel.

Understanding the long-term effects of mechanical or chemical conditioning are important for advancements in tissue engineering. In our previous study, we proposed that cells can adapt to mechanical stimuli when applied over a long culture period. We showed that step-wise increase in the strain magnitude during cyclic stretching over long-term culture apparently overcame adaptation and led to increased tensile properties and collagen deposition (14). A similar concept has been published by Rubbens *et al*, demonstrating that intermittent cyclic stretch led to better engineered tissue than constant cyclic stretch (20).

This study was conducted to understand the long-term effects of TGF-β during cyclic stretching of tubular constructs seeded with nHDF in fibrin gel. We examined the effects of TGF-β on collagen and elastin deposition and cell proliferation after 2 weeks

of static culture. The constructs were then mounted in a cyclic distension bioreactor and conditioned for 3-5 weeks. Studies were conducted both in the presence and absence of TGF-β for the entire duration. In addition, subsequent studies were conducted to optimize the duration of stretching and TGF-β supplementation to fabricate a tissue with elastin as well as physiological UTS and modulus.

3.3: Results

Experiments were conducted with tubular constructs (TC) as described previously (14). After casting, TC were statically incubated for 2 weeks to allow for gel compaction and remodeling that facilitate bioreactor loading. All experiments were conducted under ICS conditioning. Here onwards, TC cultured in medium supplemented with TGF-β are referred to as +TGF-β and TC cultured in the absence of TGF-β are referred to as –TGF-β. All difference mentioned in the results and discussion are based on a significance level of $p<0.05$.

3.3.1: TGF-β supplemented samples possessed inferior mechanical properties

TC were evaluated after 2 weeks of static culture, when they were mounted in the bioreactor, and after 3 and 5 weeks of ICS (corresponding to 5 and 7 week of total culture time). As shown in Fig. 1a&b, at 2 weeks, there was no difference in tensile properties of TC with or without TGF-β, even though +TGF-β samples have 101% higher collagen concentration (Fig. 1c). By week 5, both UTS and modulus were significantly higher for -TGF-β samples and by week 7, the UTS and modulus were

192% and 107% higher for -TGF-β samples. In addition, the UTS (1382±298 kPa) and modulus (2508±595 kPa) were comparable to sheep pulmonary valve leaflet properties, also measured in the circumferential (aligned collagen) direction (UTS = 1472±445 kPa, modulus = 3221±711 kPa).

3.3.2: Improvement in mechanical properties of -TGF-β samples correlated with increased collagen deposition and organization.

Collagen was visualized in TC by trichrome staining and qualitatively assessed for organization using picrosirius red staining. Figure 2 shows trichrome and picrosirius staining under polarized light of samples at 2, 5 and 7 weeks. Both at weeks 5 and 7, the picrosirius red stain is brighter for –TGF-β compared to +TGF-β samples. In trichrome staining, green color indicates collagen which is visible in all TC cross-sections at 5 and 7 weeks.

Collagen was quantified by hydroxyproline assay (Fig. 1c). At 2 weeks, +TGF-β samples had 101% higher collagen concentration (2.85±0.2 mg/ml). However, at 5 and 7 weeks, –TGF-β samples had a 49% and 74% higher collagen concentration, respectively (18.7±2.4 mg/ml and 32.6±6.8 mg/ml). In comparison, the native leaflet tissue had a collagen concentration of 37.8±8.4 mg/ml, which was not different from –TGF-β samples at 7 weeks.

Cellularity of TC was quantified by DNA assay. Figure 1e shows the cell density, which showed no difference between treatment groups at both weeks 5 and 7.

Hence, at 7 weeks, there was a greater collagen deposited per cell (by 66%) in -TGF-β samples compared to +TGF-β samples (Fig. 1f).

3.3.3: TGF-β increased elastin deposition by the nHDF

As shown in fig. 1d, after 5 and 7 weeks, elastin content was 45% (0.07±0.01 mg/ml) and 366% (0.18±0.04 mg/ml) higher in +TGF-β samples respectively, compared to –TGF-β samples.

3.3.4: TGF-β increased αSMA expression and phosphorylation of SMAD-2

Figure 3a shows a western blot for αSMA expression in TC at week 5. All +TGF-β samples showed a 16-fold higher αSMA expression when compared to -TGF-β samples. Upon harvest, +TGF-β samples coiled, a behavior not seen in -TGF-β samples (Fig. 3b).

Western blotting revealed a 10-fold higher expression of pSMAD-2 in +TGF-β samples at week 5 compared to –TGF-β samples (Fig. 4a). The results show that the TGF-β dose administered to the TC had induced both phenotypic (αSMA-expressing cells) and signaling changes (increased pSMAD-2 expression).

3.3.5: TGF-β decreased phosphorylation of ERK1/2

Samples from week 5 were further tested for phosphorylation of ERK1/2. The pERK1/2 signal was 70% higher in the -TGF-β samples compared to +TGF-β samples

(Fig. 4b). These findings are consistent with previously published studies that showed that a higher collagen production by fibroblast correlates with higher pERK1/2 signal in fibroblast (14, 21).

3.3.6: Sequential cyclic stretching and TGF-β supplementation leads to both improved mechanical properties and increased elastin deposition

The aforementioned results demonstrated strong evidence that TGF-β supplementation is detrimental to long-term growth and remodeling of engineered tissue during cyclic stretching, leading to inferior tensile properties. However, experiments also showed that TGF-β is beneficial for elastin deposition, which is an important ECM component of native tissue. Hence, subsequent experiments were conducted to combine superior tensile properties of TC with enhanced elastin deposition by adding TGF-β at a late time-point, specifically at week 5. The subset with this treatment is denoted as the ∗TGF-β group.

Figure 5 shows enhanced elastin deposition in the 7 week samples that were treated with TGF-β only for the last 2 weeks of culture. Compared to -TGF-β samples at 7 weeks, the ∗TGF-β samples had 4-fold higher elastin, which corresponds to an elastin concentration (0.19±0.1 μg/ml) 10% of native tissue (1.8±0.4 μg/ml). Elastic fibers were observed in the ∗TGF-β samples using Verhoeff and elastin immuno-staining (Fig. 6). Tensile testing, biochemical analysis, trichrome and picrosirius red staining showed no decrease in tensile properties and collagen concentration by changing conditions from -TGF-β to +TGF-β for the last 2 weeks of culture.

3.4: Discussion

Functional cardiovascular tissue-engineered constructs require both mechanical strength to withstand physiological forces and elasticity for functional performance. The purpose of this study was to evaluate the effects of TGF-β in long-term culture of fibrin-based tubular constructs seeded with neonatal human dermal fibroblasts, under incremental cyclic stretching (ICS) conditions. The results showed that addition of TGF-β initially promoted collagen deposition, as seen after 2 weeks of static culture. However, for longer culture times, which are required to attain the desired tensile properties of cardiovascular engineered tissue, the omission of TGF-β was more favorable for better tensile properties, collagen deposition and maturation. After 7 weeks of culture with ICS, tensile mechanical properties and collagen content were comparable to that of native pulmonary leaflet tissue (used as native control in this study for relevance to tissue engineered heart valve, (22)). The higher collagen content in –TGF-β samples correlated with a higher expression of pERK1/2. One major benefit of using TGF-β was the enhanced elastin production by cells. Hence, subsequent experiments were conducted where tissue samples were incubated without TGF-β for 5 weeks followed by the addition of TGF-β to induce elastin production for the last 2 weeks of cyclic stretching. The sequential approach produced tissue with substantial elastin (10% of native tissue) as well as comparable tensile mechanical properties.

The most relevant study for comparison was conducted by Grouf *et al*, also seeding nHDF in fibrin gel formed as hemispherical constructs adherent to underlaying

tissue culture plastic (5). They found that after 3 weeks of static culture with TGF-β there was a 33% increase in collagen content compared to –TGF-β treated samples. The results by Grouf *et al* at 3 weeks are similar to our findings (Fig. 1c), as +TGF-β samples had 101% higher collagen after 2 weeks. However, in our experiments using cyclic stretching to promote tissue growth, after 5-7 weeks, the –TGF-β samples developed better mechanical properties (Fig 1a,b), more deposited collagen (Fig. 1c) and more mature collagen (Fig. 2). Our findings are consistent with previously published short-term studies and provide new insight into long-term culture using cyclic stretching. To further explore the long-term culture effects of TGF-β, we examined the phenotypic transformation of fibroblasts to myofibroblasts, which potentially influences cell-matrix interactions and there by effect maturation of deposited collagen; and the activation of the intercellular signaling proteins ERK1/2 and SMAD-2, which regulate important pathways involved in the production and organization of major ECM proteins like collagen and elastin.

An important difference between +TGF-β and –TGF-β samples was the maturation of collagen as indicated by picrosirius red staining. In Fig. 2, picrosirius strain showed brighter staining in –TGF-β samples at both weeks 5 and 7. Others have shown that alginate gel seeded with nHDF and treated with TGF-β had lower crosslinking of collagen compared to –TGF-β samples (13). Though crosslinking was not directly measured in this study, the results of picrosirius red staining indicate similar crosslinking differences. Balguid *et al* have shown a strong correlation between intensity of picrosirius red stain and crosslinking in collagen matrix (23).

TC at week 5, corresponding to 3 weeks of ICS, were analyzed for αSMA, pSMAD-2, and pERK1/2 signal using the western blotting technique. +TGF-β samples had 16-fold higher expression of αSMA. The collagen maturation difference as seen with picrosirius red staining could potentially be related to fibroblasts transformation to myofibroblasts in the presence of TGF-β. Myofibroblasts, which have a stiffer cyto-skeleton, may prevent further crosslinking of collagen to maintain tensional homeostasis between the cell and the surrounding matrix. The cell-matrix stiffness has been studied by Karamichos *et al*, who varied the matrix stiffness of collagen gel and measured the traction force of nHDF (24). They found reduced traction force with increased gel stiffness. Translating their results to our study, cells in +TGF-β samples, having higher αSMA expression and exhibiting tissue retraction at week 5 (Fig. 4), should exit in a less stiff matrix (less mature collagen and lower modulus), while cells in –TGF-β samples should be in homeostasis with a more stiff matrix (more mature collagen and higher modulus).

One of the downstream signaling proteins of TGF-β treatment is SMAD-2 (15, 16). Western blot analysis showed a large increase in phosphorylation of SMAD-2 in TGF-β samples (Fig. 5a). Phosphorylation of ERK1/2 in contrast, was increased in –TGF-β TC (Fig 5b). In a study by Papakrivopoulou *et al,* it was shown that pERK1/2 signal when subjecting cardiac fibroblast to cyclic stretching was obligatory for increased collagen expression (21). Though activation of SMAD-2 has not been shown to have a direct inhibition effect on ERK1/2 phosphorylation, there are other downstream proteins in the TGF-β activation pathway that can inhibit phosphorylation of ERK1/2, such as p38 (19). In addition, the study by Papakrivopoulou *et al* showed

that activated p38 inhibited phosphorylation of ERK1/2. Further evidence of p38 activation can be deduced from higher elastin expression in +TGF-β samples. A study demonstrated that activation of p38 leads to a stabilization of elastin mRNA (25). Though evidence presented in this study suggests that downstream signaling proteins in the TGF-β pathway can explain the observed differences in tissue development, further studies are required to fully understand cellular signals and there role in tissue development.

Functional tissue-engineered constructs require mechanical stiffness, strength, and elasticity. This study showed that while TGF-β can lead to enhanced elastin production, it is detrimental to the development of engineered tissue when using long-term cyclic stretching. However, this study also demonstrated that use of TGF-b following extended cyclic stretching in the absence can yield both physiological UTS and modulus and substantial elastin content. A similar sequential approach to use of mechanical and chemical stimuli has been studied for bone cells by Lima *et al* (26). This study demonstrates a rationalized approach to maximize the benefits of mechanical (cyclic stretching) and chemical (TGF-β) stimuli that can be applied to engineered connective tissue and potentially improved by optimized regimens for both.

3.5: Materials and Methods

3.5.1: Cell culture

Neonatal human dermal fibroblasts (nHDFs, Clonetics) were maintained in DMEM/F12 culture medium (Gibco) supplemented with 10% FBS,100 U/ml penicillin,

100 μg/ml streptomycin, and 2.5 μg/ml amphotericin-β. Cells were passaged at 100% confluency and harvested for use from passage 7-9.

3.5.2: Tubular construct (TC) preparation and culture

A cell-seeded fibrin gel was molded by mixing cells suspended in DMEM into a solution of bovine fibrinogen (Sigma) in 20mM HEPES-buffered saline. A mixture of bovine thrombin (Sigma) and calcium chloride in DMEM was then added to the fibrinogen/cell mixture. The final concentrations of the suspension were 6.6 mg/ml fibrinogen, 0.4 U/ml thrombin, 3.6mM Ca^{2+}, and 500,000 cells/ml. Suspensions were well-mixed by pipette action and injected into a tubular molds. The details of the experiment have been previously described (14). Constructs were cultured in DMEM media supplemented with 10% FBS, 100 U/ml penicillin, 100 μg/ml streptomycin, 2 μg/ml insulin, 50 μg/ml ascorbic acid, 2.5 μg/ml ε-amphotericine-β, and 1 ng/ml TGF-β (for TGF-β samples only). Constructs were cultured for two weeks, after which they were transferred to the CD bioreactor. This two-week culture period allowed for cell-mediated fibrin compaction and initial ECM deposition so that the constructs could withstand the transfer to the bioreactor.

3.5.3: CD Bioreactor

Constructs were transferred onto a distensible mandrel in a custom built bioreactor described previously in detail (27). Briefly, a distensible mandrel was

constructed using a thin-walled latex tube (Kent Elastomer, Kent, OH). One end of the latex tube was closed with a polycarbonate stopper using epoxy sealant, while the other end was connected to an in-house air line, which was controlled by a pressure regulator. The frequency and duty of the air cycle were controlled by a solenoid valve connected downstream of the pressure regulator. For all studies, a frequency of 0.5 Hz with 12.5% duty cycle was used, corresponding to 0.25 sec stretch time in a 2 second cycle period. CD experiments were conducted with strain amplitude increased in 4 equal steps from 5% to 15% over 5 weeks. The medium in the CD bioreactor was changed 3 times per week with only 70% of the medium replaced.

For the ∗TGF-β treated group, after 3 weeks of cyclic stretching at week 5, the media conditions was altered to include TGF-β and remove ascorbic acid.

After harvest, each construct was divided into four equal-length sections, one for uniaxial tensile testing followed by biochemical analysis, and the others for western blotting, DNA quantification, and histology.

3.5.4: Uniaxial Tensile Testing

One fourth strip of a construct was tested for uniaxial properties in the circumferential direction. The thickness of each strip was measured using a 50 g-force probe attached to a displacement transducer. Tissue strips were placed in compressive grips, attached to the actuator arm and load cell of a Microbionix material testing system (MTS system, Eden Prairie, MN) and straightened with a load of 0.005 N. This position was used as the reference length of the strip. Following 6 cycles of 0-10% strain at 2 mm/min, constructs were stretched to failure. True strain was calculated

based on the change in length of the tissue over time. The stress was calculated as force divided by the initial cross sectional area. Young's modulus (E) was determined by linear regression of the stress-strain curve.

3.5.5: Histology

Constructs for histology were fixed in 4% paraformaldehyde, infiltrated with a solution of 30% sucrose and 5% DMSO, frozen in OCT (Tissue-Tek), and sectioned into 9 μm cross-sections. Sections were stained with Lillie's trichrome, Verhoeff's stain and picrosirius red. Images were taken using a color CCD camera. For Picrosirius red staining, images were taken with the samples placed between crossed plane polarizers.

Elastin immuno-staining was performed by blocking tissue section slides with 5% donkey serum, followed by elastin antibody (Elastin Inc) at 1:200 dilution and secondary cye2 antibody (Jackson Immuno Inc) at 1:200 dilution. The images were taken on a florescent microscope in rodamine channel. For all staining, sheep pulmonary valve leaflet was used as a positive control.

3.5.6: Collagen and Cell quantification

Collagen content was quantified with the hydroxyproline assay (22). Sample volume was calculated using the measured length, width, and thickness of the strips (as described above in uniaxial testing). Collagen concentrations were calculated as the amount per unit volume in each sample.

DNA content was quantified with a modified Hoechst assay (22). Cell numbers were obtained from DNA contents assuming 7.6 pg of DNA per cell. Cell

concentrations were calculated as the number of cells per unit volume using the dimensions of the strip.

3.5.7: Western Blotting Analysis

Samples were flash frozen in liquid nitrogen at harvest. The proteins were extracted as previously described (14). For each sample, 40 μg of total protein was boiled in a reducing sample buffer and separated by SDS-PAGE. The proteins were transferred to nitrocellulose (Whatman) using a wet transfer buffer (10% methanol, 2.2 g/L CAPS, pH 11). The blot was incubated in blocking solution (5% dry milk, 0.1% Tween-20 in PBS) for one hour and then incubated with respective primary antibody overnight at 4ºC (mouse monoclonal phospho-ERK antibody p-Thr202/p-Tyr204, Cell Signaling, 1:1000, rabbit monoclonal phosphor-SMAD2 antibody p-Ser465/467, Cell Signaling, 1:1000). The blot was then probed with HRP-conjugated secondary anti-IgG (Amersham) at a dilution of 1:10000 and developed using enhanced chemiluminescence. The blot was then stripped of antibodies using Restore Plus (Pierce) and re-probed using a primary antibody for the respective proteins (rabbit polyclonal ERK antibody, Cell Signaling, 1:1000, rabbit polyclonal SMAD2/3 antibody, Cell Signaling, 1:1000). The phosphorylated protein to total protein ratio was determined by densitometry of scanned auto-radiograms.

3.5.8: Statistics

For all experiments, n= 6-8 for each treatment and time point was used. The statistical difference between groups was determined using one-way ANOVA with

Tukey post hoc test in GraphPad Prism® software for Windows. In all cases where the error bars (plus or minus standard deviation) are non-overlapping, the differences are found to be significant; hence, for clarity, no symbols are used. In cases where error bars are overlapping and the difference is statistically significant, paired symbols are used to indicate the difference. Any reference to a difference in the Results and Discussion implies statistical significance at the level $p < 0.05$.

3.6: References

1. Thom, T., *et al.* (2006) Heart disease and stroke statistics--2006 update: a report from the American Heart Association Statistics Committee and Stroke Statistics Subcommittee. *Circulation* **113,** e85-151.
2. Isenberg, B. C., *et al.* (2006) Small-diameter artificial arteries engineered in vitro. *Circ Res* **98,** 25-35.
3. Yacoub, M., Nerem, R. (2007) Introduction. Bioengineering the heart. *Philos Trans R Soc Lond B Biol Sci* **362,** 1253-1255.
4. Bilodeau, K., Mantovani, D. (2006) Bioreactors for tissue engineering: focus on mechanical constraints. A comparative review. *Tissue Eng* **12,** 2367-2383.
5. Grouf, J. L., *et al.* (2007) Differential effects of EGF and TGF-beta1 on fibroblast activity in fibrin-based tissue equivalents. *Tissue Eng* **13,** 799-807.
6. Neidert, M. R., *et al.* (2002) Enhanced fibrin remodeling in vitro with TGF-beta1, insulin and plasmin for improved tissue-equivalents. *Biomaterials* **23,** 3717-3731.
7. Clark, R. A., *et al.* (1995) Collagen matrices attenuate the collagen-synthetic response of cultured fibroblasts to TGF-beta. *J Cell Sci* **108 (Pt 3),** 1251-1261.
8. Long, J. L., Tranquillo, R. T. (2003) Elastic fiber production in cardiovascular tissue-equivalents. *Matrix Biol* **22,** 339-350.
9. Ross, J. J., Tranquillo, R. T. (2003) ECM gene expression correlates with in vitro tissue growth and development in fibrin gel remodeled by neonatal smooth muscle cells. *Matrix Biol* **22,** 477-490.
10. Kucich, U., *et al.* (2002) Transforming growth factor-beta stabilizes elastin mRNA by a pathway requiring active Smads, protein kinase C-delta, and p38. *Am J Respir Cell Mol Biol* **26,** 183-188.
11. Merryman, W. D., *et al.* (2007) Synergistic effects of cyclic tension and transforming growth factor-beta1 on the aortic valve myofibroblast. *Cardiovasc Pathol* **16,** 268-276.
12. Poobalarahi, F., *et al.* (2006) Cardiac myofibroblasts differentiated in 3D culture exhibit distinct changes in collagen I production, processing, and matrix deposition. *Am J Physiol Heart Circ Physiol* **291,** H2924-2932.
13. Bastiaansen-Jenniskens, Y. M., *et al.* (2008) TGFbeta Affects Collagen Cross-Linking Independent of Chondrocyte Phenotype but Strongly Depending on Physical Environment. *Tissue Eng Part A*.
14. Syedain, Z. H., *et al.* (2008) Cyclic distension of fibrin-based tissue constructs: evidence of adaptation during growth of engineered connective tissue. *Proc Natl Acad Sci U S A* **105,** 6537-6542.
15. Massague, J. (2000) How cells read TGF-beta signals. *Nat Rev Mol Cell Biol* **1,** 169-178.
16. Massague, J., *et al.* (2005) Smad transcription factors. *Genes Dev* **19,** 2783-2810.

17. Bujor, A. M., *et al.* (2008) Akt blockade downregulates collagen and upregulates MMP1 in human dermal fibroblasts. *J Invest Dermatol* **128,** 1906-1914.
18. Kuang, P. P., *et al.* (2007) Activation of elastin transcription by transforming growth factor-beta in human lung fibroblasts. *Am J Physiol Lung Cell Mol Physiol* **292,** L944-952.
19. Sato, M., *et al.* (2002) Role of p38 MAPK in transforming growth factor beta stimulation of collagen production by scleroderma and healthy dermal fibroblasts. *J Invest Dermatol* **118,** 704-711.
20. Rubbens, M. P., *et al.* (2008) Intermittent Straining Accelerates the Development of Tissue Properties in Engineered Heart Valve Tissue. *Tissue Eng Part A.*
21. Papakrivopoulou, J., *et al.* (2004) Differential roles of extracellular signal-regulated kinase 1/2 and p38MAPK in mechanical load-induced procollagen alpha1(I) gene expression in cardiac fibroblasts. *Cardiovasc Res* **61,** 736-744.
22. Robinson, P. S., *et al.* (2008) Functional tissue-engineered valves from cell-remodeled fibrin with commissural alignment of cell-produced collagen. *Tissue Eng Part A* **14,** 83-95.
23. Balguid, A., *et al.* (2007) The role of collagen cross-links in biomechanical behavior of human aortic heart valve leaflets--relevance for tissue engineering. *Tissue Eng* **13,** 1501-1511.
24. Karamichos, D., *et al.* (2007) Collagen stiffness regulates cellular contraction and matrix remodeling gene expression. *J Biomed Mater Res A* **83,** 887-894.
25. Kuang, P. P., Goldstein, R. H. (2005) Regulation of elastin gene transcription by proteasome dysfunction. *Am J Physiol Cell Physiol* **289,** C766-773.
26. Lima, E. G., *et al.* (2007) The beneficial effect of delayed compressive loading on tissue-engineered cartilage constructs cultured with TGF-beta3. *Osteoarthritis Cartilage* **15,** 1025-1033.
27. Isenberg, B. C., Tranquillo, R. T. (2003) Long-Term Cyclic Distention Enhances the Mechanical Properties of Collagen-Based Media-Equivalents. *Annals of Biomedical Engineering* **31,** 937-949.

3.7: Figures

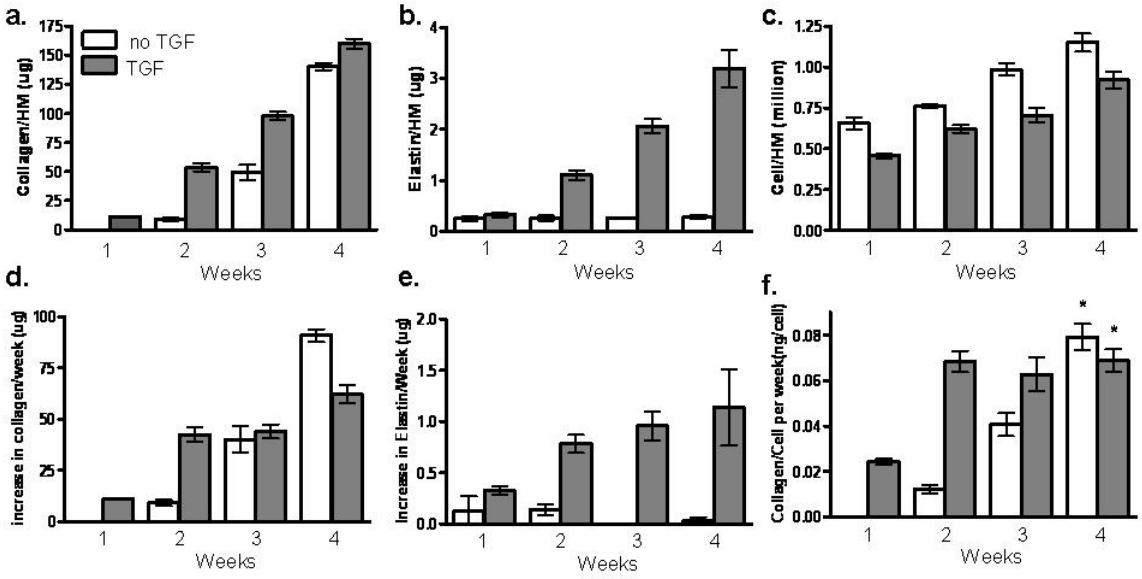

Figure 3-1: Time course of fibrin-based TC with and without TGF-β supplementation during incremental cyclic stretching a: UTS, b: Modulus, c: Collagen concentration, d: Elastin concentration, e: Cell concentration and f: Collagen/Cell concentrations after 2, 5 & 7 weeks of incubation. In all cases where error bars are not overlapping, the means are different ($p<0.05$); for groups with overlapping error bars, difference ($p<0.05$) between means is shown with paired symbols.

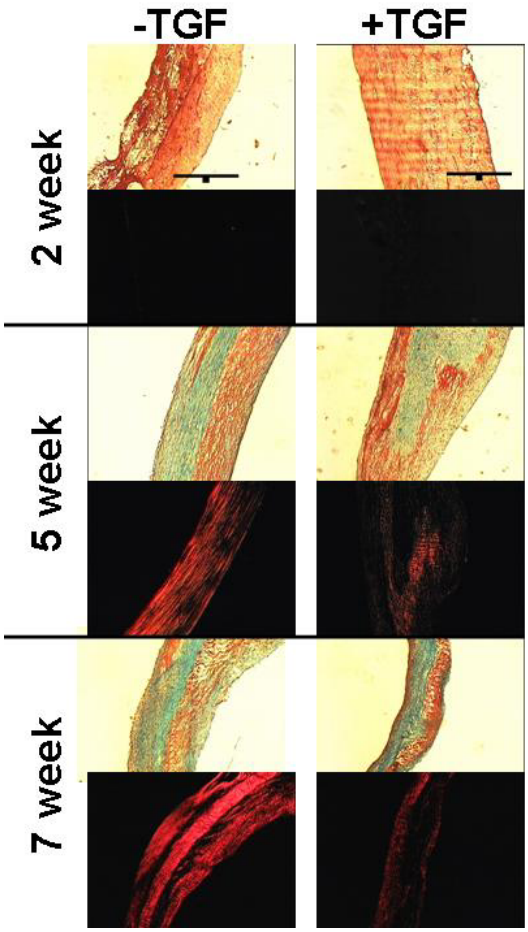

Figure 3-2: Trichrome and picrosirius red staining of TC after 2, 5 and 7 weeks. In trichrome stained section, collagen stains green and fibrin (and other proteins) stain red. In picrosirius red stained sections, brighter intensity of red color indicate more mature collagen. All images were taken at same magnification with 200μm scale bar (black line) shown in 2 weeks trichrome images. The lumen of TC is on the left side of all sections.

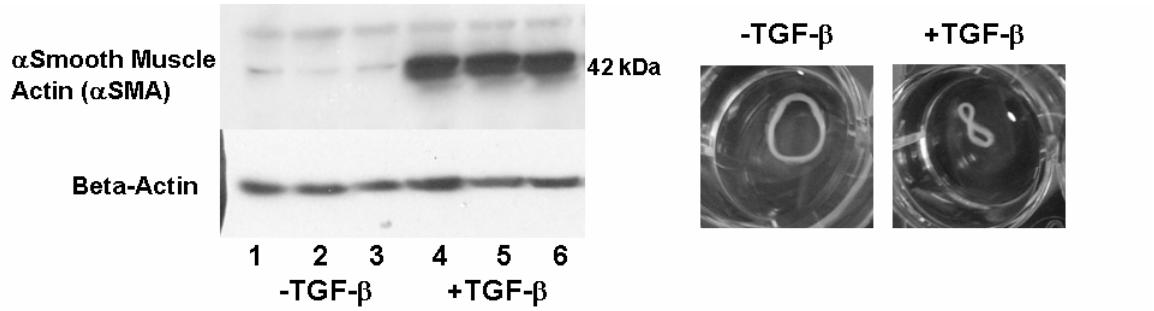

Figure 3-3: a: Western blot of αSMA expression by nHDF in TC constructs at week 5. β-actin bands indicate the same protein loading in all lanes, implying TGF-β induced expression of αSMA. b: TC in PBS at week 5 after removal from latex tube of the cyclic stretch bioreactor shows curling of TGF-β samples.

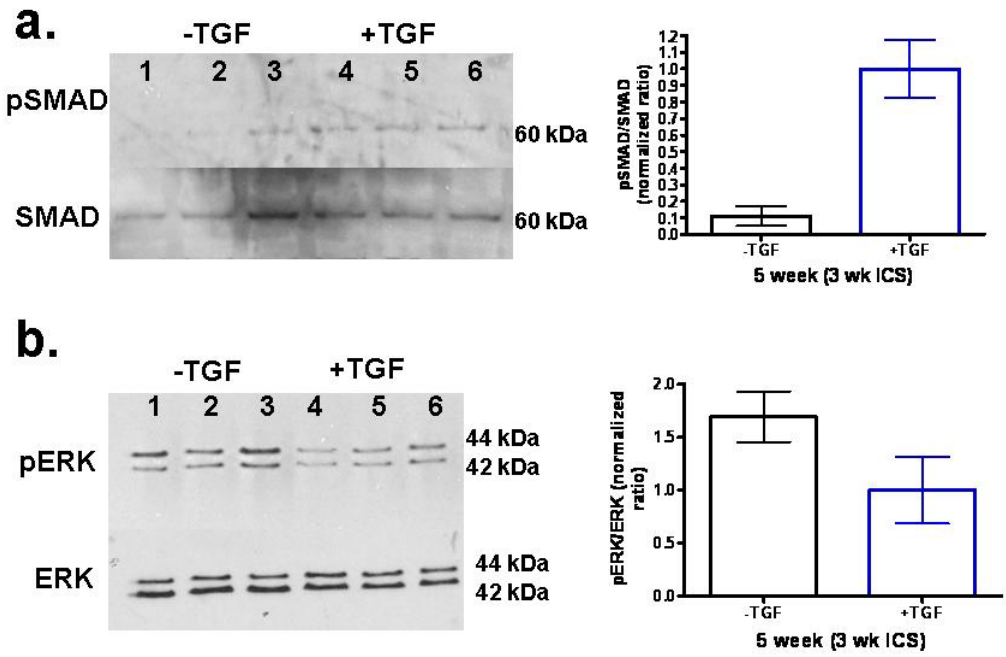

Figure 3-4: **a: Western blotting for ERK 1/2 and SMAD activation of nHDF in TC (n=3) with and without TGF-β supplementation at 5 weeks.**
a: Western blot for SMAD and phosphorylated SMAD (pSMAD).b: Western Blot for levels of total (tERK) and threonine 202/tyrosine204 phosphorylated ERK 1/2 (pERK). Band intensity was determined by densitometry and expressed as the ratio of phosphorylated protein band to total protein band and then normalized o the +TGF-β value. TGF-b is shown to increase fraction of SMAD that is phosphroylated but decrease the fraction of ERK that is phosphroylated .Statistical significance at $p<0.05$ is shown by paired symbols.

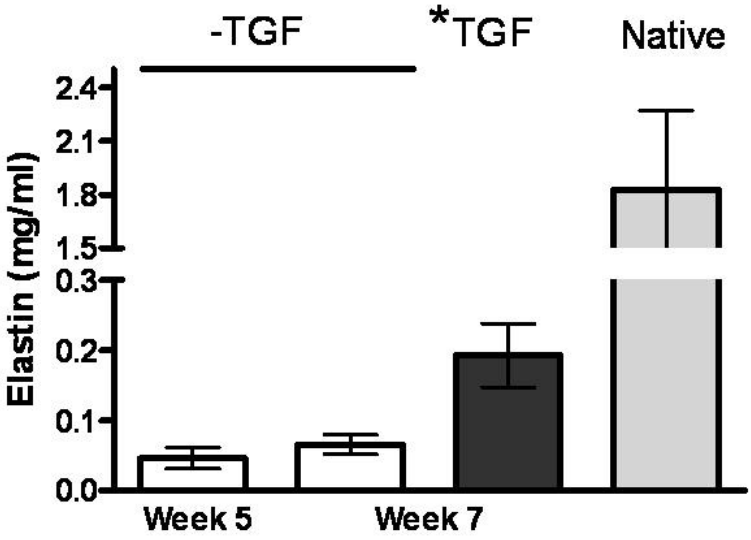

Figure 3-5: Elastin concentration comparison of –TGF-β samples at weeks 5 and 7 with the ∗TGF-β treated group and native tissue control. Statistical significance at $p<0.05$ is shown by paired symbols.

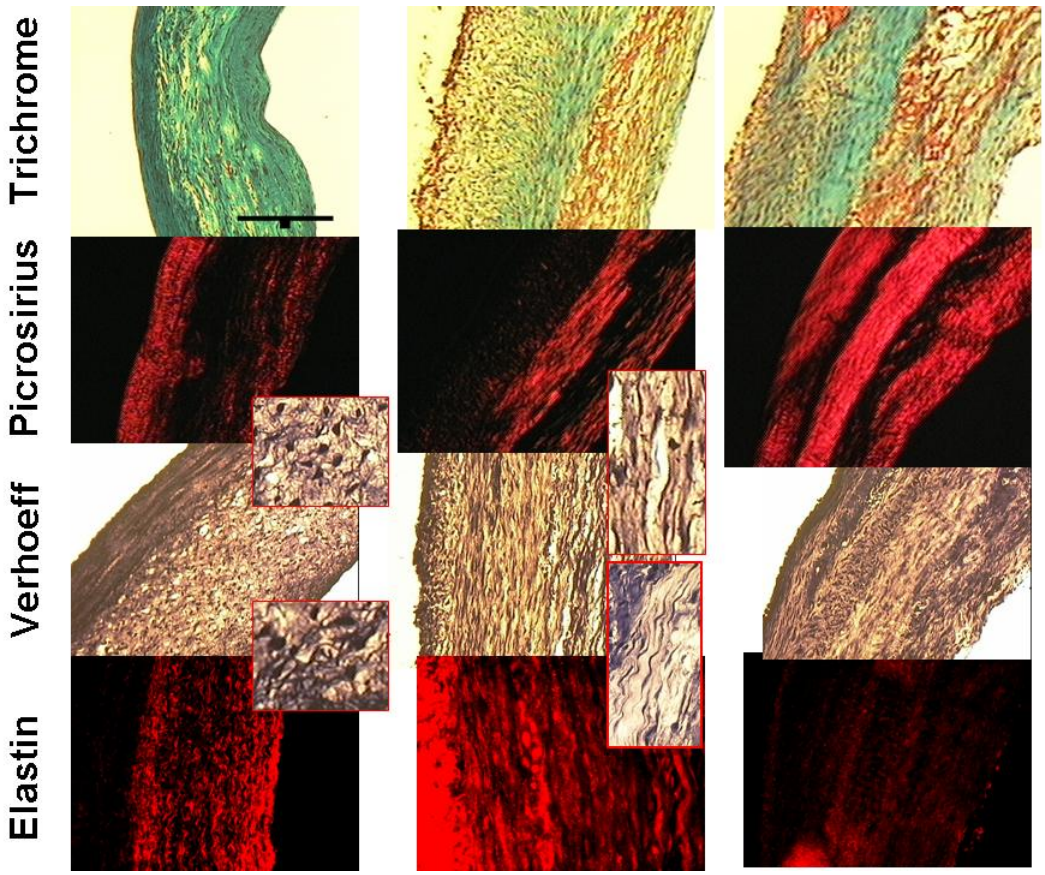

Figure 3-6: Trichrome, picrosirius red, Verhoeff, and elastin immunostaining for –TGF-β samples and ∗TGF-β samples at week 7 with native tissue control. Inset of Verhoeff stain shows magnified image of elastin fiber strands in native control and ∗TGF-β treated TC. All images were taken at same magnification with 200μm scale bar (black line) shown in native trichrome images. The lumen of TC and ventricular side of native leaflet is on the left side of all sections.

.

Chapter 4: A Novel Bioreactor for Tissue Engineered Heart Valves Based on Controlled Cyclic Stretching

Submitted Revision to *Biomaterials*, 2009

4.1: Summary

A tissue-engineered heart valve (TEHV) represents the ultimate valve replacement, especially for juvenile patients given its growth potential. To date, most TEHV bioreactors have been developed based on pulsed flow of culture medium through the valve lumen to induce strain in the leaflets. Using a strategy for controlled cyclic stretching of tubular constructs reported previously, we developed a controlled cyclic stretch bioreactor for TEHVs that leads to improved tensile and compositional properties. The TEHV is mounted inside a latex tube, which is then cyclically pressurized with culture medium. The root and leaflets stretch commensurately with the latex, the stretching being dictated by the stiffer latex and thus controllable. Medium is also perfused through the lumen at a slow rate in a flow loop to provide nutrient delivery. Fibrin-based TEHVs prepared with human dermal fibroblasts were subjected to three weeks of cyclic stretching with incrementally increasing strain amplitude. The TEHV possessed the tensile stiffness and stiffness anisotropy of leaflets from sheep pulmonary valves and could withstand cyclic pulmonary pressures with similar distension as for a sheep pulmonary artery.

4.2: Introduction

Tissue engineering provides a means to create living heart valve replacements with the ability to remodel and grow, which is an ideal solution for pediatric patients. Tissue-engineered heart valves (TEHV) may also benefit adult patients with life expectancies exceeding the typical lifetime of bioprosthetic valves or those unable to tolerate the anticoagulant therapy required for mechanical valves. There have been many advances in the field of TEHV [1-3], including bioreactors used to provide mechanical stimulation for tissue growth and associated nutrient supply [4-7]. Most bioreactors designed for TEHV generate pulsatile flow of cell culture medium through the lumen in order to provide mechanical conditioning and nutrient supply [4-6]. These pulse-flow bioreactors generate complex and often ill-defined mechanical conditioning, including shear, tensile and compressive strains, that vary with time and position. Since scaffold remodeling and tissue growth correlate with strain amplitude [8-11], TEHV development cannot be readily controlled using these pulse-flow systems.

A more controlled mechanical conditioning, specifically the use of controlled cyclic stretching, has been well studied for tissue engineered vascular grafts and shown to yield significant improvement in tensile properties and ECM production [9, 10, 12-15]. Implementation of controlled cyclic stretching via cyclic distension is facilitated by simpler tubular geometry. Mol *et al* used a stretching approach by applying cyclic back-pressure on coaptating TEHV leaflets [16]. Since pressure-induced stretching is regulated by tissue stiffness, which continually changes during culture due to tissue growth and scaffold degradation, this approach does not allow for conditioning with controlled strain amplitude unless the pressure is continuously varied [17].

Our laboratory's approach to TEHV fabrication is based on the entrapment of dermal fibroblasts into fibrin gel within a mold, which, following static incubation in the mold, yields the gross geometry and alignment patterns of the native aortic valve [18]. The dermal fibroblast is used because it is a readily available source and generates extensive remodeling of fibrin into a collagenous tissue with tensile mechanical properties approaching those of native tissue [18]. Dermal fibroblasts have also been successfully used for a vascular graft in clinical studies [19]. The fibrin-based TEHVs (hereafter termed "valve-equivalents", or VEs) are cast such that the tubular root and leaflets are a single entity. By using molds with two or three channels cut into the central mandrel, bi- and tri-leaflet VEs have been fabricated. The current study is focused on bi-leaflet VEs for comparison to previous results [18].

In contrast to synthetic biodegradable polymers whose initial strength and stiffness values are greater than heart valve tissue, those of biological scaffolds like collagen or fibrin are orders of magnitude smaller. Realizing tissue growth to achieve physiological values of leaflet tensile and bending stiffness (along with tensile strength exceeding normal leaflet stresses) prior to implantation is crucial for their success, previous research in our laboratory with fibrin-based tubular constructs prepared with porcine aortic valve interstitial cells has shown that cyclic stretching with an incremental strain amplitude over three weeks can lead to at minimum an 84% greater ultimate tensile strength compared to statically-incubated controls, which correlates with increased collagen deposition and maturation [10]. Hence in the current study, a controlled stretch TEHV bioreactor was designed that can apply prescribed cyclic stretching to the VE root and leaflets during the entire incubation (even as the tissue

mechanical properties change), while independently controlling the nutrient delivery. The motivation to keep nutrient delivery independent of cyclic stretching was to allow flexibility of changing stretching parameters (frequency and magnitude) without influencing the nutrient supply. The VEs were conditioned with incremental strain amplitude cyclic stretching in the bioreactor for three weeks and then assessed for structure, composition, and mechanical property differences relative to VEs cultured statically for the duration. Values were compared to native tissue obtained from sheep pulmonary valve and artery since it is a common large animal implant model.

4.4: Results

4.4.1: Controlled cyclic stretching leads to improved TEHV leaflet properties and anisotropy in stiffness comparable to native leaflet.

Incremental strain amplitude cyclic stretching was applied to VEs over a 3-week period using the bioreactor (Fig. 1) following a 2-week static incubation on the VE mold. The initial circumferential strain amplitude of the root was set at 5%, yielding an average strain amplitude in the leaflets of 5% in the circumferential direction and 3% in the radial direction. Fig. 2 shows the measured average leaflet strain in the circumferential (commissure-to-commissure) and radial directions.

After cyclic stretching, the VE was harvested by sliding it out of the latex tube, with no apparent cohesion. Tensile mechanical properties were measured in both the circumferential and radial directions. Figure 3 shows the ultimate tensile strength (UTS), modulus (E), thickness, maximum tension, and membrane stiffness of leaflets from static control VEs, ICS VEs, and sheep pulmonary valves. There were no

differences of the leaflet circumferential E or UTS values between VE castings for neither the static control nor the ICS VE groups based on two-way ANOVA, so results for pooled values from multiple castings are reported hereafter, In the circumferential direction, UTS and E were 97% (to 951±258 kPa) and 77% (to 2529±409 kPa) greater, respectively, for VE leaflets subjected to ICS compared to static control leaflets. Compared to sheep pulmonary valve leaflets, UTS of the ICS leaflets was 50% lower; however, E was not statistically different. There was no difference in the radial tensile properties of static, ICS, and native leaflets. There was no difference in the leaflet thickness between VEs incubated statically for 2 or 5 weeks, ICS VEs, and to sheep pulmonary valves, all being in the range of 300-350 μm (Fig. 3c). Maximum tension and membrane stiffness, defined as the UTS and E values multiplied by the average thickness of the leaflets, thus showed similar improvement as found for UTS and E when comparing the ICS to the static leaflets (Fig. 3). Also, there was no statistical difference in membrane stiffness between ICS leaflets and native leaflets. The index of anisotropy, defined as the ratio of circumferential to radial modulus, for static, ICS, and native leaflets was 2.0±0.2, 2.8±0.4 and 2.4±0.3, respectively, showing an improvement in anisotropy due to ICS, which yields a comparable anisotropy of leaflet stiffness to native leaflets.

4.4.2: Cyclic stretching improves ECM organization and collagen maturation of TEHV leaflet and root

Figure 4 shows a comparison of alignment maps and cross-sections stained with trichrome and picrosirius red stains for static, ICS, and native leaflets. The alignment

maps indicate that VE leaflets, for both static and ICS VEs, have primarily circumferential alignment, which correlates with the mechanical anisotropy noted above, consistent with native leaflets.

Based on the trichrome staining, which shows collagen in green, fibrin (for VEs) and other non-collagenous proteins in red, and cell nuclei in blue-black, it can be seen in VE leaflets that most of the fibrin degraded by 5 weeks of culture and there is a distribution of collagen across the entire thickness of the leaflet. The ICS VE also shows a homogeneous cellularity, which indicates there was no limitation to nutrient transport in the bioreactor.

Picrosirus red staining imaged under cross-polarizers shows a bright red stain indicative of mature collagen fibers [21]. Native leaflets had the highest intensity followed by ICS leaflets. The braided red fibers, which could indicate organized collagen fibers [22], are seen in the native leaflets and the ICS leaflets, but not in the static leaflets.

The collagen density in ICS leaflets (26±2 mg/ml was 86% greater than static leaflets (14±2 mg/ml) but 37% less than native leaflets (41±4 mg/ml). The cell density was not statistically different between static (160±60 $x10^6$ cells/ml), ICS (137±20 $x10^6$ cells/ml), and native (155±12 $x10^6$ cells/ml) leaflets.

4.4.3: VE root tensile properties improve with cyclic stretching and VE withstands cyclic pulmonary pressures

Figure 5a shows UTS and E of root tissue in the circumferential direction for static VE, ICS VE, and the pulmonary artery (PA). UTS and E of ICS root were 112%

and 62% greater, respectively, compared to static root and were 92% and 392% greater, respectively, than PA. Considering that the VE root is about 0.4 mm thick compared to 3 mm thick for the PA, the maximum tension and membrane stiffness of the PA were much higher than ICS VE (Fig. 5b). Trichrome staining showed cellularity and collagen deposition throughout the thickness of the VE root (Fig. 6). Picrosirius red staining indicated more mature collagen in ICS root as compared to the static root.

Upon harvest of ICS VEs from the bioreactor, the latex sleeve was removed and the VE was cyclically pressurized to 40 mmHg at 0.5 Hz for 180 cycles. The root was then incrementally pressurized until rupture (at 150 mmHg or greater). A section of PA was mounted on the bioreactor and similarly tested. The data for pressure *vs.* lumen diameter were compared to the PA, as shown in Fig. 5c. The data show comparable distension for ICS VE and PA at lower (but physiological) pressures, with the PA being stiffer at higher strains.

4.5: Discussion

In this study, a unique bioreactor design was developed for the mechanical conditioning of TEHVs. Previously, our laboratory showed significant improvements in tensile and compositional properties of fibrin-based tubular constructs conditioned with controlled incremental cyclic distension, with incremental strain amplitude being superior to constant strain amplitude [10].Taking advantage of our VE design comprised of a tubular root to which leaflets are contiguously attached, a bioreactor was developed that allows for controlled stretching, without compromising the leaflets within the lumen. This required mounting the VE inside a latex tube and pressurizing it with culture medium. The control results from the use of a latex housing stiffer than the

growing tissue, which allows for constant strain regardless of the changes in the tissue mechanical properties. The VE subjected to ICS had improved tensile and compositional properties, both in the leaflets and root section, compared to static controls, and also had the ability to withstand pulmonary pressures.

Circumferential strain in the root was calculated by measuring the distension of then latex housing with a laser micrometer. Since the TEHV was axially constrained by attachment of both ends of the root to bioreactor mounting end-pieces, there was also an axial component to cyclic strain; however, in the current study, circumferential root strain was used as the controlled variable. In the leaflets, an average strain in the belly region was calculated from image analysis of displacement of ink marks on the leaflet surfaces. The applied circumferential strain in the root resulted in essentially the same induced circumferential strain in the leaflets, because the leaflets are attached to the root. However, the radial strain in the leaflet for a given root distension was lower than the circumferential strain, because of the leaflet free edge being unconstrained. This led to non-equibiaxial strain in the leaflet, with only the circumferential strain being controlled. However, this non-equibiaxial strain evidently maintained the anisotropy developed during the 2-week static incubation phase prior to the bioreactor conditioning based on the circumferential alignment (Fig. 4) and anisotropic stiffness (Fig. 3) of leaflets following conditioning. These particular properties have been shown to be important for proper physiological function [23, 24]. For the current study, a direct measurement approach was utilized to calculate average circumferential and radial strains in the leaflet belly during controlled cyclic stretching of TEHV in the bioreactor based on the displacement of four ink marks. It was assumed that no axial movement of

the leaflet occurs during cyclic stretch, hence allowing for single head-on camera imaging. In future studies, a full 2D strain field could be calculated by using more markers on the leaflet surface to allow for local strain measurements [25, 26] or by analyzing an anisotropic mechanical model [27]. Figure 2 shows the maximum strain amplitude calculated in the circumferential and radial directions in a VE leaflet.

ICS VEs showed improved tensile mechanical properties in the circumferential direction in both the leaflets and root. Compared to static controls, UTS and E were 97% and 77% greater, respectively (Fig. 3), for ICS leaflets. Compared to sheep pulmonary valve leaflets, the UTS of ICS VE leaflets was 50% less, but there was no difference in E. Figure 3 also shows maximum tension and membrane stiffness for the three groups, which show similar trends, due to a very similar thickness of the VE and native leaflets. The improvements in mechanical properties with ICS conditioning correlated with increases in collagen density (Fig. 4). The collagen density in the ICS leaflets was 86% greater than the static value and 37% lower than the native leaflet value. These improvements seen in tensile properties and collagen density with the 2-step ICS are comparable to previously reported improvements with a fibrin-based tubular constructs seeded with porcine valve interstitial cells [10], which used 2- and 4-step ICS. In contrast to these improvements for ICS VE, when Mol et al [16] compared static-strained to dynamic-strained leaflets in their diastolic pulse duplicator bioreactor, they found no significant improvement in tensile properties after 3 weeks of culture.

If the VE is used as an interpositional graft, it is essential that it possess the critical mechanical properties in the root of the VE as well as in the leaflets. In comparing the ICS VE root properties to those of a sheep pulmonary artery (PA), the

UTS and E of the VE root were 92% and 392% greater, respectively. However, since the PA is approximately an order of magnitude thicker (3 mm versus 400 μm for VE root), it can withstand higher pressures as compared to the VE root. A short-term durability test was performed by cyclic stretching an ICS VE with internal pressure of 40 mmHg for 180 cycles at 0.5 Hz, followed by ramping the pressure to VE failure. The pressure-diameter curve for the ICS VE was similar to the PA at lower (still physiological) pressures; the ICS VE was more compliant at higher pressures and failed quicker (Fig 5). These results demonstrate the ability of the ICS VE to withstand pulmonary pressure with similar root distension as the sheep PA if implanted interpositionally in the PA.

Static controls were left on the Teflon mold with gentle shaking to allow for well-mixed culture medium. The total culture medium volume per VE was similar for both static control jars and the bioreactor nutrient loop. Thus, the reported differences should not be merely due to differences in nutrient availability. In support of this, there was no difference in cell concentrations of static control *vs.* ICS VEs. Another control which could have been used is the VE mounted in the bioreactor and perfused with medium, but without cyclic stretching. However, this would require maintaining the lumenal pressure needed to counteract lumen narrowing due to cell traction forces acting in the root and was not pursued.

Further studies will involve a sheep pulmonary valve implant model, which has been used previously to assess the remodeling of TEHVs [28, 29]. This model is relevant for human applications as our measured E of 3.2 ± 0.8 MPa for the sheep pulmonary valve leaflet is comparable to reported human values (5.89 ± 3.05 MPa [30];

16.05 ± 2.02 MPa [31]) as is our measured UTS value of 2.0 ± 0.2 MPa (3.5 - 7MPa [30]; 2.78±1.05 MPa [31]). Due to its open lumen design and separate perfusion loop, the bioreactor can also be used for endothelialization post-conditioning; we have shown that endothelial cells adhere strongly to the ECM resulting from fibroblast-mediated fibrin remodeling [32]. Further optimization of the medium composition and ICS conditions could lead to improvement in VE properties so that the VE is also suitable as an aortic valve (AV) replacement; specifically, an increased leaflet tensile modulus comparable to AV leaflets and an increased UTS so as to exceed normal stresses in the AV leaflets, as previously detailed [18].

To date, several TEHV models have been presented in the literature . Using fibrin-based VEs prepared with human dermal fibroblasts, we have demonstrated the ability to create a TEHV with circumferential fiber alignment in the leaflet manifested as anisotropic stiffness comparable to native leaflets, a property that has not been achieved with TEHVs based on synthetic biodegradable polymers. Though several bioreactors have been proposed to mechanically condition TEHVs, they do not allow for controlled strain to be applied without complicated feedback regulation, which has not been proposed. Using a strategy for controlled cyclic stretching of tubular constructs that we presented previously, we developed a controlled cyclic stretch bioreactor for TEHVs that leads to improved tensile and compositional properties. The leaflets of ICS VEs fabricated for this study possessed the tensile stiffness of native leaflets and the ICS VEs can withstand cyclic pulmonary pressures with similar distension to that of the native ovine pulmonary artery.

4.3: Materials and Methods

Cell culture

Neonatal human dermal fibroblasts (Clonetics) were maintained in DMEM/F12 culture medium (Gibco) supplemented with 10% FBS,100 U/ml penicillin, 100 μg/ml streptomycin, and 2.5 μg/ml amphotericin-β. Cells were passaged at 100% confluency and harvested for use at passage 9.

VE preparation and culture

A fibroblast-seeded fibrin gel was formed by adding thrombin (Sigma) and calcium chloride to a mixture of cells in fibrionogen (Sigma) solution in 20mM HEPES-buffered saline. All components were at room temperature. The final concentrations of the suspension were 6.6mg/ml fibrinogen, 1.1 U/ml thrombin, 5.0 mM Ca^{++}, and 500,000 cells/ml. Suspensions were well mixed by pipette action and injected into bi-leaflet VE molds as described previously [18].

After injection of the suspension, the VE molds were placed vertically in an incubator for 30 minutes. After gelation, the outer housing was removed, and the VEs were placed horizontally in culture medium, comprising DMEM supplemented with 10% FBS, 100 U/ml penicillin, 100 μg/ml streptomycin, 2 μg/ml insulin, 50 μg/ml ascorbic acid. Medium (250 mL) was changed 3 times per week and 1 ng/ml TGF-β1 (R&D Systems) was included for the first two to three feedings after casting to promote cell-mediated fibrin compaction. VEs were cultured for 2 weeks on the mold with gentle rocking, after which they were transferred to the cyclic stretch bioreactor. The 2 week static culture allowed for sufficient stiffening and strengthening of the VE to withstand handling during mounting in the bioreactor.

Controlled Cyclic Stretch Bioreactor

The bioreactor consists of a distensible latex tube, in which the TEHV is mounted, and two flow circuits for controlled stretching and nutrient supply. Figure 1 shows the schematic of the bioreactor system and the image of a VE inside the bioreactor. VEs (n=8) were taken off the Teflon mold after 2 weeks of static culture and mounted in the bioreactor, whereas static control samples (n=8) were cultured on the Teflon molds in culture medium with gentle rocking. The maximum strain and frequency of cyclic load was controlled by a custom-designed reciprocating syringe pump, which injected/withdrew culture medium from both ends of the latex tube at the same rate. The strain amplitude was increased incrementally during cyclic stretching (ICS) by adjusting the stroke volume in two equal steps from 5% to 15% over 3 weeks (i.e. set at 5%, 10%, and 15% during weeks 1, 2, and 3, respectively). For all studies, a frequency of 0.5 Hz with sinusoidal wave form was used. The nutrient supply to the VE was delivered by a perfusion loop, which circulated the culture medium through the latex tube, and therefore the VE lumen, at a low flow-rate (10-15ml/min) using a MasterFlex peristaltic pump. The use of a separate loop for nutrient supply allowed for independent change of stretching parameters (frequency and amplitude) without affecting the nutrient transport. The reservoir culture medium in the perfusion loop (250 mL) was changed three times per week.

The circumferential stretch amplitude in the root of the VE was calculated using diameter measurements from laser micrometer and was used as control input parameter. The corresponding average strain in the leaflet was calculated by image analysis of ink

marks on the leaflet surface as they displaced due to the stretching. On a subset of VEs (n=3), four ink dots were placed in the central belly region on each leaflet at approximately equal separation distance and the VE was mounted in the tube. The ink dots were placed such that they formed a square with sides parallel to the circumferential and radial direction of the leaflet (Fig. 1c). The flow circuits were connected to the syringe pump. The laser micrometer and end-on digital camera were mounted such that simultaneous root distension and leaflet images were acquired. For each VE, the lumen diameter required to achieve a root circumferential strain of 5%, 7.5%, 10%, 12.5% and 15% were calculated based on the initial lumen diameter as measured by the laser micrometer. The syringe pump was ramped until the laser micrometer measured the calculated distension for each assigned strain value, paused at maximum distension, and a digital image from the end piece view window was taken (Fig. 1c). Hence for each VE, 6 sets of images were acquired (including un-pressurized, or 0%). The imaging sequence was repeated several times for each VE.

Based on VE mold geometry, the leaflets are at an angle of 42^{o} with respect to the upper root. With the assumption that the leaflet angle does not change during stretching, a head-on image of the angled surface with the ink marks can be used to measure the 2D strain by virtue of geometrical properties of “similar triangles”. For each assigned root strain, pixel distances parallel to the circumferential direction from the edge of one ink marker to the other were measured to record the circumferential displacement denoted as ‘C’. Similarly, the radial displacement was recorded as ‘R’. The true strain (ε) was calculated both directions by defining C_{min} and R_{min} as the displacement at 0% root strain using:

$$\varepsilon_{circ} = \ln\left(C_{\max} / C_{\min}\right) \qquad \varepsilon_{rad} = \ln\left(R_{\max} / R_{\min}\right)$$

The average strains with standard deviations of all measurements are plotted as a function of root circumferential strain in Figure 2.

Cyclic Loading of TEHV root at pulmonary pressures

After cyclic stretching, the latex tube was removed and the VE was cyclically distended (n=2) to pulmonary pressures of 40 mmHg for 1 hour at 0.5 Hz and then pressurized to failure by injecting culture medium at 60 ml/min. During pressurization, both luminal pressure (via an inline pressure transducer (Omega)) and VE diameter (via video recording) were measured. The video was used to measure the VE root diameter and from which the true strain was calculated.

Uniaxial Tensile Testing

VEs were dissected to obtain tissue strips for evaluation of tensile properties. For leaflets, strips were obtained in both the circumferential and radial directions. For the root, one circumferential strip was obtained from both the upper (aortic side) and lower (ventricular side) root sections. The thickness of each strip was measured using a 50 g-force probe attached to a displacement transducer. Tissue strips were placed in compressive grips, attached to the actuator arms and load cell of a Microbionix material testing system (MTS system, Eden Prairie, MN), and straightened with a load of 0.005 N. This position was used as the reference length of each strip. Following 6 cycles of 0-10% strain at 2 mm/min, tissue strips were stretched to failure. True strain was calculated based on the change in the length of the tissue over time. The engineering

stress was calculated as the force divided by the initial cross-sectional area. Young's modulus (E) was determined by regression of the linear region of stress-strain curve. The ultimate tensile strength (UTS) was measured as the peak stress (at tissue failure). Maximum tension and membrane stiffness were calculated by multiplying UTS and E with thickness of the tissue strip.

Polarimetry and Histology

Fiber alignment in the dissected leaflets was measured using polarized light imaging[20]. Samples from the leaflet belly region and root were fixed in 4% paraformaldehyde, infiltrated with a solution of 30% sucrose and 5% DMSO, frozen in OCT (Tissue-Tek), and sectioned into 9 μm cross-sections. Sections were stained with Lillie's trichrome and picrosirius red [10]. Images were taken at 10x magnification using a color CCD camera. For picrosirius red, images were taken with the samples placed between crossed plane polarizers.

Collagen and Cell quantification

The collagen content was quantified with the hydroxyproline assay assuming 7.46 μg of collagen per 1 μg of hydroxyproline [18]. The sample volume was calculated using the measured length, width, and thickness of the strips (as described above in uniaxial testing). Collagen concentrations were calculated as the amount per unit volume in each sample.

DNA content was quantified with a modified Hoechst assay [18]. Cell numbers were obtained from DNA contents assuming 7.6 pg of DNA per cell [18]. Cell

concentrations were calculated as the number of cells per unit volume using the dimensions of the strip.

Statistics

For each group of VEs casted, a subset was randomly chosen as the paired static controls. The mechanical testing data were statistically compared between static control VEs, ICS VEs, and pulmonary valves from Dorset sheep of age 6 months. Statistical differences between groups were determined using one-way ANOVA in GraphPad Prism software for Windows. The Tuckey post hoc analysis was conducted to evaluate significant differences. Statistical differences between groups pooled from multiple castings were assessed using two-way ANOVA with Bonferroni post hoc analysis. A difference between groups is indicated by paired symbols. Any reference to a difference in the Results and Discussion implies statistical significance at the level $p < 0.05$.

4.6: References

1. Vesely I. Heart valve tissue engineering. Circ Res 2005;97(8):743-755.
2. Schoen FJ. Evolving concepts of cardiac valve dynamics: the continuum of development, functional structure, pathobiology, and tissue engineering. Circulation 2008;118(18):1864-1880.
3. Neuenschwander S, Hoerstrup SP. Heart valve tissue engineering. Transpl Immunol 2004;12(3-4):359-365.
4. Hoerstrup SP, Sodian R, Sperling JS, Vacanti JP, Mayer JE, Jr. New pulsatile bioreactor for in vitro formation of tissue engineered heart valves. Tissue Eng 2000;6(1):75-79.
5. Dumont K, Yperman J, Verbeken E, Segers P, Meuris B, Vandenberghe S, et al. Design of a new pulsatile bioreactor for tissue engineered aortic heart valve formation. Artif Organs 2002;26(8):710-714.
6. Hildebrand DK, Wu ZJ, Mayer JE, Jr., Sacks MS. Design and hydrodynamic evaluation of a novel pulsatile bioreactor for biologically active heart valves. Annals of biomedical engineering 2004;32(8):1039-1049.
7. Engelmayr GC, Jr., Hildebrand DK, Sutherland FW, Mayer JE, Jr., Sacks MS. A novel bioreactor for the dynamic flexural stimulation of tissue engineered heart valve biomaterials. Biomaterials 2003;24(14):2523-2532.
8. Boerboom RA, Rubbens MP, Driessen NJ, Bouten CV, Baaijens FP. Effect of strain magnitude on the tissue properties of engineered cardiovascular constructs. Ann Biomed Eng 2008;36(2):244-253.
9. Isenberg BC, Tranquillo RT. Long-term cyclic distention enhances the mechanical properties of collagen-based media-equivalents. Ann Biomed Eng 2003;31(8):937-949.

10. Syedain ZH, Weinberg JS, Tranquillo RT. Cyclic distension of fibrin-based tissue constructs: evidence of adaptation during growth of engineered connective tissue. Proc Natl Acad Sci U S A 2008;105(18):6537-6542.
11. Mol A, Bouten CV, Zund G, Gunter CI, Visjager JF, Turina MI, et al. The relevance of large strains in functional tissue engineering of heart valves. Thorac Cardiovasc Surg 2003;51(2):78-83.
12. Solan A, Mitchell S, Moses M, Niklason L. Effect of pulse rate on collagen deposition in the tissue-engineered blood vessel. Tissue Eng 2003;9(4):579-586.
13. Seliktar D, Nerem RM, Galis ZS. Mechanical strain-stimulated remodeling of tissue-engineered blood vessel constructs. Tissue Eng 2003;9(4):657-666.
14. Seliktar D, Black RA, Vito RP, Nerem RM. Dynamic mechanical conditioning of collagen-gel blood vessel constructs induces remodeling in vitro. Ann Biomed Eng 2000;28(4):351-362.
15. Cummings CL, Gawlitta D, Nerem RM, Stegemann JP. Properties of engineered vascular constructs made from collagen, fibrin, and collagen-fibrin mixtures. Biomaterials 2004;25(17):3699-3706.
16. Mol A, Driessen NJ, Rutten MC, Hoerstrup SP, Bouten CV, Baaijens FP. Tissue engineering of human heart valve leaflets: a novel bioreactor for a strain-based conditioning approach. Ann Biomed Eng 2005;33(12):1778-1788.
17. Kortsmit J, Driessen NJ, Rutten MC, Baaijens FP. Nondestructive and Noninvasive Assessment of Mechanical Properties in Heart Valve Tissue Engineering. Tissue Eng Part A 2008.
18. Robinson PS, Johnson SL, Evans MC, Barocas VH, Tranquillo RT. Functional tissue-engineered valves from cell-remodeled fibrin with commissural alignment of cell-produced collagen. Tissue Eng Part A 2008;14(1):83-95.
19. L'Heureux N, Dusserre N, Marini A, Garrido S, de la Fuente L, McAllister T. Technology insight: the evolution of tissue-engineered vascular grafts--from research to clinical practice. Nat Clin Pract Cardiovasc Med 2007;4(7):389-395.
20. Tower TT, Neidert MR, Tranquillo RT. Fiber alignment imaging during mechanical testing of soft tissues. Ann Biomed Eng 2002;30(10):1221-1233.
21. Dayan D, Hiss Y, Hirshberg A, Bubis JJ, Wolman M. Are the polarization colors of picrosirius red-stained collagen determined only by the diameter of the fibers? Histochemistry 1989;93(1):27-29.
22. Balguid A, Rubbens MP, Mol A, Bank RA, Bogers AJ, van Kats JP, et al. The role of collagen cross-links in biomechanical behavior of human aortic heart valve leaflets--relevance for tissue engineering. Tissue Eng 2007;13(7):1501-1511.
23. Luo XY, Li WG, Li J. Geometrical stress-reducing factors in the anisotropic porcine heart valves. J Biomech Eng 2003;125(5):735-744.
24. Li J, Luo XY, Kuang ZB. A nonlinear anisotropic model for porcine aortic heart valves. J Biomech 2001;34(10):1279-1289.
25. Gao ZB, Pandya S, Hosein N, Sacks MS, Hwang NH. Bioprosthetic heart valve leaflet motion monitored by dual camera stereo photogrammetry. J Biomech 2000;33(2):199-207.
26. He Z, Ritchie J, Grashow JS, Sacks MS, Yoganathan AP. In vitro dynamic strain behavior of the mitral valve posterior leaflet. J Biomech Eng 2005;127(3):504-511.
27. Driessen NJ, Mol A, Bouten CV, Baaijens FP. Modeling the mechanics of tissue-engineered human heart valve leaflets. J Biomech 2007;40(2):325-334.
28. Hoerstrup SP, Sodian R, Daebritz S, Wang J, Bacha EA, Martin DP, et al. Functional living trileaflet heart valves grown in vitro. Circulation 2000;102(19 Suppl 3):III44-49.
29. Sodian R, Hoerstrup SP, Sperling JS, Daebritz SH, Martin DP, Schoen FJ, et al. Tissue engineering of heart valves: in vitro experiences. Ann Thorac Surg 2000;70(1):140-144.
30. Clark RE. Stress-strain characteristics of fresh and frozen human aortic and mitral leaflets and chordae tendineae. Implications for clinical use. J Thorac Cardiovasc Surg 1973;66(2):202-208.
31. Stradins P, Lacis R, Ozolanta I, Purina B, Ose V, Feldmane L, et al. Comparison of biomechanical and structural properties between human aortic and pulmonary valve. Eur J Cardiothorac Surg 2004;26(3):634-639.
32. Isenberg BC, Williams C, Tranquillo RT. Endothelialization and flow conditioning of fibrin-based media-equivalents. Ann Biomed Eng 2006;34(6):971-985.

4.7: Figures

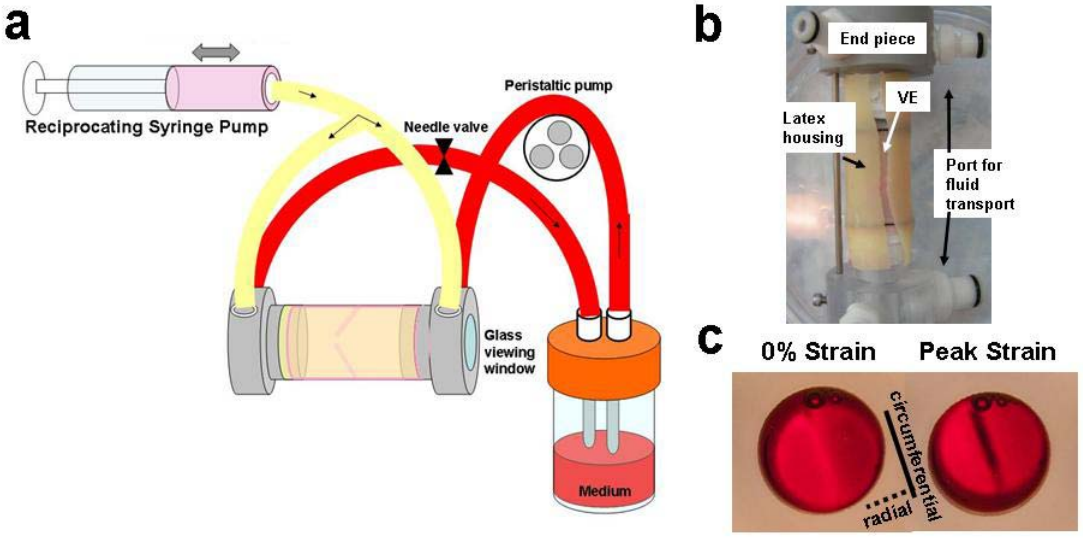

Figure 4-1: (a) Schematic of controlled cyclic stretching TEHV bioreactor, showing the reciprocating syringe pump for cyclic pressurization and stretching of the VE mounted within the latex tube, (b) Image of the bioreactor with the latex housing slit to reveal the VE mounted within and its tie-down to both endpieces, and (c) End-on view of the VE through the glass window of the bioreactor during a stretching cycle, showing the leaflets coapting when the lumen is not pressurized, and separated when the lumen is pressurized and the root and leaflets are stretched.

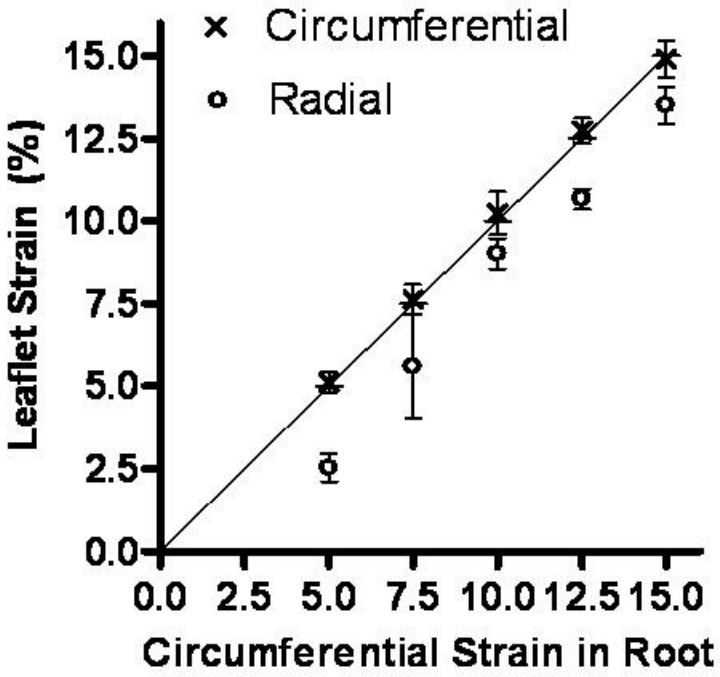

Figure 4-2: Average strain amplitude in circumferential and radial directions in the VE leaflets during cyclic stretching.

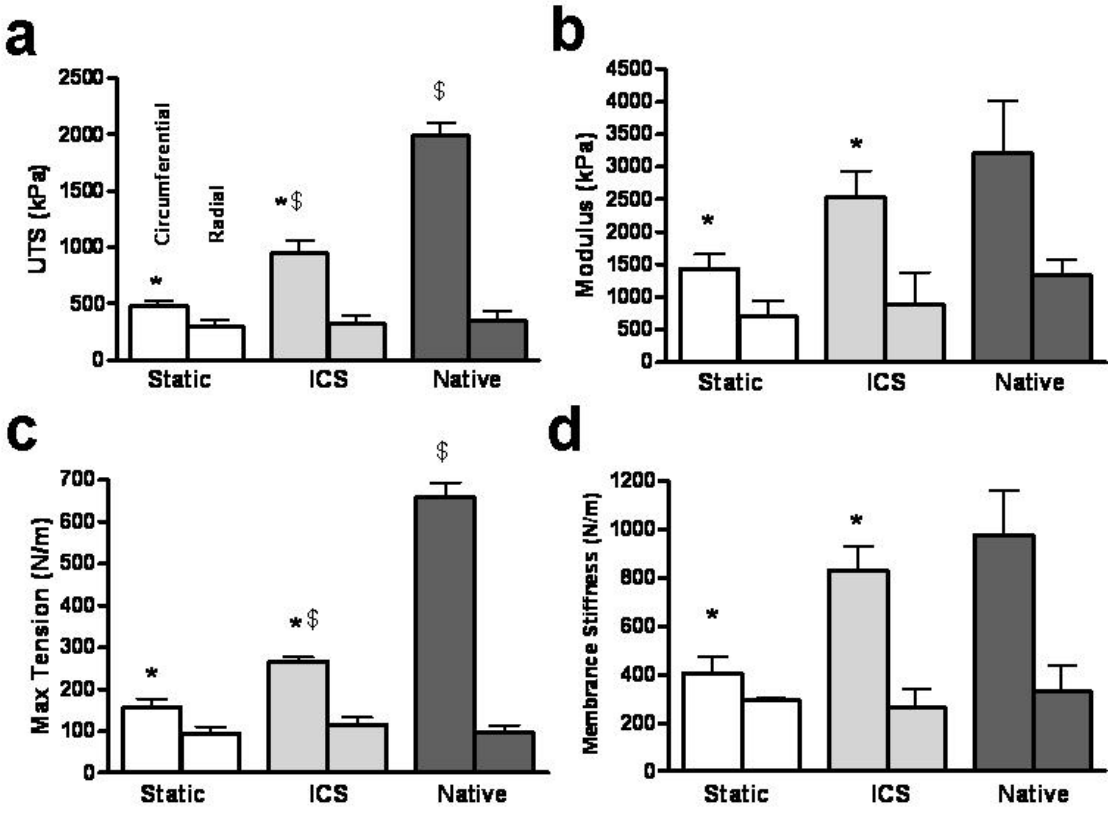

Figure 4-3: Tensile mechanical properties of ICS VE leaflets. (a) Ultimate tensile stress (UTS), (b) Modulus (E), (c) Thickness, (d) Maximum tension, and (e) Membrane stiffness, showing comparison of static control VE, ICS VE, and sheep pulmonary valve leaflets. Differences between groups ($p < 0.05$) are indicated by paired symbols (n=8).

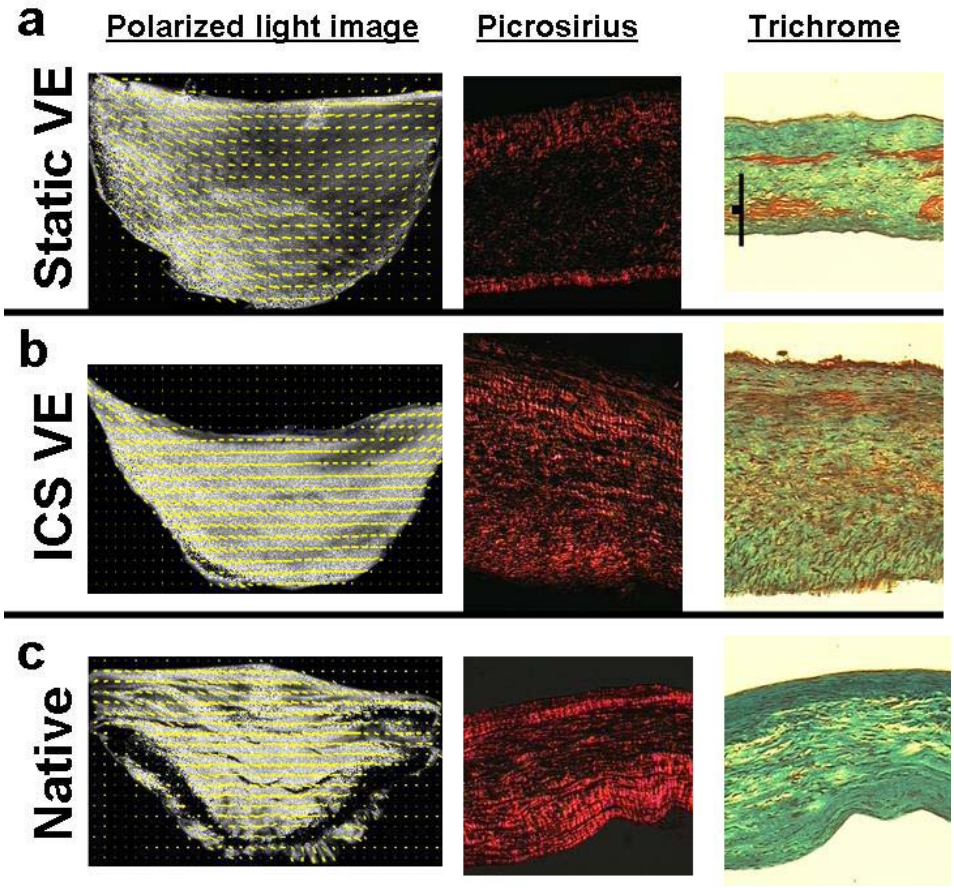

Figure 4-4: Structural comparison of VE and native valve leaflets: (from left to right) polarized light image of a whole leaflet, picrosirius red stain of a cross-section under polarized light, and trichrome stain of a cross-section. The orientations of the yellow segments in the polarized light images correspond to the local average fiber direction, and their lengths are proportional to the local average retardation, a measure of the fiber alignment strength. The pixel gray level is mapped from isotropic (black) to maximally aligned (white). A 200 μm scale bar is shown in trichrome image of a control VE, with all images acquired at the same magnification.

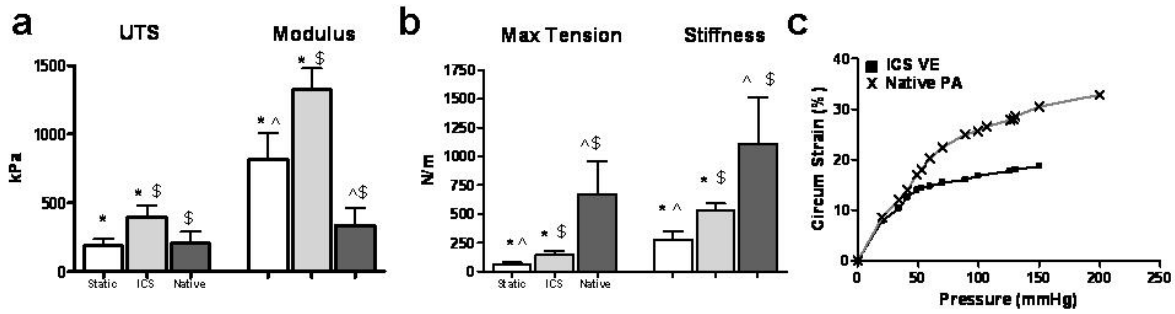

Figure 4-5: Comparison of tensile mechanical properties in the circumferential direction of static and ICS VE root with native pulmonary artery. (a) UTS and modulus, (b) maximum tension and membrane stiffness, and (c) pressure-strain curve of ICS VE *vs.* sheep pulmonary artery (PA).

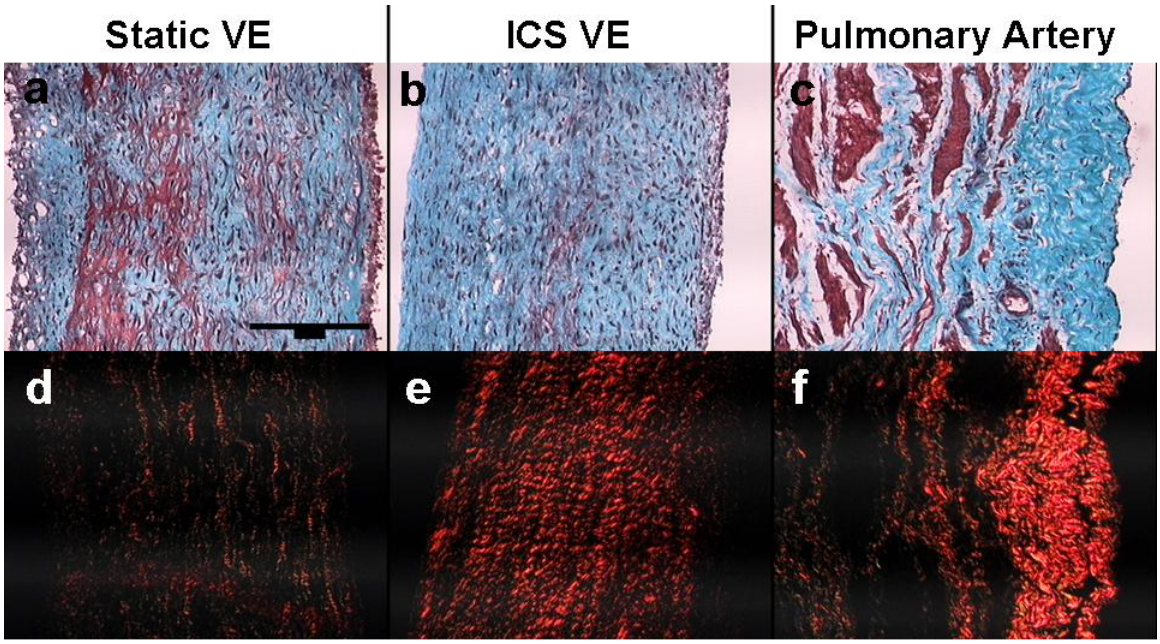

Figure 4-6: Trichrome and picrosirius red staining comparison of VE root with sheep pulmonary artery on cross-section in the circumferential direction. A 200 μm scale bar is shown in trichrome of the control VE, with all images acquired at the same magnification.

Chapter 5: *In vivo* Assessment of a Completely Biological Tissue Engineered Heart Valve

5.1: Summary

A tissue engineered heart valve (TEHV) is the ultimate valve replacement option for the pediatric patients. It has the advantage of being able to grow and remodel with the patient. Biological scaffolds like collagen or fibrin provide the ability to achieve alignment of fibers in the TEHV comparable to that of native leaflets and to create tissue with physiological tensile properties derived solely from cell produced ECM. Using a novel controlled cyclic stretch bioreactor, we have developed a TEHV with tensile stiffness and mechanical anisotropy comparable to that of sheep pulmonary valve leaflets. Fibrin-based TEHV were conditioned *in vitro* in the bioreactor for 3 weeks before implantation in to the pulmonary artery of the sheep. Echocardiogram of the TEHV immediately post-implantation showed a functional valve with normal flow and pressure profile. TEHV were explanted at 4.5 weeks and 8 weeks. At 4.5 weeks, the valve was functional with moderate regurgitation and turbulence. Explanted leaflets showed no change in the tensile properties or thickness, and had increased collagen and elastin concentration. The cell density was comparable between the pre-implanted and explanted TEHV. The lumen of the TEHV root showed evidence of endothelium formation. The tensile properties of the remodeled root were comparable to the native pulmonary artery, with collagen fibers aligned circumferentially. The inner wall of the explanted TEHV root showed vasculature formation, with lumens comparable in size to those found in the native pulmonary artery wall. The *in vivo* study is unprecedented for a TEHV developed with a biological scaffold.

5.2: Introduction

The ultimate evaluation of a tissue engineered heart valve (TEHV) is implantation in to an animal model. To date only the Mayer group has successfully implanted a TEHV, made with a synthetic biodegradable scaffold [1, 2]. The *in vivo* assessment with the PGA scaffold has shown remodeling with collagen and cell content reaching native leaflet values. However, during *in vivo* remodeling, the leaflets tensile properties decreased with time as the stiff PGA scaffold degraded [1]. The PGA scaffold at implant had stiffness several fold higher than the native leaflet, and at explant it was reduced to lower than the native leaflets.

A fibrin gel has stiffness and strength much less than PGA and hence requires extensive *in vitro* tissue development before it attains the tensile properties needed to withstand physiological stresses. The novel cyclic stretch bioreactor system presented in Chapter 4 was utilized in this study to improve the tensile properties of fibrin based TEHV (valve equivalent or VE) prior to implant. After 3 weeks of incubation in the bioreactor, the VE leaflets had similar stiffness and mechanical anisotropy as the sheep pulmonary valve leaflet. The sheep pulmonary artery has been used previously for TEHV implants and provides an appropriate model for assessing the *in vivo* remodeling of the VE.

5.3: Material and Methods

5.3.1: Cell culture

Neonatal human dermal fibroblasts (Clonetics) were maintained in DMEM/F12 culture medium (Gibco) supplemented with 10% FBS, 100 U/ml penicillin, 100 μg/ml streptomycin, and 2.5 μg/ml amphotericin-β. Cells were passaged at 100% confluency and harvested for use at passage 9.

5.3.2: VE preparation and culture

A fibroblast-seeded fibrin gel was formed by adding thrombin (Sigma) and calcium chloride to a mixture of cells in fibrionogen (Sigma) solution in 20mM HEPES-buffered saline. All components were at room temperature. The final concentrations of the suspension were 6.6mg/ml fibrinogen, 1.1 U/ml thrombin, 5.0 mM Ca^{++}, and 500,000 cells/ml. Suspensions were well mixed by pipette action and injected into bi-leaflet VE molds as described previously [3].

After injection of the suspension, the VE molds were placed vertically in an incubator for 30 minutes. After gelation, the outer housing was removed, and the VEs were placed horizontally in culture medium, comprising DMEM supplemented with 10% FBS, 100 U/ml penicillin, 100 μg/ml streptomycin, 2 μg/ml insulin, 50 μg/ml ascorbic acid. Medium was changed 3 times per week and 1 ng/ml TGF-β1 (R&D Systems) was included for the first two to three feedings after casting to promote cell-mediated fibrin compaction. VEs were cultured for 2 weeks on the mold with gentle rocking, after which they were transferred to the cyclic stretch bioreactor. The 2 week static culture allowed for sufficient stiffening and strengthening of the VE to withstand handling during mounting in the bioreactor.

5.3.3: Controlled Cyclic Stretch Bioreactor

The bioreactor is described in details in Chapter 4. In brief, the bioreactor consists of a distensible latex tube, in which the TEHV is mounted, and two flow circuits for controlled stretching and nutrient supply. The maximum strain and frequency of cyclic load was controlled by a custom-designed reciprocating syringe pump, which injected/withdrew culture medium from both ends of the latex tube at the same rate. The nutrient supply to the VE was delivered by a perfusion loop, which circulated the culture medium through the latex tube, and therefore the VE lumen, at a low flow-rate (10-15ml/min) using a MasterFlex peristaltic pump. The use of a separate loop for nutrient supply allowed for independent change of stretching parameters (frequency and amplitude) without affecting the nutrient transport. The reservoir culture medium in the perfusion loop was changed three times per week.

For all studies, a frequency of 0.5 Hz with sinusoidal wave form was used. The circumferential stretch amplitude in the root of the VE was calculated using diameter measurements from laser micrometer and was used as control input parameter. For all studies, a two-step ICD was applied with steps going from 5% to 15%.

To maintain coapting leaflets, Blebbistatin at 10mM was used after 3 weeks of culture for 2-4 days prior to implant in sheep.

5.3.4: Animal Implant Studies

After 5 weeks of *in vitro* culture, VE were implanted inter-positionally in the pulmonary artery of a 6 month old Dorset sheep. All protocols were approved by the Institutional Animal Care and Use Committee (IACUC). The surgeries were performed by the University of Minnesota Experimental Surgical Services (ESS). To facilitate

surgical handling of the VE for implantation a thin non-woven synthetic fabric sleeve (Poly-Lactic acid/Poly-ester) was placed around the VE root. Sheep were placed on by-pass under general anesthesia and the heart was exposed by a left lateral thoracotomy with dissection through the fourth intercostals space. Sheep were given 400 IU/kg heparin during surgery. The inter-thoracic echocardiogram was performed post-implant (within 1 hr) after animals were off by-pass. Post-implantation, animals were given immunosuppressants and continued on heparin. Daily, animals were given Cyclosporine (10mg/kg), Azathioprine (2mg/kg), Methylprednisolone (0.5mg/kg), and Heparin. At 4.5 week, inter-thoracic echocardiogram was performed prior to sacrificing the animal. Additionally for NAVT 8, intercardiac echocardiogram (ICE) was performed which showed end-diastolic pressure gradient indicative of leaflet function.

5.3.5: Uniaxial Tensile Testing

Both *in vitro* and *in vivo* explanted VEs were dissected to obtain tissue strips for evaluation of the tensile properties. For leaflets, strips were obtained in both the circumferential and radial directions. The thickness of each strip was measured using a 50 g-force probe attached to a displacement transducer. Tissue strips were tested in Microbionix material testing system (MTS system, Eden Prairie, MN) to failure. The stress was calculated as the force divided by the initial cross-sectional area. Young's modulus (E) was determined by regression of the linear region of stress-strain curve. The ultimate tensile strength (UTS) was measured as the peak stress (at tissue failure). Maximum tension and membrane stiffness were calculated by multiplying UTS and E with thickness of the tissue strip. For root tissue, circumferential strip were measured in similar method.

5.3.5: Histology

VE samples from leaflet region and root in circumferential direction were fixed in 4% paraformaldehyde, infiltrated with a solution of 30% sucrose and 5% DMSO, frozen in OCT (Tissue-Tek), and sectioned into 9 μm cross-sections. Sections were stained with Lillie's trichrome and picrosirius red stain. Images were taken at 10x magnification using a color CCD camera. For Picrosirius red stain, images were taken with the samples placed between crossed plane polarizers.

5.3.6: Collagen and Cell quantification

The collagen content was quantified with the hydroxyproline assay assuming 7.46 mg of collagen per 1 mg of hydroxyproline [3]. The sample volume was calculated using the measured length, width, and thickness of the strips (as described above in uniaxial testing). Collagen concentrations were calculated as the amount per unit volume in each sample.

DNA content was quantified with a modified Hoechst assay [3]. Cell numbers were obtained from DNA contents assuming 7.6 pg of DNA per cell [3]. Cell concentrations were calculated as the number of cells per unit volume using the dimensions of the strip.

5.3.7: Statistics

The mechanical and biochemical data were statistically compared between *in vitro* VE, *in vivo* VE and native sheep pulmonary valves. Statistical differences between groups were determined using one-way ANOVA in GraphPad Prism software for

Windows. The Tuckey post- hoc analysis was conducted to evaluate significant differences. The difference between groups is shown by paired symbols. Any reference to a difference in the Results and Discussion implies statistical significance at the level $p < 0.05$.

5.4: Results

To date, 10 implant experiments has been performed (acronym 'NAVT' followed by a number). The three successful ones (NAVT 7, 9 & 10) are reported here. In all failed attempts, the animal did not survive longer than 6 hours and the failure mode was either a complication of the implant procedure or mechanical failure of the VE. NAVT 8 survived for 4.5 weeks, however it was the only implant of a tri-leaflet VE and the VE leaflets were not functional in post-implant echo (the leaflets had become adherent to the root). A brief summary of all the implant attempts is given in Table 1.

5.4.1: Leaflet functionality post implant and after 4.5 weeks *in vivo*

Echocardiography conducted on animals (NAVT 7, 9, & 10) post-implant showed coapting valve leaflets with normal physiological flow and pressure profile. Figure 1 shows still image of a VE (NAVT 9) fully opened and closed post-implant from both side and end-on views. There was mild regurgitation through the VE during diastole in the two animals where one leaflet of the pulmonary valve (PV) was removed. Due to the location of the implanted VE (obstructed by lungs),

echocardiograms could not be performed between implant and explant. Two VE were explanted at 4.5 weeks (NAVT 7 and 9). Both VE had functional leaflets, but NAVT 9 had one leaflet half-way torn from the root. Figure 2 shows still image from the echo of NAVT 7. Doppler flow profile showed mild to moderate regurgitation and turbulence. The echocardiogram of NAVT 10 at 8 weeks showed no functional leaflets, which was confirmed upon explant.

5.4.2: Explanted VE leaflets had unaltered tensile mechanical properties

The explanted VE leaflets and root from the NAVT-7 implant are shown in Figure 3. Both leaflets were intact and had a thickness comparable to the native leaflet and the VE at implant (Fig. 3a). The VE root at anastomosis had smooth surface with no indication of reactive or inflammatory tissue (Fig. 3b). A stress-strain curve for the explanted VE leaflet is shown in Figure 4 along with that for a native pulmonary valve leaflet. Figure 5 shows the UTS and modulus of implanted VE, explanted VE and native pulmonary valve leaflets. There was no significant difference in modulus of VEs and pulmonary valve. The UTS was increased for the explanted VE (1115±99 kPa) compared to the implanted VE (822±65 kPa).

5.4.3: Explanted VE leaflets had increased collagen and elastin concentrations

Biochemical analysis showed increased collagen and elastin concentrations in the explanted VE leaflets compared to implant valves. Collagen concentration after *in vivo* increased by 28% to 24±2 mg/ml compared to implanted VE leaflets (19±2 mg/ml). The elastin concentration increased by 73% compared to implanted VE leaflets.

There was no difference in cell concentration of the explanted leaflets compared to implanted leaflets. Trichrome and picrosirius red staining showed collagen bands across the thickness of the explanted VE (Fig. 6).

5.4.4: VE root tissue was compliant and remodeled with evidence of endothelium formation

The explanted VE root was 2-3 mm thick at explant, which included the original engineered tissue of 300-400μm thick with additional reactive tissue grown around the root and supporting polymeric sleeve. The lumen surface showed remodeled collagen with some endothelial cell coverage (Fig. 7). However, the endothelial lining was not fully developed in all regions, especially near the leaflets. Within the root tissue, a micro vasculature was present as observed by vWF staining (Fig. 8). The micro-vessel lumen was comparable in diameter to those in the native pulmonary artery wall. Trichrome and picrosirius red stain showed collagen organized with circumferential alignment (Fig. 8c). The circumferential modulus of the explanted VE root was 222±20 kPa, which was comparable to the sheep pulmonary artery (337±123 kPa). Similarly, the membrane stiffness was comparable between the explanted VE root (863±13 N/m) and the pulmonary artery (1111±405 N/m).

5.5: Discussion

A fibrin-based tissue engineered heart valve provides the means to create a fully biological heart valve replacement. Cells seeded in fibrin gel have been shown to

deposit more collagen and elastin compared to other biopolymers, such as collagen [4, 5], and with cyclic stretching, the tensile and biochemical properties of the growing tissue construct improved [6]. Based on our previous studies with a cyclic distension bioreactor, we have shown improved tensile properties and collagen density in nHDF-seeded fibrin tubular constructs. Hence, a novel bioreactor was design for the VE to impart controlled cyclic stretching of the root and leaflets. The VE were cultured statically for 2 weeks followed by bioreactor conditioning for 3 weeks with incremental strain amplitude cyclic stretching. Following 3 weeks of cyclic stretching, the VE were implanted in the pulmonary artery of 6 month old Dorset sheep.

As cell traction force can compact the fibrin gel, to accommodate for compaction without losing coaptation of the leaflets, the VE mold was designed to allow for casting of leaflets with extended length [3]. During the 3 weeks of culture in the bioreactor, leaflets compaction occurred to the limit for coaptation; hence, Blebbistatin, a myosin inhibitor, was used to reduce compaction of the leaflets. Blebistatin has been shown to reduce compaction of collagen and fibrin gel seeded with dermal fibroblasts [7, 8].

To facilitate suturing of the VE to the native PA, Dacron cuffs were embedded on both ends of the root during casting of the VE [3]. Also to accommodate for surgical handling, a non-woven polymer sleeve was placed over the VE root. This is meant to be a “temporary fix” until an implant method that doesn’t cause significant tissue stretching or greater root tensile strength is achieved.

Three long-term implants were performed, one with the native PV leaflets intact and two with the PV made incompetent by surgically removing one of the pulmonary

leaflets. Post implant, echocardiography was performed on all animals. All implanted VE had coapting leaflets with mild regurgitation but no turbulence. There was some variability in flow profile and acceleration of blood among the animals but in all cases, the right-side of the heart had normal function immediately after implantation with flow and pressures within the physiological range. Figure 1 shows a post-implant echo still images of the leaflets from side and end-on views. To our knowledge, only the fibrin-based VE used in this study has the physiological compliance needed for the leaflet deformation that confer valve function with normal flow and pressure waveform.

All animals were asymptomatic at sacrificed. Two sheeps, one with intact native leaflets (NAVT 7) and one without intact native leaflets (NAVT 9) were explanted at 4.5 weeks. The third animal was sacrificed at 8 weeks (NAVT 10). Figure 3 shows the gross anatomy of the lumen surface and the leaflets of NAVT 7 after 4.5 weeks. The leaflets had comparable thickness to the VE at implantation and native pulmonary leaflets. The root was integrated with the pulmonary artery and the gross surface texture of the VE root was comparable to the lumen of the artery. There was angiogenic response on the lumen surface near leaflets at 4.5 weeks, however at 8 weeks the entire lumen surface had gross texture comparable to native PA. Echocardiography showed minor turbulence in the region near the leaflets, which could have potentially led to clotting or an inflammatory response. One potential way to mitigate this would be by pre-endothelialization of the leaflets and root lumen.

The leaflets and root section were comparable in gross anatomy between the two explants at 4.5 week. However, in the case of the NAVT 9, one of the VE leaflets was torn away from the root half-way. Prior to explants, inter-thoracic echocardiography

was performed on all animals. In all cases, moderate regurgitation and turbulence was observed in the vicinity of the implants. Figure 2 shows functional leaflets at 4.5 weeks for NAVT 7, as observed in echo and regurgitation evident from the doppler flow profile.

Tensile properties of the explanted VE leaflets and root were measured. Figure 4 shows the stress-stain curve of an explanted VE leaflet (NAVT 7) with native sheep pulmonary valve leaflet in the circumferential direction (commissure-to-commissure direction). The explanted VE failed at a lower break force compared to the native tissue, which is shown in Figure 5b by the UTS comparison, since the thickness of the explanted VE leaflets was also comparable to the native pulmonary leaflets (Fig. 5a).. However, the stress-strain curve was comparable between the native and explanted VE leaflets. This is indicated by the comparable modulus of the leaflets (Fig. 5c).

Biochemical analysis showed increased collagen and elastin concentrations in the explanted VE tissue compared to the VE at implantation. The modest increase in the collagen did not have any effect on the tensile properties. However, it is noteworthy that no massive inflammatory response or tissue degeneration was seen, which would have led to a major changes in the tensile properties. The cell concentration was comparable between the implanted and explanted VE leaflets, though it is unknown what percentage of the original nHDF were still present and if any host cells had infiltrated. The cells were still homogeneously distributed across the thickness of the leaflets as shown in Figure 7. Trichrome and picrosirius red staining (Fig. 7) also showed collagen bands interspersed across the thickness of the leaflets from both VE explanted at 4.5 weeks.

There was outgrowth of reactive tissue on root with thickness of 3mm. This could be associated with reaction to PLA that was used as a support or an inflammatory response to the VE root tissue. Even though there was significant thickening of the root, the UTS and modulus of the VE root at explant were comparable to the native pulmonary artery values. Trichrome stains showed collagen bands organized with circumferential alignment in the root wall and formation of a micro-vasculature (Fig 8, Fig 9a). The micro-vessel lumens were of comparable size to one found in the pulmonary artery wall, as identified by vWF staining (Fig. 9). The lumenal surface of the VE showed formation of an endothelial lining by vWF staining (Fig. 8b). The endothelium was not observed in all regions and was dominant near the proximal and distal ends of the VE root. This could potentially be due to endothelial cells migrating from the adjacent pulmonary artery. However, due to the short implant duration or turbulence near the leaflets the endothelial coverage was not present on or around the leaflets.

The functional leaflets with comparable thickness and mechanical properties represents major progress in the development of a fibrin based TEHV. Considering that the tensile properties and cellularity of the implanted VE are comparable to native pulmonary valves, major remodeling should not be expected in 4.5 weeks *in vivo*.

This study is unprecedented in terms of a successful *in vivo* assessment of a completely biological heart valve (replacement fabricated from a bio-polymeric scaffold and cells). This study demonstrates our ability to create a functional VE that can withstand physiological conditions for an extended period of time without significant change in biochemical or tensile properties. The implanted and explanted VE leaflets

both had tensile properties comparable to native pulmonary valve leaflets, which has not been accomplished with synthetic polymer scaffolds. The study will also lead to a better understanding of *in vivo* remodeling of the engineered construct and further advance the development of the VE for human use.

5.6: References

1. Hoerstrup SP, Sodian R, Daebritz S, Wang J, Bacha EA, Martin DP, et al. Functional living trileaflet heart valves grown in vitro. Circulation 2000 Nov 7;102(19 Suppl 3):III44-49.
2. Sodian R, Hoerstrup SP, Sperling JS, Daebritz SH, Martin DP, Schoen FJ, et al. Tissue engineering of heart valves: in vitro experiences. The Annals of thoracic surgery 2000 Jul;70(1):140-144.
3. Robinson PS, Johnson SL, Evans MC, Barocas VH, Tranquillo RT. Functional tissue-engineered valves from cell-remodeled fibrin with commissural alignment of cell-produced collagen. Tissue Eng Part A 2008 Jan;14(1):83-95.
4. Grassl ED, Oegema TR, Tranquillo RT. Fibrin as an alternative biopolymer to type-I collagen for the fabrication of a media equivalent. Journal of biomedical materials research 2002 Jun 15;60(4):607-612.
5. Long JL, Tranquillo RT. Elastic fiber production in cardiovascular tissue-equivalents. Matrix Biol 2003 Jun;22(4):339-350.
6. Syedain ZH, Weinberg JS, Tranquillo RT. Cyclic distension of fibrin-based tissue constructs: evidence of adaptation during growth of engineered connective tissue. Proceedings of the National Academy of Sciences of the United States of America 2008 May 6;105(18):6537-6542.
7. Abe M, Ho CH, Kamm KE, Grinnell F. Different molecular motors mediate platelet-derived growth factor and lysophosphatidic acid-stimulated floating collagen matrix contraction. The Journal of biological chemistry 2003 Nov 28;278(48):47707-47712.
8. Grinnell F, Ho CH. Transforming growth factor beta stimulates fibroblast-collagen matrix contraction by different mechanisms in mechanically loaded and unloaded matrices. Experimental cell research 2002 Feb 15;273(2):248-255.

5.7: Figures

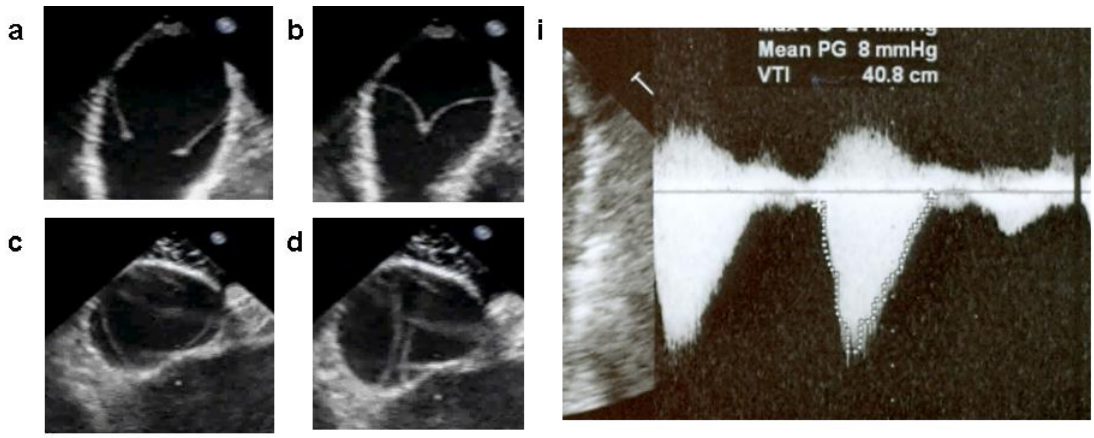

Figure 1: Post implant echocardiogram images of NAVT 9 showing leaflets in open (a&c) and close (b&d) positions from side (a&b) and end-on view (c&d). i. Doppler flow profile

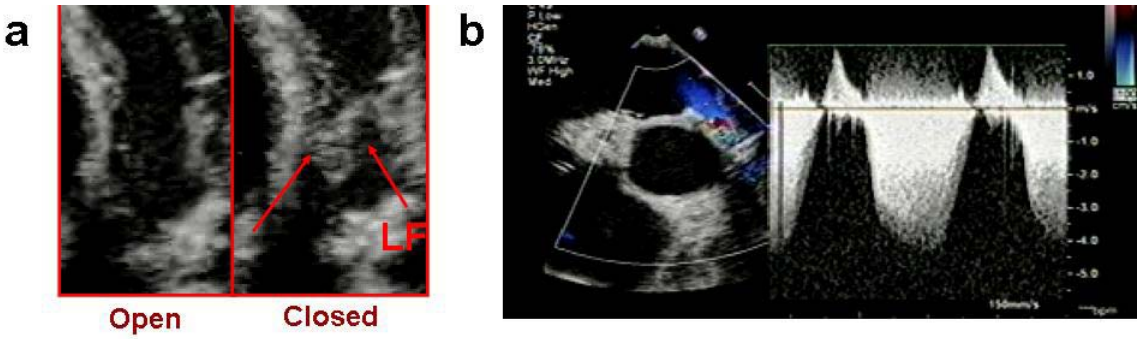

Figure 2: Echocardiogram images at 4.5 week of NAVT 7. a. valve leaflets in opened and closed position, b. Doppler flow profile

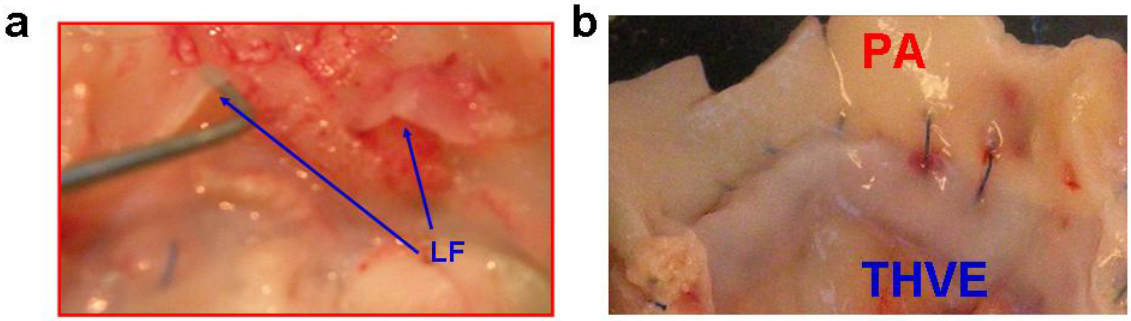

Figure 3: Gross images of explanted VE (NAVT 7), a. Surface view showing intact leaflet (LF), b. Surface view of proximal end of VE root and suture line with native pulmonary artery.

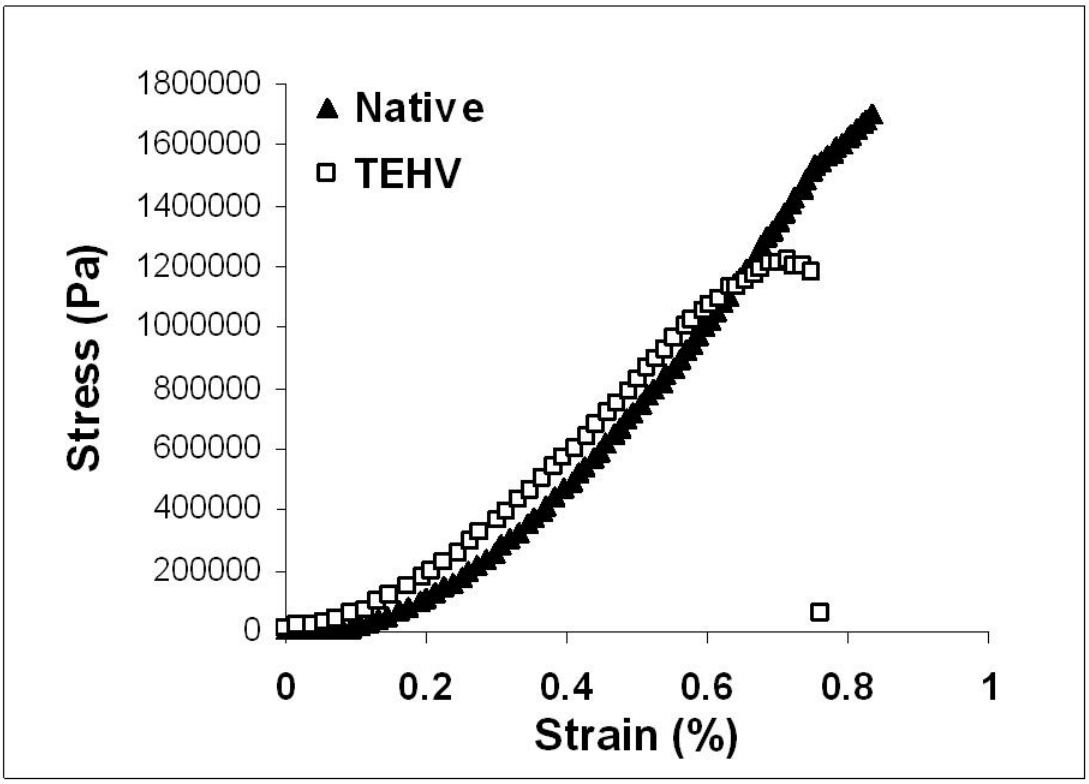

Figure 4: Stress-strain profile comparison of explanted VE leaflet with native pulmonary valve leaflet.

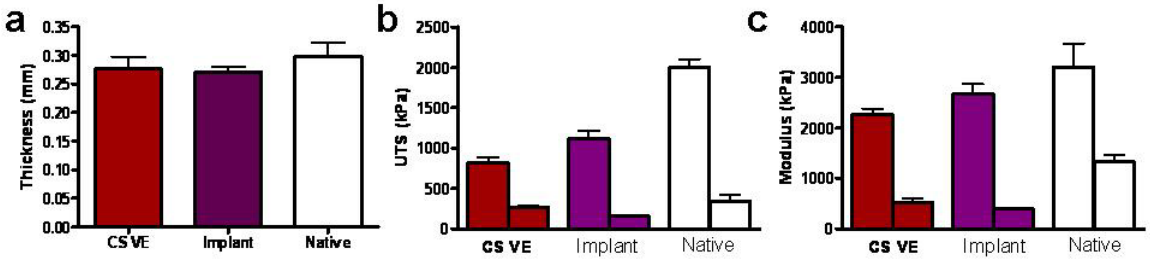

Figure 5: Tensile mechanical properties of explanted VE (Implant) in comparison to properties of paired VE at implantation (CSVE) and native pulmonary leaflet. a. thickness, b. UTS and c. modulus.

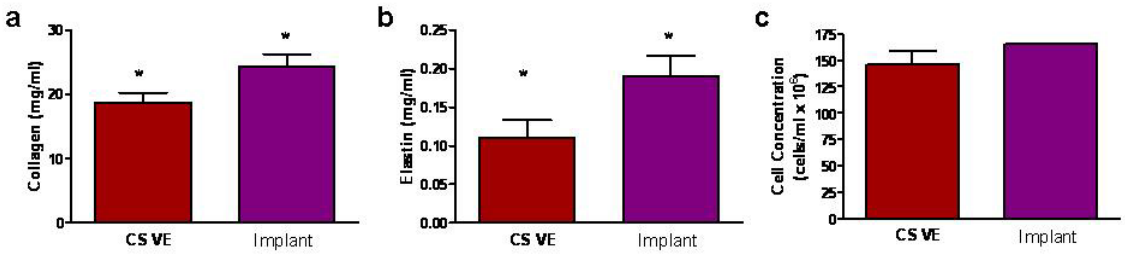

Figure 6: Biochemical analysis of explanted VE with *in vitro* VE. a. Collagen concentration, b. Elastin concentration and c. cell concentration

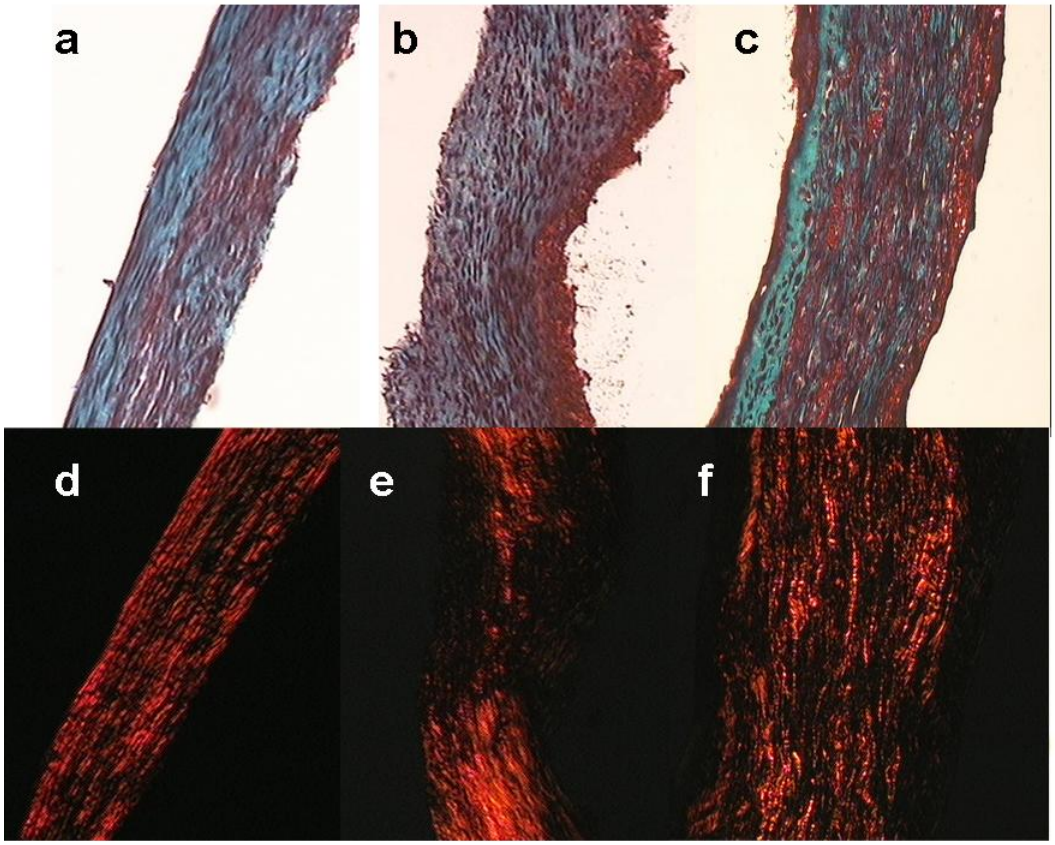

Figure 7: Trichrome and Picrosirius red stained cross-section of paired implanted VE (a&d), explanted VE at 4.5 weeks from sheep with intact native leaflets (NAVT 7 b&e) and sheep without native leaflets intact (NAVT 9 c&f).

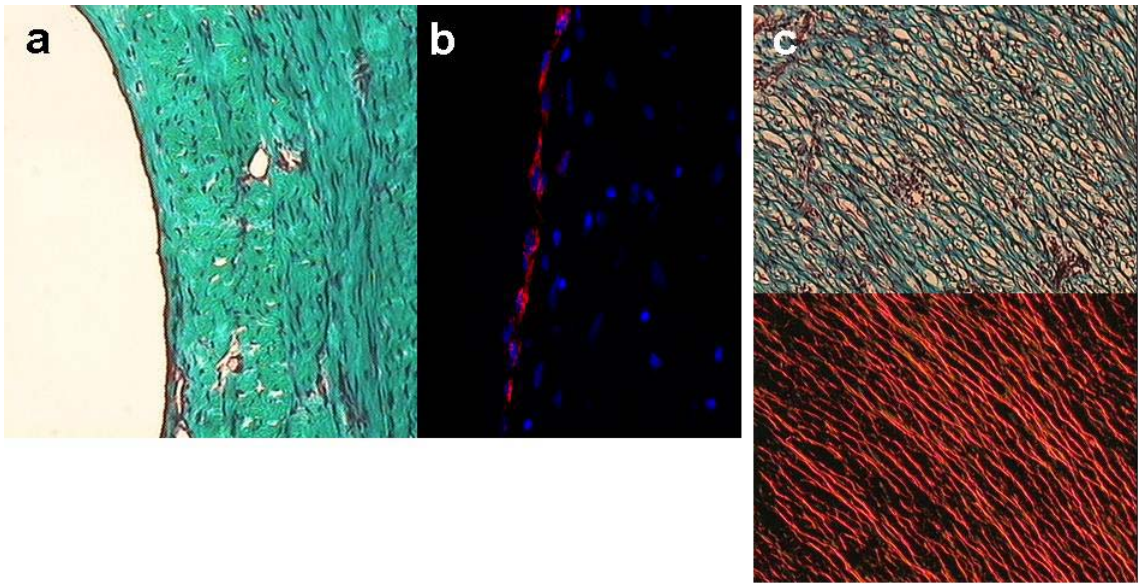

Figure 8: Lumen surface of explanted VE root at 4.5 week NAVT 9, a. Trichrome stain, b. vWF immuno staining (red) with DAPI cell nuclei (blue) and c. Trichrome and picrosirius red stain of collagen fibers aligned in circumferential direction inside the wall of VE root.

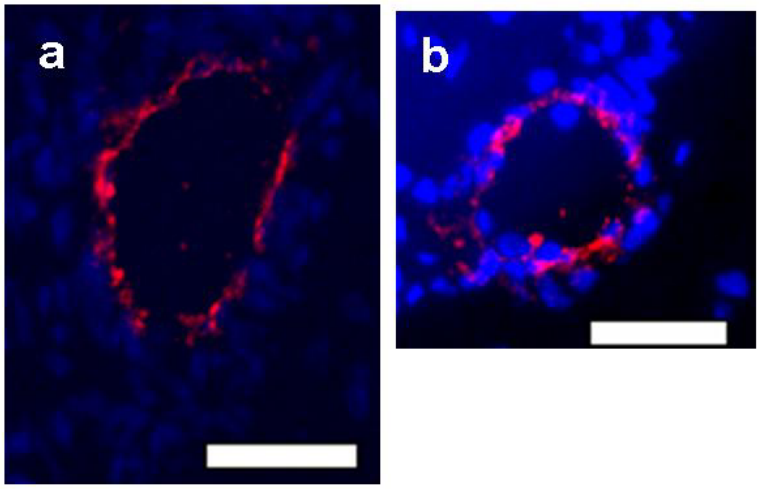

Figure 9: Vasculature lumen inside the wall of a. VE root and b. native pulmonary artery stained with vWF (red) and DAPI cell nuclei (blue).

Sheep Implant Summary

Implant ID	Date of Implant	Implant Mode	Outcome
NAVT 1	2-01-07	VE inside Pulmonary Artery (PA)[1]	No Echo, Animal died for 6 hrs. Explant had torn root from Dacron cuff
NAVT 2	3-13-7	VE inside PA[1]	Failed Surgery
NAVT 3	4-13-07	VE inside PA[1]	Echo showed one torn leaflet post-implant, sheep died 4 hrs post-implant. Explant showed inverted root torn from Dacron cuff.
NAVT 4	5-20-08	VE inside PA	Root folded inside PA causing restriction of flow, sheep died 3 hrs post implant
NAVT 5	8-13-08	Interpositional implant	VE failed upon implant, proximal end constricted by sutures
NAVT 6	9-05-08	Interpositional implant	VE failed upon implant, VE root thinner than normal
NAVT 7	9-29-08	Root sleeved, PV leaflet intact	Echo showed coapting leaflets at implant, Explant at 4.5 week with both VE leaflets intact
NAVT 8	12-01-08	Trileaflet valve[2], Root sleeved, one PV leaflet removed	Echo showed no functional leaflets. Explant at 4.5 week
NAVT 9	1-23-09	Root sleeved, one PV leaflet removed	Echo showed coapting leaflets at implant, Explant at 4.5 week with one VE leaflet partially detached from root
NAVT 10	1-26-09	Root sleeved, one PV leaflet removed	Echo showed coapting leaflets at implant, Explant at 8 week with only one over-compacted leaflet

1: Static cultured VE (VE fabricated led by Paul Robinson).
2: Only trileaflet implant, used after initial two bi-leaflet VE failed to implant correctly using a paneled sleeve.

Table 1: Summary of VE implant attempts to date in sheep pulmonary artery of TEHV

Chapter 6: Controlled Compaction of Cell Seeded Fibrin Constructs

6.1: Summary

Tissue engineering based on fibrin as a scaffold has the advantage of creating a completely biological graft via fibrin inducing its cellular remodeling. Cells seeded in fibrin gel can compact the gel and with appropriate mechanical constrains induce alignment of the fibers. This phenomenon has been used to induce circumferential alignment in the leaflets of the TEHV. However, as gel compaction depends on cells retraction force and the surrounding matrix stiffness, cells can over-compact the fibrin gel during remodeling. In the case of TEHV, the valve leaflets can compact beyond the point of coaptation, which is catastrophic to valve function. Several approach have been proposed to control the compaction of the fibrin gel. Here, two different approaches are presented, one at the cellular level and another at the matrix level. The first approach utilizes inhibition of cellular traction by using the myosin blocker Blebbistatin and the Rho dependent kinase blocker 'Y-27632'. The second approach at the matrix level is by photo-cross-linking the cell seeded fibrin gel using Ruthenium as a catalyst.

Blebbistatin and Y-27632 were effective in reducing the compaction of the fibrin gel seeded with nHDF in tubular constructs; however, both drugs also negatively affected cell proliferation and collagen deposition. Blebbistatin was more potent, and the effects lasted more than 72 hrs in monolayer culture. In tubular constructs, Y-27632 had less detrimental effects on the collagen production and cell proliferation compared to Blebbistatin. The study showed that pharmacological drugs can be used to prevent cellular traction without toxic effects on cells, but can inhibit remodeling of the fibrin gel into tissue.

The second approach was investigated by cross-linking the tyrosine phenyl groups in the fibrin protein utilizing Ruthenium as a catalyst. The cross-linking was

effective in increasing the initial stiffness of the fibrin gel by 93% without any cell death. In long-term culture of cross-linked tubular constructs there were no effects on cell proliferation and ECM deposition between cross-linked and control samples. The cross-linked samples compacted 4-6 fold less than un-treated controls. This study showed that photo cross-linking is a viable option to stiffen the fibrin matrix and reduce cellular traction of the fibrin gel, which can allow for longer incubation period and more tissue growth without compaction below a useful size.

6.2: Introduction

Fibrin gel is used as a tissue engineering scaffold for its good cell compatibility, the ability to mold into desired shape, and its compaction leading to alignment of the fibers (1). In the development of the tissue engineered heart valve (TEHV), by constraining the fibrin gel scaffold, circumferential alignment can be achieved in the valve leaflets, which then guides the cell-deposited ECM to align with the fibrin fibers (2). Over time as cells deposit stiffer extracellular matrix (ECM) proteins like collagen, the cell induced traction would be minimized. However, due to slow remodeling (slow stiffening) of the fibrin gel, effects of over-compaction is problematic with long-term incubation, which is required to achieve the mechanical properties to withstand physiological forces.

Several approaches have been developed to reduce/control the compaction of cell-seeded fibrin gel either by reducing the cell's ability to contract matrix, inhibiting enzymes to reduce fibrin matrix degradation, or stiffening the initial fibrin matrix. Aprotinin and ε-aminocaproic acid have been used to prevent plasmin and MMP mediated degradation of the fibrin; however at low dose they are not very effective and at high dose they inhibit cell proliferation and collagen production (3).

The cell's contractile ability can be inhibited by adding actin, myosin or Rho kinase inhibitors (4). Blebbistatin has been investigated as a myosin blocker for fibroblasts in fibrin gel and shown to reduce compaction of the gel by inhibiting cell's traction (5). Blebbistatin works by binding to large cleft in the motor domain (50 kDa Cleft), which opens and closes during the contractile cycle (6). Similarly, Y-27632 [(+)-(R)-*trans*-4-(1-aminoethyl)-*N*-(4-pyridyl)cyclohex-anecarboxamide dihydrochloride], a

drug that inhibits the Rho-associated protein serine/threonine kinase (ROCK) family of protein kinases has been shown to reduce cell traction force and compaction of the collagen gel (5, 7, 8). Blebbistatin and Y-27632 were shown to be effective in preventing compaction of the fibrin gel (7, 8), however no studies to date have investigated the effects of these drugs on long-term cell proliferation and ECM deposition. Hence, we conducted a study with Blebbistatin and Y-27632 to investigate their long-term effects on remodeling of fibrin gel seeded with nHDF in the form of tubular constructs.

Since enzyme inhibitors like ACA and cellular inhibitors like Blebbistatin can affect the cell's ability to produce ECM proteins, stiffening the initial fibrin gel has been considered an alternate option for reducing gel compaction. Though fibrin gel stiffness can be increased by increasing the density of fibrin fibers, previous research (3, 9) has shown this to also reduce the cell's ability to remodel the fibrin and achieve desirable tensile properties (3, 9). Another approach to stiffen the fibrin network is to cross-linking the fibrin fibrils. Previous research in our lab has used Factor XIII (involved in blood clotting) and other transglutanimases to cross-link fibrin. They were successful in increasing the initial stiffness of the fibrin gel; however, due to the expensive cost and only modest increase in stiffness, this was not pursued. Another approach to cross-link fibrin involves covalently linking tyrosine residue that are abundant in two of the three protein chains in fibrinogen (β-chain = 4.9%, γ-chain =5.6%) (10). The chemistry involves ruthenium trisbypyridyl chloride $[Ru(II)(bpy)_3]^{2+}$ as a catalyst which act as an electrophile to remove electrons, which is energized by blue light absorbed by the tyrosine phenyl group. The reactive tyrosine radical can then

react with another tyrosine phenyl group to create a covalent di-tyrosine bond, with sodium persulfate (SPS) acting as an electron donor (11). The experiments were performed to access toxic effects of ruthenium and sodium persulfate on cell-seeded fibrin tubular constructs and the effects on long-term remodeling during static and cyclic distension culture (12, 13).

6.3: Blebbistatin and Y-27632 effects on compaction of fibrin gel

6.3.1: Material and Methods

6.3.1.1: Cell culture

Neonatal human dermal fibroblasts (HDFs, Clonetics) were maintained in DMEM/F12 culture medium (Gibco) supplemented with 10% FBS,100 U/ml penicillin, 100 μg/ml streptomycin, and 2.5 μg/ml amphotericin-β. Cells were passaged at 100% confluency and harvested for use from passage 7-9.

6.3.1.2: Monolayer culture and migration assay for nHDF cells

To qualitatively observe the effects of Blebbistatin and Y-27632 on nHDF morphology and migration on tissue culture plastic, cells were plated and incubated for 48 hrs in the cell culture medium. For a migration assay, a scrap of 100 μm was created in each well and monitored every 4 hours over 72 hrs after supplemented with 20μm blebbistatin or 10 μM Y-27632. Cell morphology was captured using an Olympus

microscope under transmitted light using 20x objective lens and black-in-white ccd camera.

6.3.1.3: Tubular construct (TC) preparation and culture

A cell-seeded fibrin gel was molded by mixing cells suspended in DMEM into a solution of bovine fibrinogen (Sigma) in 20 mM HEPES-buffered saline. A mixture of bovine thrombin (Sigma) and calcium chloride in DMEM was then added to the fibrinogen/cell mixture. The final concentrations of the cell suspension were 6.6 mg/ml fibrinogen, 0.4 U/ml thrombin, 3.6mM Ca^{2+}, and 500,000 cells/ml. Suspensions were well-mixed by pipette action and injected into tubular molds. The resulting TC had initial length of 8 cm, inner lumen diameter of 2 mm, and outer diameter of 8 mm. Constructs were cultured in DMEM supplemented with 10% FBS, 100 U/ml penicillin, 100 μg/ml streptomycin, 2 μg/ml insulin, 50 μg/ml ascorbic acid, 2.5 μg/ml ε-amphotericine-β, and 1 ng/ml TGF-β. At each feeding, 70% of the medium was changed 3 times per week

6.3.1.4: Blebbistatin and Y-27632 treatment of TC

Drugs were introduced to a sub-set of TC after 11 days of culture. This time-point was determined based on previous experiments that showed rapid compaction beyond 2 weeks of culture without drug treatment. Blebbistatin (B) (Sigma EI-315) was used at 20 μM and Y-27632 (Y) (Sigma Y0503) at 10 μM. A subset was incubated with both drugs (B+Y). The same concentrations were used for the monolayer culture and TC studies. After harvest, each construct was divided into four equal-length sections

and then slit longitudinally to form four tissue strips, one for uniaxial tensile testing followed by biochemical analysis, and the others for western blotting, DNA quantification, and histology.

6.3.1.5: Uniaxial Tensile Testing

One tissue strip from each construct was tested for tensile properties in the circumferential direction. The thickness of each strip was measured using a 50 g-force probe attached to a displacement transducer. Tissue strips were placed in compressive grips, attached to the actuator arm and load cell of a Microbionix material testing system (MTS systems) and straightened with a load of 0.005 N. This position was used as the reference length of the strip. Following 6 cycles of 0-10% strain at 2 mm/min, strips were stretched to failure at the same rate. True strain was calculated based on the change in length of the tissue over time. The stress was calculated as force divided by the initial cross-sectional area. Young's modulus (E) was determined by linear regression of the linear region of the stress-strain curve just prior to failure.

6.3.1.5: Collagen and Cell quantification

Collagen content was quantified with the hydroxyproline assay assuming 7.46 mg of collage per 1 mg of hydroxyproline (2). Tissue strip volume was calculated using the measured length, width, and thickness of the strips (as described above in uniaxial testing). Collagen concentrations were calculated as the amount per unit volume in each strip.

DNA content was quantified with a modified Hoechst assay (2). Cell numbers were obtained from DNA contents assuming 7.6 pg of DNA per cell. Cell concentrations were calculated as the number of cells per unit volume using the dimensions of the strip.

6.3.2: Results

6.3.2.1: Cell morphology and migration assay of Blebbistatin and Y-27632 treated nHDF

nHDF were plated on the tissue culture plastic and incubated for 48 hrs prior to drug treatment. Cell migration and morphology were qualitatively assessed. Figure 1 shows time-lapse images of cells migrating into the scrapped region over 72 hrs. The cell migration was very similar regardless of the drug treatment. At 72 hrs, a live/dead assay was conducted on all groups and no difference was found between the control and the drug treatment groups (Fig. 2). Cell morphology was similar for the Y-27632 treatment compared to the control group; however, for Blebbistatin and B+Y, the cells exhibited a less elongated morphology, indicating drug effects were present after 72 hrs. Cell proliferation was quantified using a DNA assay and showed that both Blebbistatin and Y-27632 inhibited cell proliferation compared to the control group; however, the effect was more significant with Blebbistatin compared to Y-27632 (Figure 3).

6.3.2.2: Blebbistatin and Y-27632 reduce TC compaction

TC were incubated under static culture conditions for 11 days before Blebbistatin and Y-27632 were introduced. By day 11, TC had compacted to 50% of

initial length. After the drugs were introduced, TC length was measured periodically (Figure 4). Blebbistatin completely abolished further compaction. Y-27632 initially abolished compaction but TC gradually compacted to 12.5% of initial length, which was still larger than for the control (4% of initial length).

6.3.2.3: Blebbistatin and Y-27632 inhibit cell proliferation with Blebbistatin reducing collagen deposition

Blebbistatin was most effective in inhibiting the compaction of the fibrin gel. However, it also inhibited cell proliferation and collagen deposition. Figure 5 shows the thickness, mechanical properties (UTS and modulus), cell, collagen and protein concentration at 3 weeks (10 days of drug treatment). The lower collagen concentration in the Blebbistatin group correlated with weaker tensile mechanical properties. TC treated with Y-27632 had the same collagen concentration and the tensile properties as the control. The B+Y group was comparable to the Blebbistatin group, indicating that Blebbistatin dominated the effects of the combined drug treatment.

6.3.2: Discussion

Over-compaction of the remodeling fibrin gel can lead to non-coapting leaflets and regurgitation of the TEHV, which are highly undesirable. Since compaction is mediated by the nHDF, compaction can be controlled by inhibiting cell traction forces. Blebbistatin (a myosin blocker) and Y-27632 (a Rho-dependent kinase inhibitor) have been shown to prevent cell-mediated compaction of fibrin and collagen gels (4, 5, 7). However, there are no reports of the effects of Blebbistatin and Y-27632 on cell proliferation and ECM deposition, which are critical for tissue engineering.

The concentrations of Blebbistatin and Y-27632 used in these studies were based on the effective concentrations used previously (4, 5, 8). Prior to use in TC, toxicity and cell motility effects were evaluated by migration assay of a scrapped nHDF monolayer on tissue culture plastic. Both Blebbistatin and Y-27632 reduced elongation 30 mins after the treatment. Over 72 hrs, the cell migration on tissue culture plastic was comparable. Y-27632-treated cells had normal cell morphology after 72 hrs, indicating drug effects to be suppressed; however, the rounder cells were still present in the Blebbistatin-treatment group (Fig. 1). Live/Dead assay showed no cell death and comparable morphology for Y-27632-treated cells and the control cells (Fig. 2). DNA quantitation showed both Blebbistatin and Y-27632 inhibited normal cell proliferation, with the difference being more prominent for Blebbistatin (Fig. 3). The results showed that Blebbistatin at 20μM and Y-27632 at 10μM were not toxic and had the typical effect on cell morphology as reported in literature (4, 5, 8). Further experiments were conducted with TC using the same concentration of drugs from the monolayer experiment.

In the 2 mm lumen diameter TC, it was commonly observed that after 2 weeks of culture, the rate of axial compaction increases significantly; hence an 11 day time-point was chosen to treat TC with Blebbistatin and Y-27632 to evaluate their effects on the compaction. Both Blebbistatin and Y-27632 inhibited further axial compaction of the TC (Fig. 4). However, in the case of Y-27632, the TC gradually compacted down to 88% of initial length compared with 96% for the control TC. For Blebbistain, there was no further compaction once the drug was introduced, indicating a much stronger and permanent effect. However, Blebbistain also greatly reduced cell proliferation and

collagen deposition (Fig. 5). Y-27632 had no effect on collagen deposition but inhibited cell proliferation. The cell proliferation data in TC for different drugs treatments was comparable to the monolayer culture (Fig. 2&5).

The TC study showed that Blebbistatin is effective in inhibiting cell-mediated compaction of the fibrin gel without being toxic to the cells. Though it can not be used for continuous culture of the fibrin-based tissue engineered constructs during the prolonged remodeling phase, the drug can be effectively used to inhibit over-compaction in a matured construct, as used for maintaining VE coaptation after 5 week of culture untill implantation in the sheep (presented in chapter 5). Y-27632 is more desirable for use during fibrin remodeling/tissue maturation as it slows compaction without influencing the collagen deposition or mechanical properties of TC, unfortunately it is a relatively expensive drug and effects on inhibition of compaction seems to mitigate over time.

6.3.4: Figures

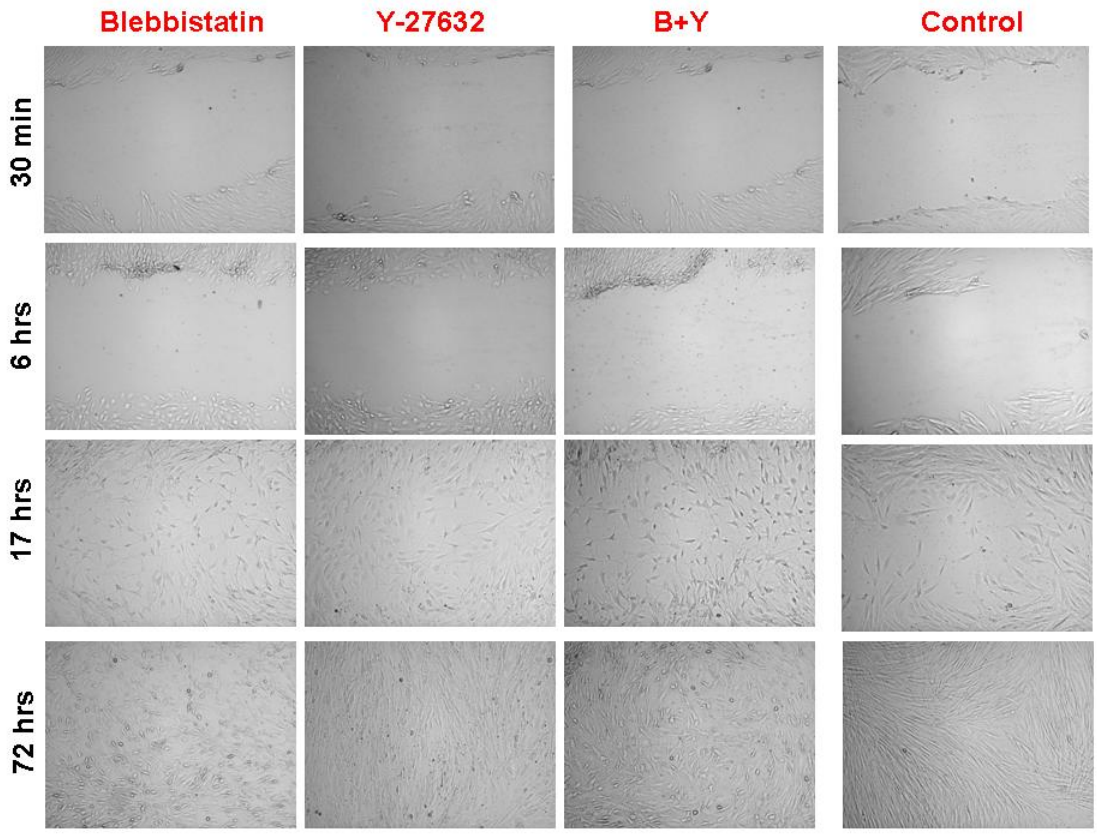

Figure 6-1: **Time-lapse images of nHDF on tissue culture plastic treated with 20 μM Blebbistatin, 10 μM Y-27632, or both (B+Y), compared to untreated control cells.**

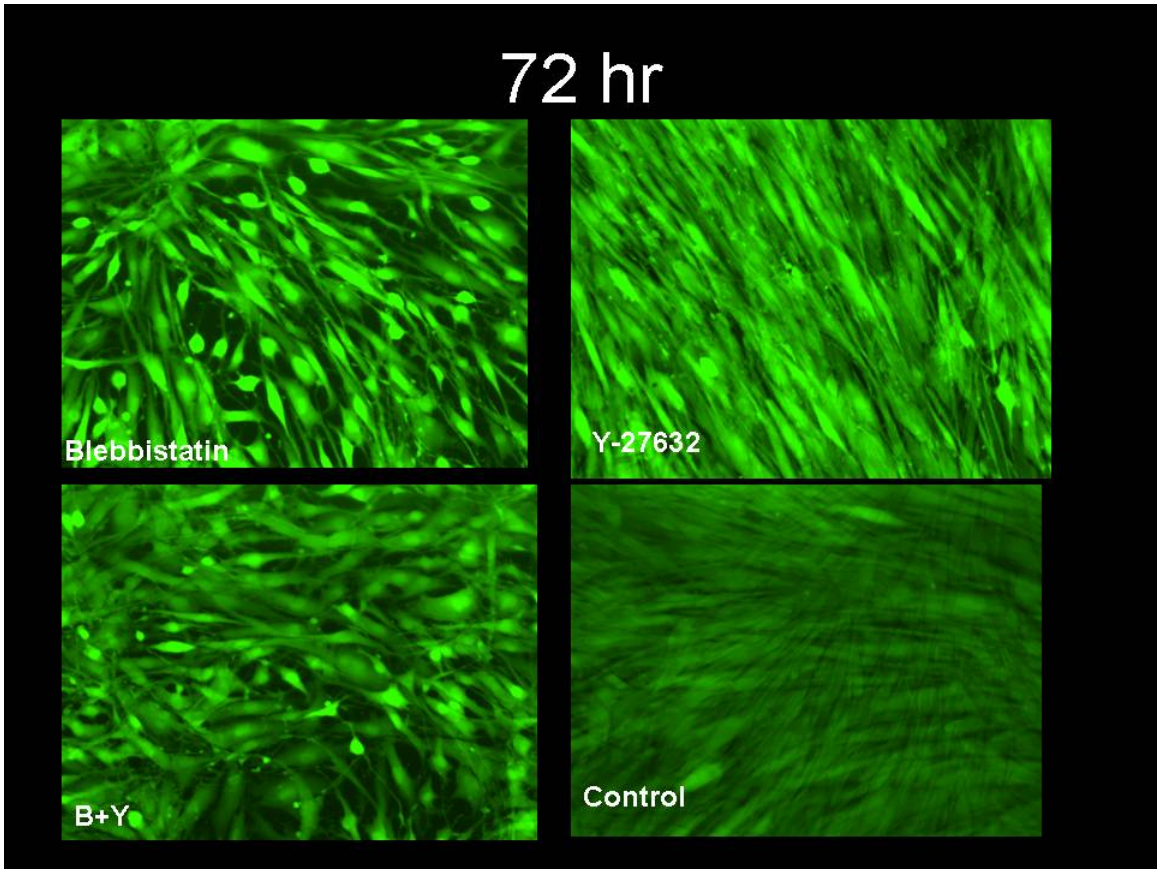

Figure 6-2: **Calcein A staining (for live cells) of Blebbistatin, Y-27632, and B+Y treated cells after 72 hrs of drug treatment.**

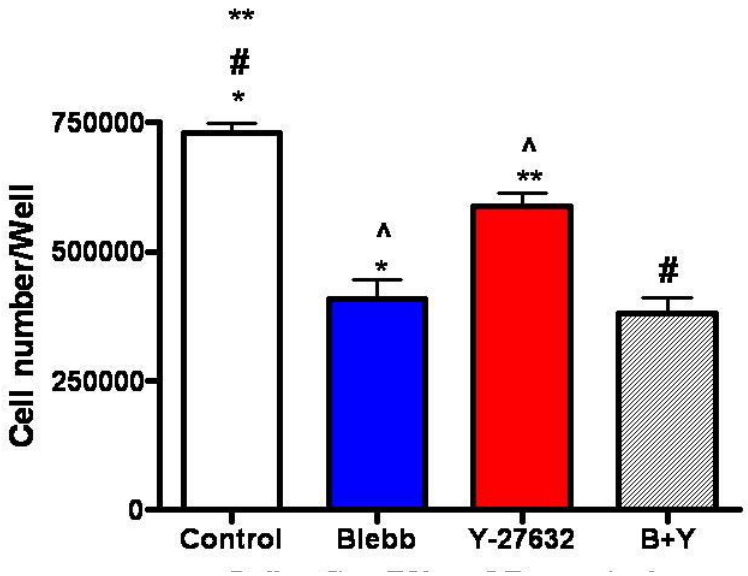

Figure 6-3: **Total cell number on tissue culture plastics after 72 hrs treatment with Blebbistatin, Y-27632, and B+Y. Paired symbols show statistically significant difference at *P<0.05.***

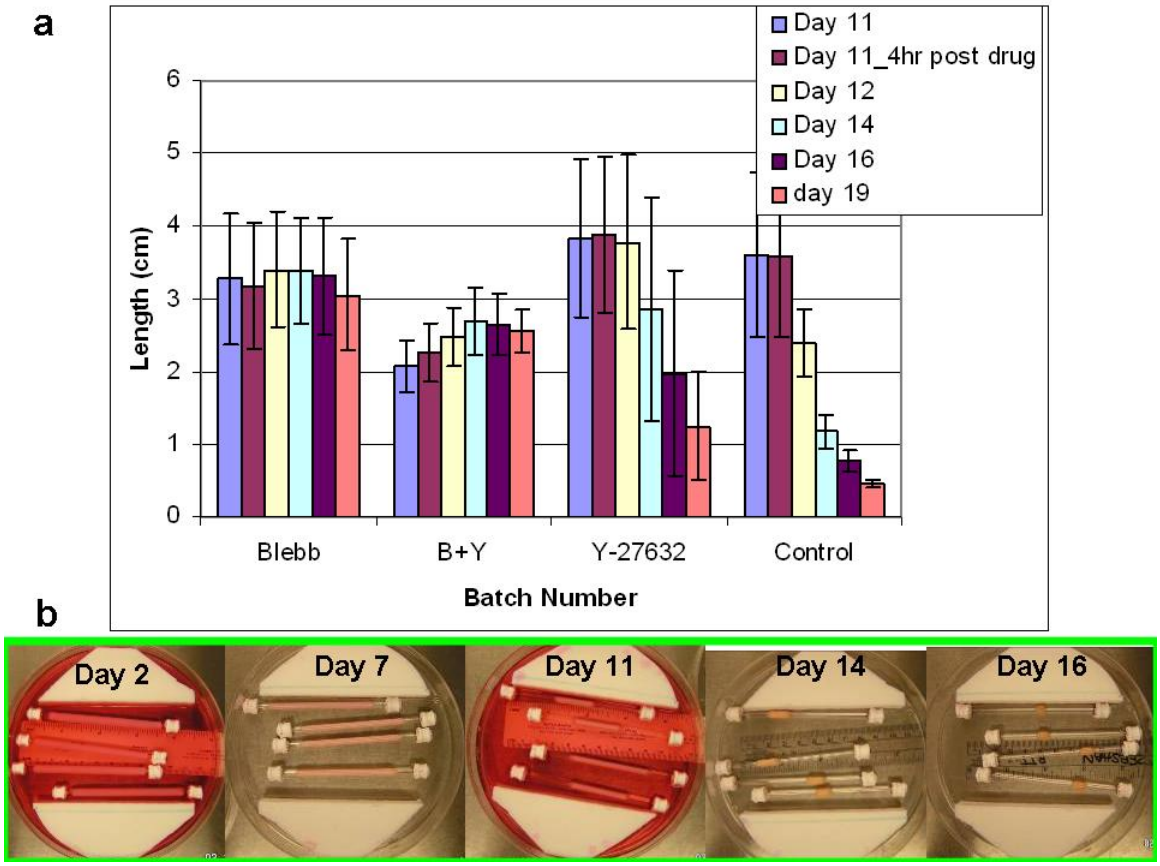

Figure 6-4: **a. Axial length of TC treated with Blebbistatin and Y-27632 (n=4-5). b. Time-lapse images of control TC.**

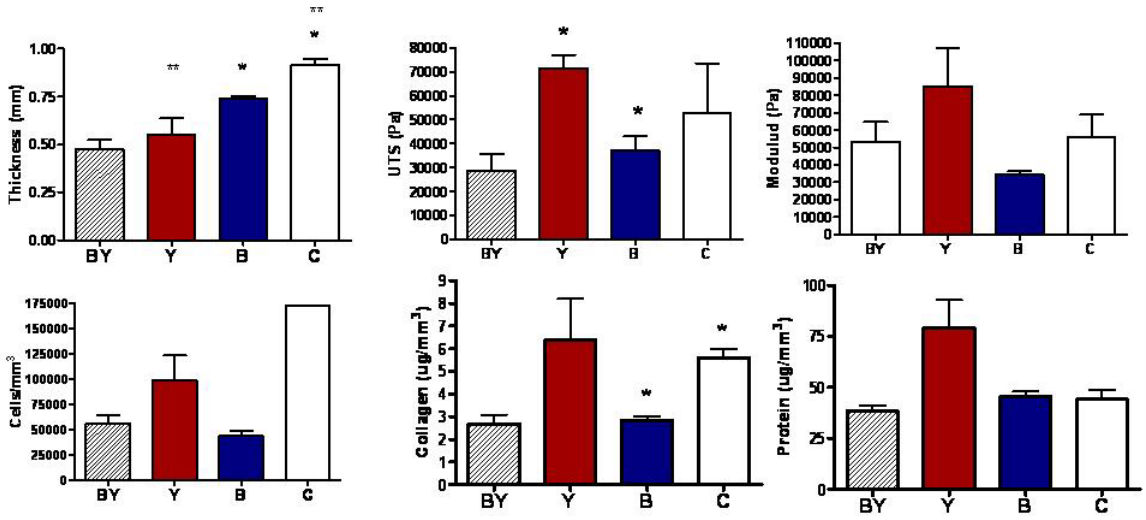

Figure 6-5: **Tensile mechanical and biochemical properties of TC after 10 days with Blebbistatin (B), Y-27632 (Y), or both (B+Y) (n = 4 to 5). See Figure 3 for statistical significance.**

6.4: Ruthenium cross-linking of fibroblast-seeded fibrin gel for tissue engineering

The photo cross-linking of the fibrin gel relies on the proximity of fibrin fibrils and, more importantly, their tyrosine groups, which are about 5% of total amino acids in two of the three protein chains in the fibrinogen used to make fibrin. Previous work by Elvin *et al* (10) has shown photo cross-linking to be highly effective in 150 mg/ml fibrin gel; however, the typical concentration used in tissue engineering is 3-6 mg/ml. Hence, initial studies were conducted to determine not only the toxic effect of the cross-linking reagents used but also whether any significant change in the stiffness of fibrin gel at 4 mg/ml would result. Cross-linking chemistry was developed with Australian Common Wealth Scientific and Industrial Research Organization collaboration (Dr. Charles Lindall and Dr. Lillian Sando). Their protocol was modified to minimize the deleterious environment for the cells. Additional experiments were performed to evaluate long-term remodeling and compaction of the cross-linked fibrin gel. The objective was to determine if sufficient stiffening of the fibrin could be achieved so as to substantially reduce compaction mediated by the nHDF without a reduction in ultimate tensile mechanical properties. If achieved, a longer incubation time could be used to improve the mechanical properties without over-compaction of the tissue formed from fibrin remodeling.

6.4.1: Material and Methods

6.4.1.1: Cell culture

Neonatal human dermal fibroblasts (HDFs, Clonetics) were maintained in DMEM/F12 culture medium (Gibco) supplemented with 10% FBS,100 U/ml penicillin, 100 μg/ml streptomycin, and 2.5 μg/ml amphotericin-β. Cells were passaged at 100% confluency and harvested for use from passage 7-9.

6.4.1.2: Tubular construct (TC) preparation and culture

The details of sample preparation and culture have been previously described (13). Briefly, a cell-seeded fibrin gel was cast in a tubular mold by mixing cells suspended in DMEM into a solution of bovine fibrinogen (Sigma) in 20mM HEPES-buffered saline. A mixture of bovine thrombin (Sigma) and calcium chloride in DMEM was then added to the fibrinogen/cell mixture. The final concentrations of the suspension were 6.6 mg/ml fibrinogen, 0.4 U/ml thrombin, 3.6mM Ca^{2+}, and 500,000 cells/ml. Suspensions were well mixed by pipette action and injected into tubular molds. Constructs were cultured in DMEM media supplemented with 10% FBS, 100 U/ml penicillin, 100 μg/ml streptomycin, 2 μg/ml insulin, and 50 μg/ml ascorbic acid. Constructs were cultured for one week, after which they were transferred to a bioreactor for cyclic stretching. This one-week culture period allowed for cell-mediated fibrin compaction and initial ECM deposition so that the constructs could withstand the transfer to the CD bioreactor. Samples were cultured on CD bioreactor for additional 2 to 4 weeks. Two set of experiments were performed, with both sets having paired non-cross-linked control for all time-points. After harvest, each construct was divided into four equal-length sections and then slit longitudinally to form four tissue strips, one for

uniaxial tensile testing followed by biochemical analysis, and the others for western blotting, DNA quantification, and histology.

6.4.1.3: Hemisphere Constructs (HC) preparation and culture

HC were formed in six-well plates with the bottom of each well being scored to yield a 1 cm diameter etch. Using the same formulation as above, 200 µl of fibrin-forming cell suspension was placed within each etch, allowed to gel for 30 minutes, and then incubated with the same medium as for TC. Samples were cross-linked (see below) after 24 hrs of culture and incubated further for 3 weeks in the same medium. For a direct assessment, the compressive stiffness of the HC was measured using a quasi-static force indenter test. Using pre-calibrated volt-meters, compressive force versus displacement data was acquired and used for calculation of compressive stiffness defined as force per unit initial surface area of HC.

6.4.1.4: SDS-PAGE analysis of photo cross-linked fibrin

To evaluate the extent of cross-linking, fibrinogen solution at 10 mg/ml was cross-linked at several dilutions of Ruthenium compound from 0.02 mM to 4 mM. To assess the kinetics of cross-linking, fibrinogen solution with Ruthenium compound at 2 mM concentration was exposed to blue light for 1,5,10, and 20 seconds. The cross-linked samples were added to a reducing buffer (4x loading dye: Tris-HCL 0.125 M, glycerol 20%, SDS 4%, bromophenol blue 0.01%, DTT 12.5 mM), heated at 95^{o}C for 5 minutes, and analyzed by electrophoresis on 10% SDS-polyacrylamide gel. 10 µg of

protein was loaded for each treatment group and the control group. The gel was stained with blue Bandit protein stain.

6.4.1.5: Ruthenium photo cross-linking of nHDF seeded fibrin gel

TC and HC were incubated in culture medium for 24 hrs or more before (as specified) cross-linking. Ruthenium trisbypyridyl chloride $[Ru(II)(bpy)_3]^{2+}$ (Ru(II)) solution was made at 10x (20 mM) concentration by dissolving it in distilled H_2O. Sodium persulfate solution was prepared at 20x (200 mM) concentration by dissolving it in distilled H_2O. Solutions were sterile filtered with a 2 μm filter (Millipore, USA). Solutions were protected from light until used and made fresh for each cross-linking experiment. Prior to cross-linking, the solutions were diluted in sterile PBS and TC/HC were incubated in a mixed solution of Ru(II) and sodium persulfate at 37^{o}C for 10 min. At the end of the incubation, blue light delivered from a custom mesh of 48 blue LEDs was applied at 10 mW/cm^2 for 20 seconds. After cross-linking, the TC/HC were rinsed 2x in PBS and 1x in DMEM, and then cultured in standard conditions. Controls were kept in normal culture medium and not exposed to blue light but otherwise subjected to the same culture conditions (including cyclic distension following static incubation).

6.4.1.6: Uniaxial Tensile Testing

One tissue strip from each construct was tested for tensile properties in the circumferential direction. The thickness of each strip was measured using a 50 g-force probe attached to a displacement transducer. Tissue strips were placed in compressive grips, attached to the actuator arm and load cell of a Microbionix material testing

system (MTS systems) and straightened with a load of 0.005 N. This position was used as the reference length of the strip. Following 6 cycles of 0-10% strain at 2 mm/min, strips were stretched to failure at the same rate. True strain was calculated based on the change in length of the tissue over time. The stress was calculated as force divided by the initial cross-sectional area. Young's modulus (E) was determined by linear regression of the linear region of the stress-strain curve just prior to failure.

6.4.1.7: Histology

Tissue strips were fixed in 4% paraformaldehyde, infiltrated with a solution of 30% sucrose and 5% DMSO, frozen in OCT (Tissue-Tek), and sectioned into 9 μm cross-sections. Sections were then stained with Lillie's trichrome, Verhoeff's stain and picrosirius red stain. Images were taken using a color CCD camera. For picrosirius red staining, images were taken with the samples placed between crossed plane polarizers.

6.4.1.8: Collagen and Cell quantification

Collagen content was quantified with the hydroxyproline assay assuming 7.46 mg of collage per 1 mg of hydroxyproline (2). Tissue strip volume was calculated using the measured length, width, and thickness of the strips (as described above in uniaxial testing). Collagen concentrations were calculated as the amount per unit volume in each strip.

DNA content was quantified with a modified Hoechst assay (2). Cell numbers were obtained from DNA contents assuming 7.6 pg of DNA per cell. Cell

concentrations were calculated as the number of cells per unit volume using the dimensions of the strip.

6.4.1.9: Statistics

For all experiments, a statistical difference between groups was determined using one-way ANOVA with the Tukey post hoc test in GraphPad Prism® software for Windows. Any reference to a difference in the Results and Discussion implies statistical significance at the level $p < 0.05$. In all cases where the error bars (plus or minus standard deviation) are non-overlapping, the differences are significant; hence, for clarity, no symbols are used. In cases where error bars are overlapping and the difference is significant, paired symbols are used to indicate the difference.

6.4.2: Results

6.4.2.1: Ruthenium cross-linking kinetics

To assess Ru(II) cross-linking kinetics, a solution of fibrinogen at 10 mg/ml was cross-linked at Ru(II) concentration of 0.02, 0.1, 0.2, 0.5, 1, 2 and 4 mM. The solution had width and depth of 2-3mm, which is comparable to a day old TC. At all concentrations, the solution was exposed to blue light at 10mW/cm^2 for 20 seconds. Figure 6a shows a visible band of un-cross-linked fibrinogen at low concentration of 0.02 mM, however at 0.2 mM and higher concentration, there are no visible band. Further, the cross-linking kinetics was assessed by exposing the fibrinogen solution at 20 mM Ru(II) concentration to blue light for 1, 5, 10 and 20 seconds. At 1 sec exposure, the bands of the fibrinogen are visible, but by 5 seconds all the fibrinogen had been

cross-linked (Fig 6b). The data shows that fibrinogen can be cross-linked at 100x lower Ru(II) concentration with exposure to blue light 4x less than used for the TC study.

6.4.2.2: Ruthenium cross-linking increased the fibrin gel stiffness without affecting cell viability

HC were incubated overnight in culture medium before cross-linking. As shown in Fig. 7a, 30 min after cross-linking, no cytotoxic effects were observed. To assess whether cross-linking influenced the stiffness of the fibrin gel, the HMs were detached from the plates and allowed to float in PBS for 5 min. In a well known phenomenon due to cell traction forces (5), immediate gel compaction occurred in the control group (maintained in cell culture medium at 37C), which was inhibited in the cross-linked HC, implying an increased stiffness from this functional assessment (Fig 7b). Using direct measurement, measured stiffness of HC increased with cross-linking by 93% (Fig 6c).

6.4.2.3: Ruthenium cross-linking of TC leads to reduced compaction

TC were cross-linked at day 1 and day 7. Figure 8 shows the process of cross-linking and a live/dead image showing no cell death 30 minutes after cross-linking. After 7 days of static incubation, TC were mounted in the CD bioreactor (as previously described (13)). TC were cultured for an additional 2 weeks and length was recorded weekly. Figure 9a shows the measured length of TC over 3 weeks. Control samples compacted to 2% of the initial length, while samples cross-linked on day 1 only

compacted to 12%, while samples cross-linked on day 7 compacted to 17%. Compared to un-treated control TC, cross-linked TC were 4-6 fold longer at week 3 (Fig. 9b).

6.4.2.4: Cross-linked TC had increased cell proliferation and comparable collagen density

After 3 weeks of culture (including 2 weeks in the CD bioreactor), the TC cell content increased by 50% for control TC and by 125% for cross-linked TC. Figure 10 shows the cell count, total deposited collagen, and collagen/cell. There was no difference in collagen deposited by the cells in the control (375±48 μg) and day 1 (409±10 μg) cross-linked TC; however the day 7 cross-linked TC had 45% less collagen (208±77 μg) compared to control TC.

6.4.2.5: Tensile properties of TC correlated with collagen density

The tensile properties (UTS and modulus) were higher for the control compared to Day 1 and Day 7 cross-linked TC (Fig. 11). The UTS value for the control (792±312 kPa) was 1.5 fold higher than Day 1 (309±34 kPa) and 4.7 fold higher than Day 7 (127±10 kPa). Similarly, the modulus for the control (2859±821 kPa) was 1.5 fold higher than Day 1 (1140±113 kPa) and 3.7 fold higher than Day 7 (609±57 kPa). The tensile properties correlated with the collagen density, which was also 1.5 fold and 4.7 fold higher than Day 1 and Day 7 for the control samples. The plot for modulus versus collagen density for all samples is shown in Figure 12, which had a linear trend (R^2 = 0.97 for linear regression).

6.4.2.6: Ruthenium cross-linked TC require a longer incubation to achieve desired tensile properties

In the first study described above, the tensile properties correlated with collagen density, which resulted in cross-linked TC having a lower UTS and modulus after 3 weeks of culture compared to control TC. Hence, a second study was performed with TC cross-linked at Day 1 and then incubated for 5 weeks (1 week static culture followed by 4 weeks in CD bioreactor). For both 3 and 5 week time-point, paired untreated control was also analyzed. The cross-linked TC further compacted during the additional 2 weeks of CD down to 8.5% of the initial length by week 5 (Fig. 13a); however they were still 120% longer than controls. The UTS and modulus both improved for the cross-linked TC from week 3 to 5, with 5 week sample properties comparable to the 3 week non cross-linked controls (Fig. 13c&d). The UTS and modulus improved by 111% and 293% from week 3 to 5, respectively. The trichrome and picrosirius red staining showed significant remodeling and maturation of collagen for the cross-linked samples from week 3 to 5 (Fig. 14).

6.4.3: Discussion

Initial experiments were conducted with HC to evaluate the toxic effects and stiffness change in fibrin gel seeded with nHDF due to Ruthenium catalyzed cross-linking. After cross-linking, a Live/Dead assay was performed, which showed no toxic effects of Ru(II) or sodium persulfate (Fig. 7a). The control gel retracted when pealed from plate compared to cross-linked HC (Fig. 7b). An indentation test showed that the cross-linked HC were twice as stiff compared to the controls (Fig. 7c).

The HC studied validated the Ru(II) cross-linking protocol to be non-toxic to nHDF inside the fibrin gel; hence further long-term effects were evaluated in the TC, which were mounted in the CD bioreactor to access remodeling under cyclic stretching. Further, to assess if cross-linking can be beneficial in partially remodeled fibrin, a subset of TC were cross-linked on day 7 rather than day 1. The 3 groups (day 1, day 7 and control) were mounted in the CD bioreactor and cyclic stretched at 10% for 2 weeks after 1 week of static incubation on the rigid mandrel used for casting. Control TC rapidly compacted to 2.7% of the initial length after 3 weeks. Compared to the control TC, cross-linked TC were 4-6 fold longer at 3 weeks. The data showed that cross-linking was effective in slowing but not abolishing the compaction of the fibrin gel. Some compaction is desirable, as under appropriate mechanical constraints it leads to the alignment of the fibrin fibrils as well as the deposited ECM fibers. In the case of TC, the alignment is circumferential.

Biochemical data showed TC cross-linked developed a higher cell content (Fig 10a). One plausible explanation would be the cell proliferation being a function of cell density and nutrient availability. It was observed that control TC rapidly compacted by week 2, and at 3 week (Fig. 11) the cell density was greater in control TC, compared to cross-linked TC. Hence, due to higher cell density in control TC, cell proliferation would potentially have slowed down between week 2 to 3 compared to cross-linked TC. The total deposited collagen was comparable between the control and day 1 cross-linked TC, with day 7 TC having 50% less collagen (Fig. 10b). Even though no toxic effects of cross-linking were not observed, it is possible that the treatment of Ru(II), sodium persulfate and blue light led to some cellular damage that required longer

incubation for the cells to recover before they could further remodel the surrounding ECM. This is supported in the trend of collagen/cell (Fig. 10c), which is highest for the controls followed by day 1 and day 7 groups.

Since the total collagen was comparable between control and 1 day cross-linked TC, but they possessed dramatically different volumes (Fig 9), the collagen density was 2-fold higher in the controls (Fig. 11c). As shown in Figure 12, the tensile modulus correlated with the collagen density. Both the UTS and modulus were highest for the controls followed by day 1 and day 7 cross-linked TC. To facilitate improvement in the tensile properties of the cross-linked TC, additional experiments with longer culture time in the CD bioreactor were performed. An additional 2 weeks of culture improved the UTS and modulus of cross-linked TC to values comparable to the 3 week control samples. The trichrome and picrosirius red stains confirmed further remodeling with more visible (trichrome) and mature (picrosirius red stain) collagen in 5 week TC compared to the 3 week TC (Fig. 14). However, during the additional 2 weeks of culture, the length further decreased down to 8.5% compared to 16% at 3 weeks. The 5 week TC were still 120% longer than control TC.

Over all, this study shows that Ru(II) cross-linking of the tyrosine groups in the fibrin can be achieved at a low initial fibrin concentration of 4 mg/ml. The cross-linking has no toxic effects on the nHDF and leads to a stiffer fibrin matrix. In long-term culture, the cell proliferates normally in the cross-linked fibrin and remodel it with comparable deposition of collagen as in control samples. Further, we showed that cross-linking can be done on partially remodeled fibrin after 1 week of incubation to inhibit further compaction after some initial compaction has occurred. The study demonstrates

Ru(II) cross-linking as a successful method to control compaction of fibrin-based tissue constructs.

6.4.4: Figures

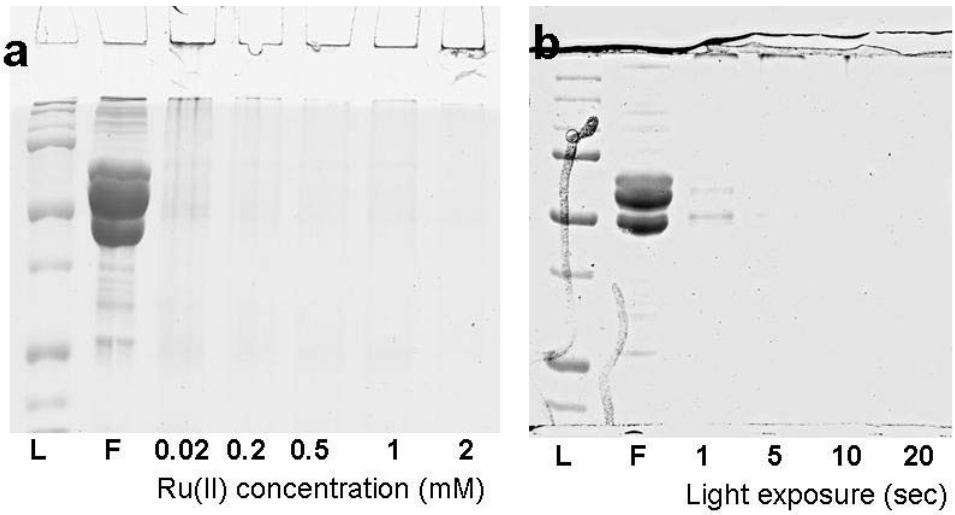

Figure 6-7: Photochemical cross-linking of fibrinogen solution at 10 mg/ml using Ru(II) as a catalyst. a. Evaluation of Ru(II) concentration effect on fibrinogen cross-linking at concentrations of Ru(II) at 0.02, 0.2, 0.5, 1 and 2 mM. b. Evaluation of blue light exposure time on the Ru(II) cross-linking with time of 1, 5, 10 and 20 seconds at 10 mW/cm^2. The first lane on the left side of each gel has a protein ladder (L) followed by untreated fibrinogen solution loaded at 10 μg (F).

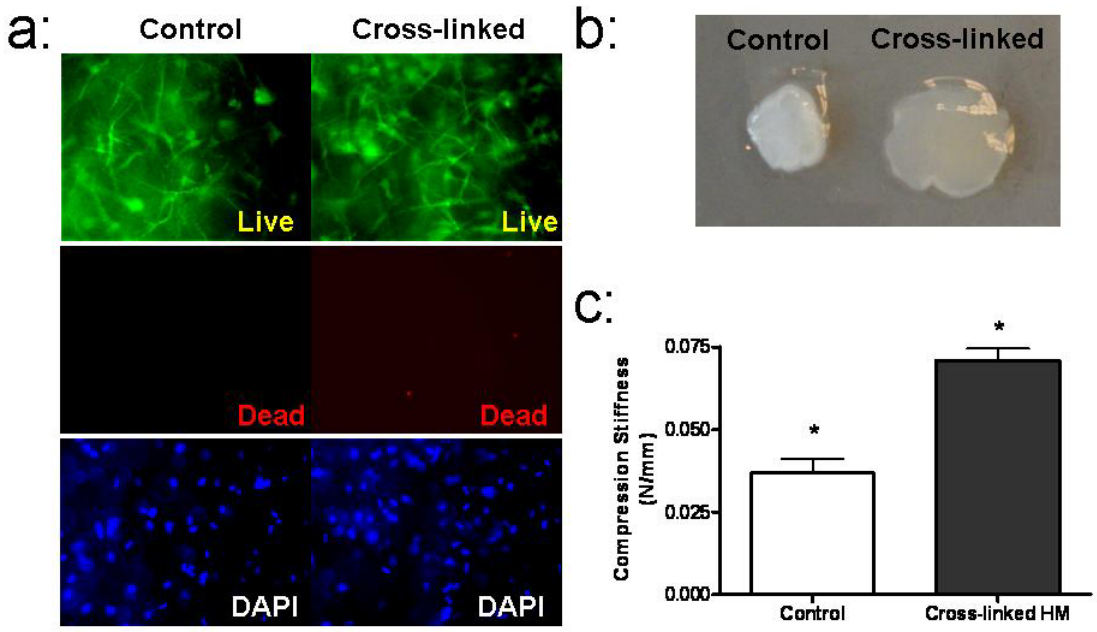

Figure 6-7: **a. Live-dead comparison of an nhDF-seeded fibrin HM photo cross-linked with Ruthenium catalyst and a control HM B. Visual comparison of HM compaction after detachment from surface c. Comparison of compression stiffness (* significantly different at $p<0.05$).**

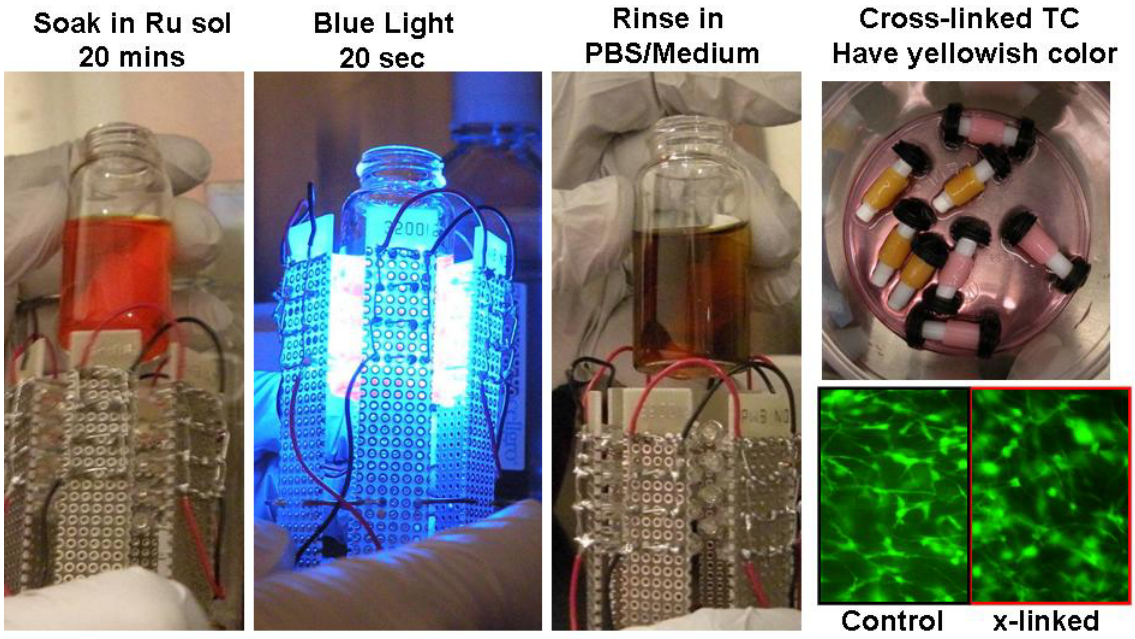

Figure 6-8: **Process of Ruthenium cross-linking. Bottom right shows Live/Dead image of TC cross-linked (x-linked) compared to untreated control.**

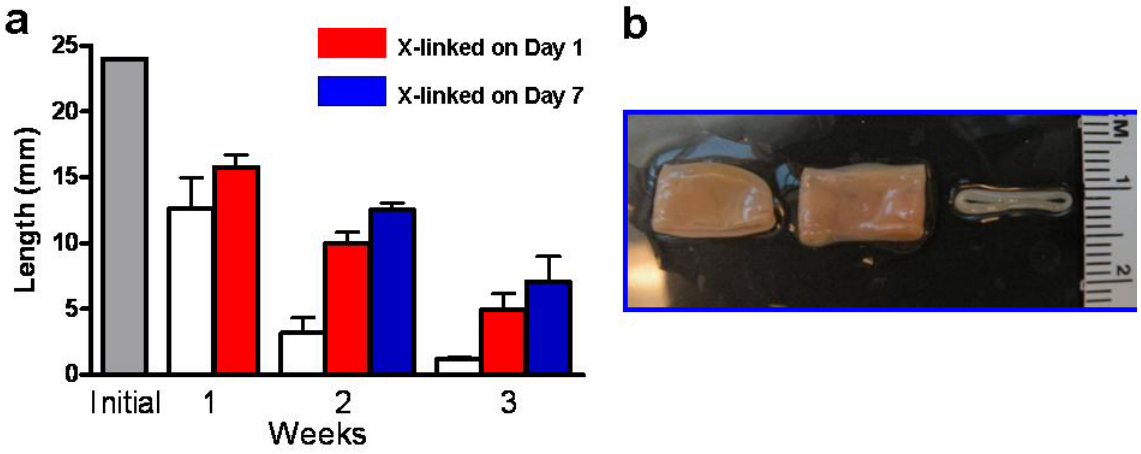

Figure 6-9: **a. Time-course of axial length of the TC, b. Image of the TC at 3 week (from left to right: 1 day, 7 day, and control)**

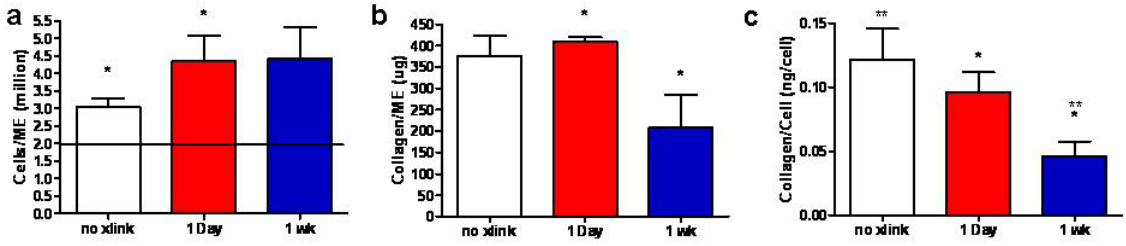

Figure 6-10: **a. Cell number, b. total collagen and c. collagen/cell for TC after 3 weeks of culture in CD bioreactor. In a. horizontal line represents the initial cell number.**

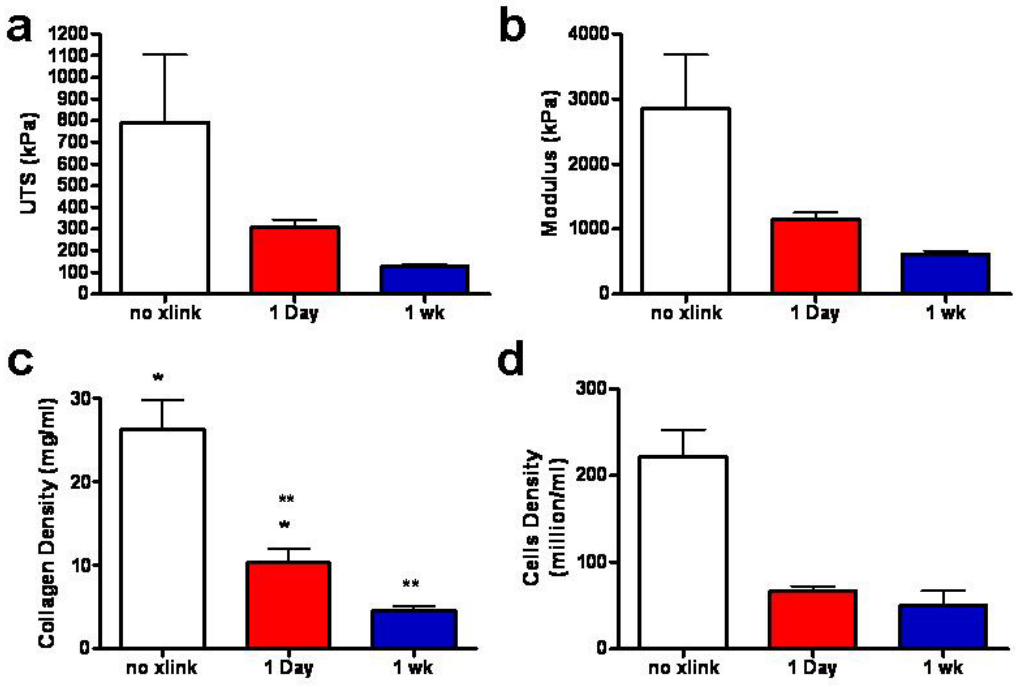

Figure 6-11: **a. UTS, b. modulus, c. collagen concentration and d. cell concentration in TC after 3 weeks**

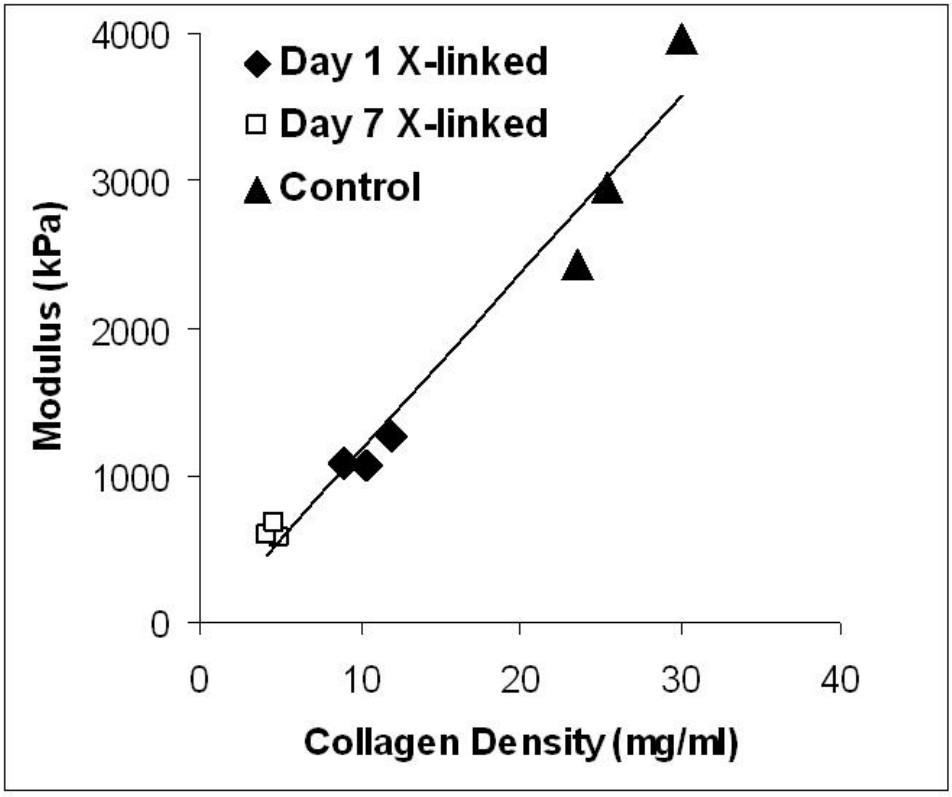

Figure 6-12: **Collagen density versus modulus of TC after 3 week of incubation, linear regression had R^2=0.97 (line on the plot).**

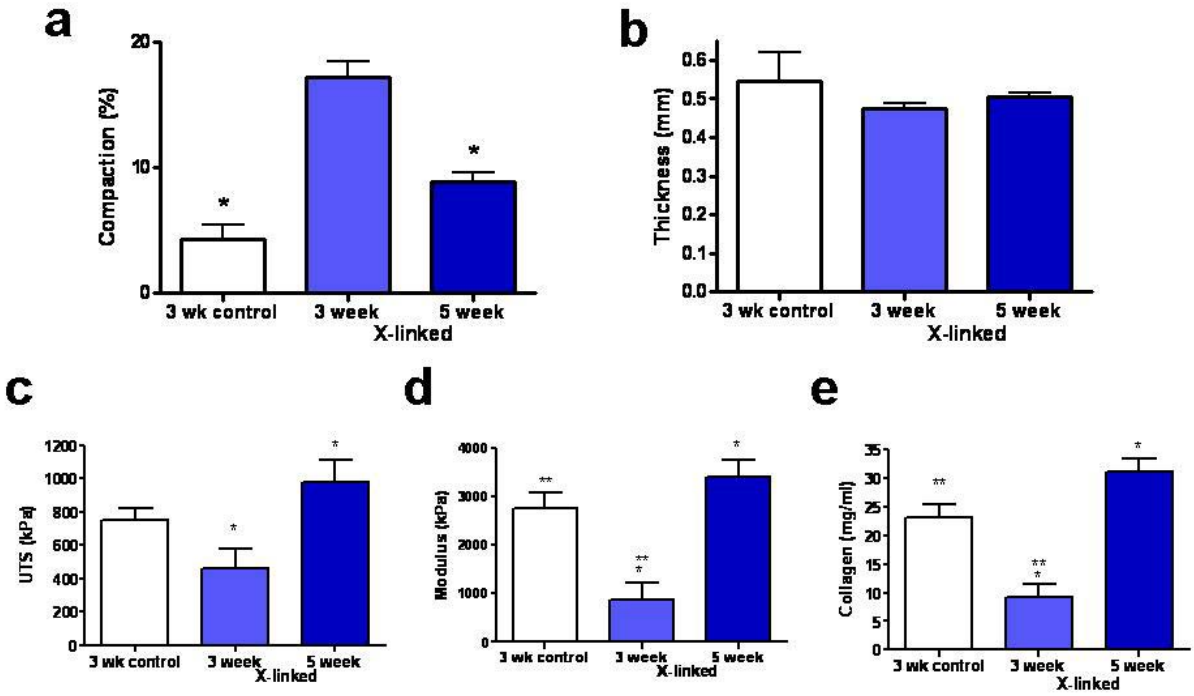

Figure 6-13: **Comparison of compaction and tensile mechanical properties of non cross-linked TC control after 3 weeks of culture to photo cross-linked TC after 3 and 5 weeks of culture. All samples were statically cultured on mandrel for 1 week followed by 2-4 weeks in the CD bioreactor. a. Overall length compaction as % of initial length, b. thickness, c. UTS, d. modulus, and e. Collagen density.**

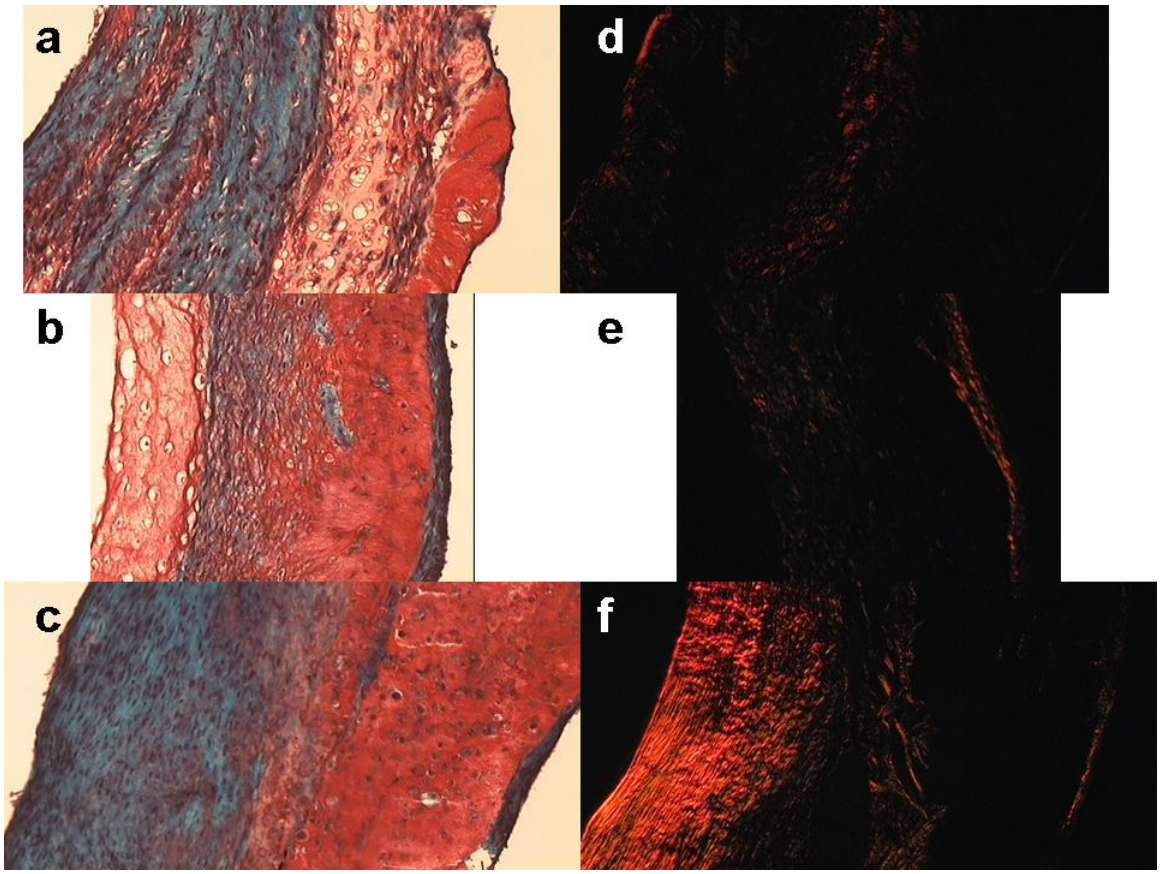

Figure 6-14: **Trichrome and Picrosirius Red Stain of the TC control (a&c) and photo cross-linked TC after 3 (b&d) and 5 (c&f) weeks of culture.**

6.5: References

1. Grassl, E. D., *et al.* (2002) Fibrin as an alternative biopolymer to type-I collagen for the fabrication of a media equivalent. *J Biomed Mater Res* **60,** 607-612.
2. Robinson, P. S., *et al.* (2008) Functional tissue-engineered valves from cell-remodeled fibrin with commissural alignment of cell-produced collagen. *Tissue Eng Part A* **14,** 83-95.
3. Yao, L., *et al.* (2005) Fibrin-based tissue-engineered blood vessels: differential effects of biomaterial and culture parameters on mechanical strength and vascular reactivity. *Tissue Eng* **11,** 991-1003.
4. Beningo, K. A., *et al.* (2006) Traction forces of fibroblasts are regulated by the Rho-dependent kinase but not by the myosin light chain kinase. *Arch Biochem Biophys* **456,** 224-231.
5. Abe, M., *et al.* (2003) Different molecular motors mediate platelet-derived growth factor and lysophosphatidic acid-stimulated floating collagen matrix contraction. *J Biol Chem* **278,** 47707-47712.
6. Allingham, J. S., *et al.* (2005) The structural basis of blebbistatin inhibition and specificity for myosin II. *Nat Struct Mol Biol* **12,** 378-379.
7. Kim, A., *et al.* (2006) Quantitative assessment of local collagen matrix remodeling in 3-D culture: the role of Rho kinase. *Exp Cell Res* **312,** 3683-3692.
8. Ishizaki, T., *et al.* (2000) Pharmacological properties of Y-27632, a specific inhibitor of rho-associated kinases. *Mol Pharmacol* **57,** 976-983.
9. Ho, W., *et al.* (2006) The behavior of human mesenchymal stem cells in 3D fibrin clots: dependence on fibrinogen concentration and clot structure. *Tissue Eng* **12,** 1587-1595.
10. Elvin, C. M., *et al.* (2009) The development of photochemically crosslinked native fibrinogen as a rapidly formed and mechanically strong surgical tissue sealant. *Biomaterials* **30,** 2059-2065.
11. Fancy, D. A., Kodadek, T. (1999) Chemistry for the analysis of protein-protein interactions: rapid and efficient cross-linking triggered by long wavelength light. *Proc Natl Acad Sci U S A* **96,** 6020-6024.
12. Isenberg, B. C., Tranquillo, R. T. (2003) Long-term cyclic distention enhances the mechanical properties of collagen-based media-equivalents. *Ann Biomed Eng* **31,** 937-949.
13. Syedain, Z. H., *et al.* (2008) Cyclic distension of fibrin-based tissue constructs: evidence of adaptation during growth of engineered connective tissue. *Proc Natl Acad Sci U S A* **105,** 6537-6542.

Chapter 7: Ongoing Work, Future Direction and Conclusions

7.1: Introduction

The science of tissue engineering has been proposed as the next generation of therapy to replace and repair tissues and organs. Several tissue engineered grafts have been used in the clinical trails but for most of the field, the science is still in the research phase. Specifically to tissue engineered heart valve (TEHV), the tissue requires both functional and tensile properties to be able to withstand the physiological conditions. The research can then look into more complex questions regarding *in vivo* performance of the valve conduit. For synthetic grafts made from biodegradable polymer, to certain extent the rigid polymer can provide the strength needed to withstand physiological conditions. John Mayer's group at Children Hospital Boston has successfully implanted the synthetic polymer TEHV in sheep pulmonary artery and reported first study 9 years ago (1, 2). In 9 years since then, the group has published several iterations to the original conduit but the progress is still far from a clinical trial. Though synthetic polymer provides durability, it has several disadvantages, which is the primary reason for the slow progress. Our laboratory approach is by using fibrin as a scaffold. Fibrin gel is extremely fragile compared to synthetic polymers and requires extensive remodeling by embedded cells to have the desired mechanical properties. The early chapters of this thesis addressed these issues and a design of a bioreactor that can be used to improve remodeling of a fibrin gel based TEHV. To this day, we have implanted fibrin based TEHV in several large animals with uneventful survival of upto 8 weeks. During development of the TEHV, numerous approaches were looked at that could be utilized in the future.

7.2: Ongoing and Future Studies

Some of the preliminary studies conducted with the fibrin system are presented here in. These ideas potentially would probe further questions on the fundamental of tissue engineering, cellular behavior, and requirements for developing a tissue engineered devices.

7.2.1: Endothelialization of valve surface

Evaluation of the VE implanted in sheep has shown inflammatory response on surface near leaflets. Histopathology showed formation of blood capillaries on luminal surface in at least one of the implant. Though the observed inflammation could be related to completely unknown phenomenon, our first assumption would be the lack of endothelial lining on implant graft, which leads to reactive response. The inflammatory response was least to none near proximal and distal end of root surface. Immuno-histology showed endothelial lining in these regions by positive Von Willebrand factor (vWF) staining (marker for endothelial cells). Most likely after implant endothelial from surrounding pulmonary artery spread onto near by VE root and over time minimize any inflammatory response.

A desirable source of endothelial cells would be the autologous endothelial cells. Previous animal implant with human cell derived tissue engineered vascular grafts have used endothelial cells extracted from the saphenous vein (3). In our lab, we are pursuing blood derived endothelial cells (BOEC), which only require with-drawl of blood hence a more convenient source for patients to donate. The BOEC technology is developed by Hebbel lab at the University of Minnesota. In preliminary studies, sheep BOEC

(isolated and passaged by Mark Roney from Hebbel Lab) were plated on nHDF seeded hemispheric constructs (HC). In brief, the HC were cultured on tissue-culture plastic for 2 weeks prior to BOEC seeding. BOEC (three million cells) were suspended in culture media over HC surface for 4 hrs. Endothelial culture media was added following seeding and HC with BOEC were cultured for additional 7 days. A HC was stained for LDL at 2, 4 and 7 days. The 7 day HC were also immuno-histochemically stained for vWF. Figure 1a shows surface image of HC coated with BOEC that are labeled with LDL. HC surface had 100% BOEC coverage after 4 days. vWF staining showed confluent lining of endothelial cells on surface of HC (Fig. 1b).

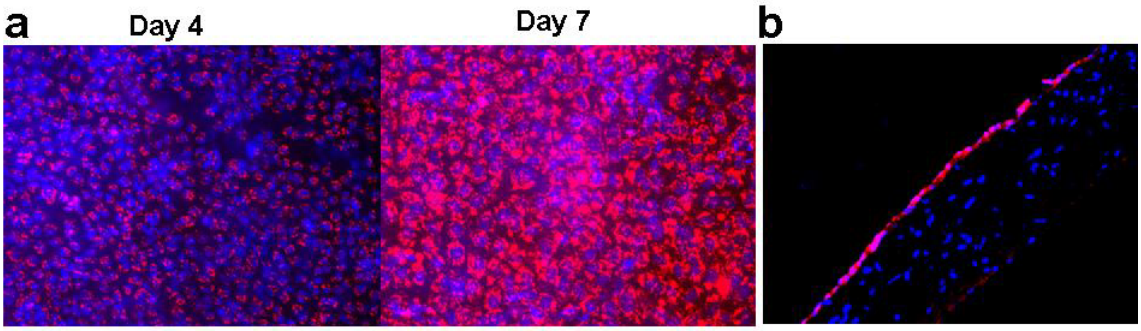

Figure 7-1: a. LDL staining of BOEC on HC surface, red represent LDL, blue is cell nuclei stained with DAPI counter stain b. vWF immuno-staining (red) of HC cross-section with nuclei (blue) DAPI counter-stain.

Further experiments were performed to coat surface of the VE inside the bioreactor with BOEC cells. In brief, VE cultured in bioreactor for 3 weeks were seeded with BOEC by injecting 20ml of BOEC cell solution at 3 million cells/ml into the lumen of the VE, while still mounted in the bioreactor. The end-caps were sealed and bioreactor was rotated at 0.5rpm for 4 hrs to achieve adhesion of BOEC on to VE lumen surface. The VE was connected back in the bioreactor flow-loop and cultured with endothelial culture media for additional 4 days with low perfusion. After harvest, luminal surface of VE root and leaflets was stained for LDL (Fig. 2). The study shows a

proof of concept for endothelialization of VE inside the bioreactor prior to implant. The protocol would need further optimization of BOEC seeding concentration, initial incubation time, rotation speed, and post culture to reach confluency and possible flow conditioning to mature the endothelial lining. Beyond coating, shear studies would be required to access adherence of endothelial coating on the VE surface under physiological flow. Ultimate test would be to implant a BOEC coated VE in the animal model with low to no heparin.

The role of endothelial cells on the leaflet surface has largely been ignored, primarily due to commercial success of bioprosthetic valve. However for the tissue engineered heart valve, it may be necessary and require further investigation.

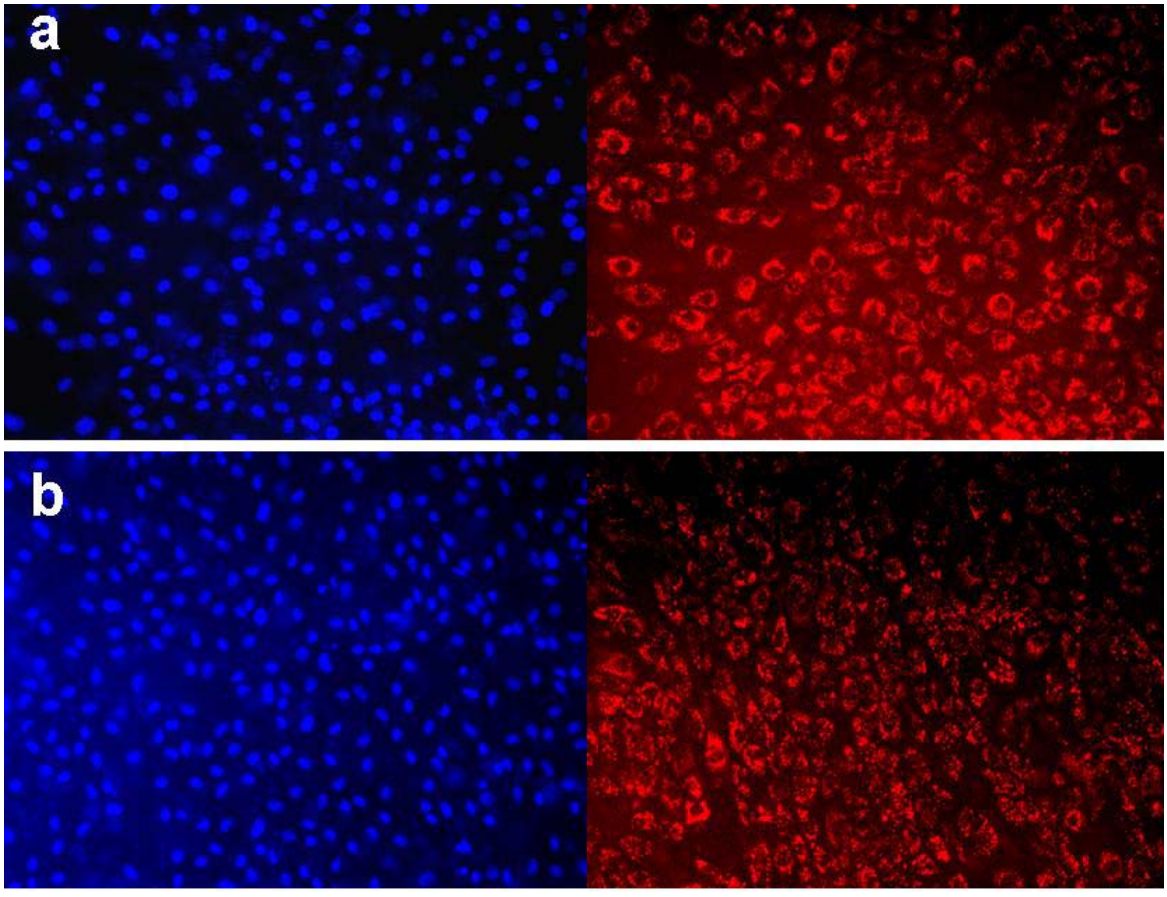

Figure 7-2: **LDL staining (red) of BOEC on VE lumen surface with DAPI (blue) for cell nuclei. a: Image of lumen surface of root section, b: Image of lumen surface on aortic side of the leaflets.**

7.2.2: Hypoxia induced remodeling of nHDF seeded fibrin constructs

Oxygen tension has long been studied to evaluate the effects on cell cycle and behavior (4). Fibroblasts have been shown to increase proliferation and ECM deposition rate at low oxygen tension (5). Recently, hypoxia has been studied as a parameter for tissue engineering and found to be effective in enhancing mechanical properties and ECM content of a engineered tissue (6).

In our lab, we have recently looked at the effects of hypoxia (5% oxygen) on tubular constructs seeded with mouse smooth muscle cells and nHDF compared to normal (21% oxygen) culture conditions. Figure 3 shows the effects of hypoxia on the tensile properties of nHDF seeded gel after 4 week of static culture. Hypoxia increased the UTS by 62% (Fig. 3a) and the maximum tension by 112% (Fig. 3c). These mechanical properties are critical in determining the structural durability of a VE. Hence, further studies that can control not only the mechanical environment (i.e. cyclic stretch) but also the nutrient environment including oxygen tension can be used to further optimize the mechanical properties and ECM content of the VE during in vitro growth. Such optimization could potentially lead to VE with enough strength to withstand aortic pressures.

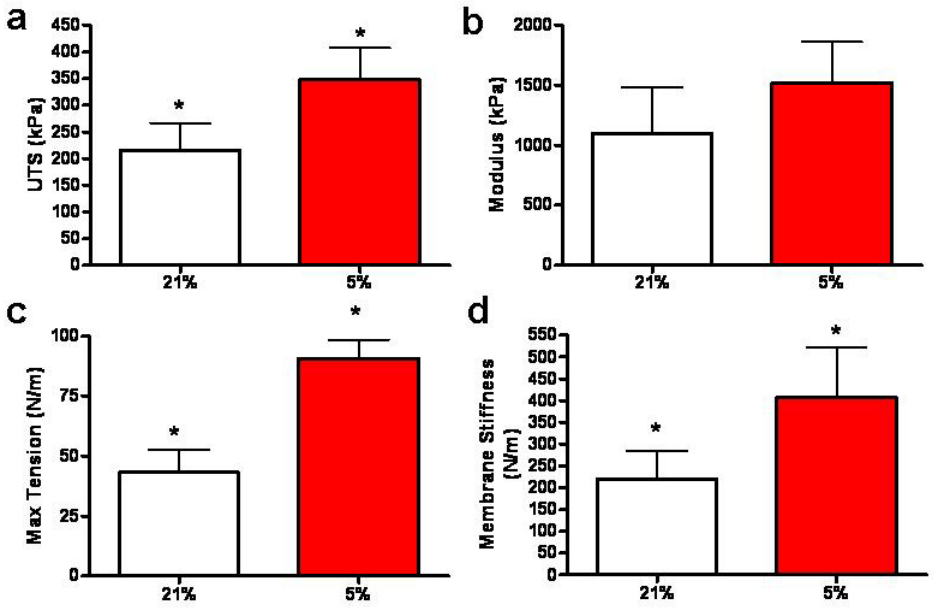

Figure 7-3: a. UTS, b. Modulus, c. Maximum Tension, and d. Membrane stiffness of nHDF seeded fibrin TC after 5 week of static culture

7.2.3: Optimizing mechno-chemical environment to manipulate protein signaling

Success of a TEHV and in general any tissue engineered construct is in manipulating the cellular environment to achieve the desired effects. In the case of TEHV, it is to induce cells to produce ECM proteins and organize them. Study in Chapter 2 showed that TC can adapt to cyclic stretch or mechanical stimulus. This was seen at protein level by plating nHDF cells on a silicon membrane and cyclically stretched for 24hrs in Flexcell system. The cell protein were extracted at several time-points and analyzed for phosphloration of ERK by western blotting. The results in showed that with cyclic stretching the pERK level initially went up but gradually declined over time, indicating that continues cyclic stretching doesn't necessary maintain higher level of pERK for long duration (Fig. 4). Another experiment was conducted where average strain of 10% was applied to three groups of TC for 3 weeks,

first was kept at 10% CD, second was incrementally stretched from 5% to 15% in equal time-steps and third was strained with random increase and decrease in strain amplitude (Fig. 5a). The results showed that to over come adaptation, not only mechanical stimuli need to be changed but also it has to be in an increasing order (Fig. 5b). The two studies mention above highlights the complexity of mechanical signal and its response at the cellular level. Similarly, TGF-β study showed that benefits of a growth factor are not seen at all time-point/under all conditions and optimize dosing can be used to improve the ECM content in the tissue engineered constructs. Recent experiments have show that even nutrients (i.e. oxygen) can be controlled to manipulate cellular response. Hence, for a true optimized TEHV, a growth system is required that can control mechanical and chemical stimulus. The bioreactor system presented in this research has elements that can be used to achieve this. The current bioreactor design allows for independent cyclic stretch control and flow control. Potentially by reducing flow to zero, one can create complete hypoxic environment for VE, or by increasing the flow to higher values, a significant pressure gradient can be induced across the VE (inducing a mechanical stress), and further any growth factors can be injected and over time removed by changing the media reservoir. Similarly cyclic stretch frequency, amplitude and duty cycle can be manipulated without effecting the controlled flow environment. However, to achieve all this requires sophisticated sets of sensory and feed-back controls, which could potentially be achieved in the next generation of TEHV bioreactor system.

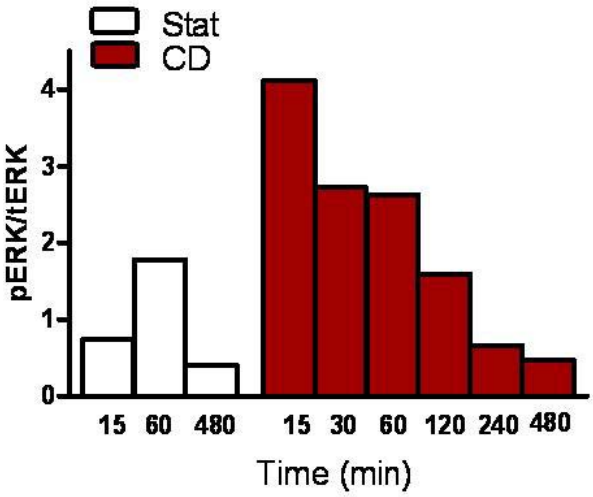

Figure 7-4: Time-course of pERK/ERK singal of nHDF cells on flex cell membrane

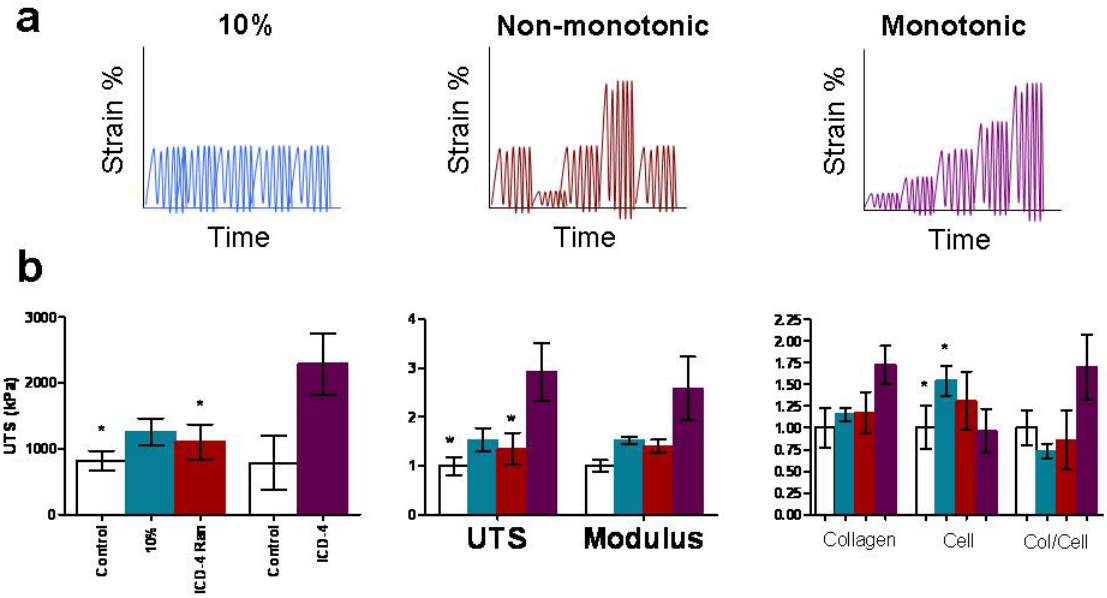

Figure 7-5: a. Schematic of constant CD, non-monotonic and incremental cyclic stretching profile applied to nHDF TC for 3 weeks, b. Comparison of tensile mechanical and biochemical properties of TC conditioned to different cyclic stretch regimes.

7.2.4: Hybrid root for the fibrin TEHV

Fibrin based TEHV provides many advantages over synthetic polymers including leaflets with comparable thickness, modulus and anisotropy to the native leaflets. However, weaker root tissue primarily due to 300-400 μm thickness compared to several millimeters for a native root has been a challenge during surgery. Additionally, fibrin remodeled tissue has weaker suture retention than one required for the surgery, hence current TEHV are embedded with Dacron cuffs for sewing. Synthetic biodegradable polymer like PGA, PLGA and PLA used in TEHV has the advantage of superior suture retention abilities (1, 2). In a completely biological tissue engineering approach, cell sheet based vascular grafts have also been shown to have the desired suture retention (3). Any future iteration in the fibrin based TEHV design can combine the success of several approaches. For instance the entire root of fibrin based TEHV can be cast out of biodegradable polymer along the lines of Baaijens group approach (7), or a completely fibrin based TEHV can be cast and a cell sheet can be rolled over the root in similar fashion as one used for vascular graft, prior to mounting in the bioreactor (3). The second approach could yield a completely biological TEHV with appropriate suturing structure. Of course, either of these hybrid approaches requires a collaborative research.

7.3: Towards clinical trial of TEHV

TEHV technology is fairly young with only one clinical study in progress with decellularized native valve seeded with human cells. The decellularized technology provides the advantage of scaffold with natural valve architecture, however it is yet to

been seen if seeded cells have the ability to remodel these constructs especially in the pediatric patients. Previous trials of decellularized valve implant without cell seeding had catastrophic results in the pediatric patients (8). It is yet to be seen, of the several approaches that are currently being developed, which one will emerge most viable for clinical trails. Since a completely biological valve like the one developed with fibrin scaffold provides the certainty that all components of the graft can be autologous and the tensile properties of the graft are from cell produced ECM, the future clinical success would most likely involve this technology. Current development of TEHV as presented in this thesis already incorporates elements that are critical to success towards clinical trial.

While we worked with bovine fibrin, mainly due to cost reason, fibrin is a highly conserved polymer among species and limited experience in our lab with human fibrin has shown to give comparable results as with bovine fibrin. We currently use human dermal fibroblast, which is relatively easy source of cells to acquire from individual patients and protocols to expand these cells are well established. The growth conditions involving fetal bovine serum (FBS) have been debated for human use, however both dermal grafts made by ATS and organogenesis and recent clinical trial of vascular grafts by Cytograft utilized the culture conditions involving FBS (3). Recently, serum free media culture conditions have been utilized to grow engineered tissue (9) and if necessary nHDF can be cultured in such conditions.

In current fibrin based TEHV, due to weak suture retention properties of the engineered tissue, embedded dacron cuffs inside the fibrin gel are used for sewing. Even though Dacron is commonly used in many commercial bioprosthetic valves, for

pediatric patients it creates a problem as darcon may not expand with growing heart of the patient. A clever zig-zag cuff design can be used that can allow for 100% expansion of lumen or cuffs made from biodegradable polymers. Beyond developmental improvements as mentioned in this thesis, the fibrin based TEHV would require extensive animal studies to evaluate growth and remodeling before clinical trial.

With *in vivo* remodeling assurance from animal studies, first clinical trials with TEHV can be conducted in pediatric patients with pulmonary valve disease. Pulmonary valve failure is a low risk and with continues monitoring, patients progress with TEHV in pulmonary position can be evaluated without significant risk to life.

7.4: Conclusions

This thesis focused on the development of TEHV based on a fibrin gel as a scaffold seeded with nHDF. The development primarily focused on cyclic stretch as a mechanical stimulus in improving the tensile mechanical properties of tissue by stimulating cells in fibrin gel to produce and organize collagen. Initial studies were focused on evaluating the role of cyclic stretching on fibrin based tubular constructs (TC). The study was conducted with porcine valve interstitial cells (PVIC) and neo-human dermal fibroblast (nHDF). Both cell types showed improvements in tensile properties with cyclic stretching. PVIC constructs showed significant variability in gel compaction, ECM production, cell proliferation and tensile properties from batch to batch, hence further studies were pursued with nHDF. The cyclic stretching studies showed that under constant cyclic stretching, over time cells can adapt to mechanical stimulus. It was also shown that by applying incremental cyclic stretching, this

adaptation can be overcome and leads to improved tensile properties and collagen production by cells. Further optimization studies involved removing TGF-β during cyclic stretch phase of TEHV growth.

The major development in this project was manufacturing of a novel cyclic stretch bioreactor for fibrin based TEHV. The TEHV cultured in the bioreactor had improved UTS and modulus. The modulus and mechanical anisotropy were comparable to the sheep pulmonary valve leaflets. TEHV tested in pulse duplicator were able to withstand physiological flow and pressure conditions. Burst testing showed that root can withstand pressure up to 150 mmHg.

The desirable mechanical properties achieved with fibrin based TEHV motivated us to conduct animal trials on the pulmonary side of the heart in sheep. Animal implanted with TEHV survived with uneventful occurrences upto 8 weeks. The evaluation of the explanted valve showed inflammatory reaction on luminal surface. The leaflets had no significant change in tensile properties with both collagen and elastin concentration increased during 4.5 week of *in vivo* remodeling. This is a major success considering the valve with human cells in bovine fibrin and without endothelial coating was implanted in a sheep. The root tissue showed areas with endothelial lining and in root wall there was evidence of vasculature. The overall root tensile properties were comparable to the native sheep pulmonary artery.

Further development of the TEHV can utilize ongoing approach to reduce compaction of the fibrin gel, improve cell's ability to produce collagen, elastin and glycoamino glycines (GAG) and coat valve with endothelial cells prior to an implant.

Overall, this study showed controlled mechanical conditioning as a viable approach towards development of a completely biological tissue engineered heart valve.

7.5: References

1. Hoerstrup, S. P., *et al.* (2000) Functional living trileaflet heart valves grown in vitro. *Circulation* **102,** III44-49.
2. Sodian, R., *et al.* (2000) Tissue engineering of heart valves: in vitro experiences. *Ann Thorac Surg* **70,** 140-144.
3. L'Heureux, N., *et al.* (2006) Human tissue-engineered blood vessels for adult arterial revascularization. *Nat Med* **12,** 361-365.
4. Falanga, V., *et al.* (1993) Low oxygen tension increases mRNA levels of alpha 1 (I) procollagen in human dermal fibroblasts. *J Cell Physiol* **157,** 408-412.
5. Siddiqui, A., *et al.* (1996) Differential effects of oxygen on human dermal fibroblasts: acute versus chronic hypoxia. *Wound Repair Regen* **4,** 211-218.
6. Balguid, A., *et al.* (2009) Hypoxia induces near-native mechanical properties in engineered heart valve tissue. *Circulation* **119,** 290-297.
7. Mol, A., *et al.* (2005) Tissue engineering of human heart valve leaflets: a novel bioreactor for a strain-based conditioning approach. *Ann Biomed Eng* **33,** 1778-1788.
8. Simon, P., *et al.* (2003) Early failure of the tissue engineered porcine heart valve SYNERGRAFT in pediatric patients. *Eur J Cardiothorac Surg* **23,** 1002-1006; discussion 1006.
9. Ahlfors, J. E., Billiar, K. L. (2007) Biomechanical and biochemical characteristics of a human fibroblast-produced and remodeled matrix. *Biomaterials* **28,** 2183-2191.

Bibliography

Abe, M., C. H. Ho, K. E. Kamm and F. Grinnell (2003). "Different molecular motors mediate platelet-derived growth factor and lysophosphatidic acid-stimulated floating collagen matrix contraction." J Biol Chem **278**(48): 47707-12.

Ahlfors, J. E., Billiar, K. L. (2007) Biomechanical and biochemical characteristics of a human fibroblast-produced and remodeled matrix. *Biomaterials* **28,** 2183-2191.

Allen, H. D., D. J. Driscoll, R. E. Shaddy and T. F. Feltes (2008). Moss and Adams' Heart Disease in Infants, Children, and Adolescents. Philadelphia, Lippincott Williams & Wilkins.

Allingham, J. S., R. Smith and I. Rayment (2005). "The structural basis of blebbistatin inhibition and specificity for myosin II." Nat Struct Mol Biol **12**(4): 378-9.

Arnaout, M. A., S. L. Goodman and J. P. Xiong (2002). "Coming to grips with integrin binding to ligands." Curr Opin Cell Biol **14**(5): 641-51.

Baaijens, F., C. Bouten, S. Hoerstrup, A. Mol, N. Driessen and R. Boerboom (2005). "Functional tissue engineering of the aortic heart valve." Clin Hemorheol Microcirc **33**(3): 197-9.

Bader, A., T. Schilling, O. E. Teebken, G. Brandes, T. Herden, G. Steinhoff and A. Haverich (1998). "Tissue engineering of heart valves--human endothelial cell seeding of detergent acellularized porcine valves." Eur J Cardiothorac Surg **14**(3): 279-84.

Balestrini, J. L. and K. L. Billiar (2006). "Equibiaxial cyclic stretch stimulates fibroblasts to rapidly remodel fibrin." J Biomech **39**(16): 2983-90.

Balguid, A., M. P. Rubbens, A. Mol, R. A. Bank, A. J. Bogers, J. P. van Kats, B. A. de Mol, F. P. Baaijens and C. V. Bouten (2007). "The role of collagen cross-links in biomechanical behavior of human aortic heart valve leaflets--relevance for tissue engineering." Tissue Eng **13**(7): 1501-11.

Balguid, A., *et al.* (2009) Hypoxia induces near-native mechanical properties in engineered heart valve tissue. *Circulation* **119,** 290-297.

Bastiaansen-Jenniskens, Y. M., W. Koevoet, A. C. De Bart, A. M. Zuurmond, R. A. Bank, J. A. Verhaar, J. Degroot and G. J. Van Osch (2008). "TGFbeta Affects Collagen Cross-Linking Independent of Chondrocyte Phenotype but Strongly Depending on Physical Environment." Tissue Eng Part A.

Beningo, K. A., K. Hamao, M. Dembo, Y. L. Wang and H. Hosoya (2006). "Traction forces of fibroblasts are regulated by the Rho-dependent kinase but not by the myosin light chain kinase." Arch Biochem Biophys **456**(2): 224-31.

Berry, C. C., J. C. Shelton, D. L. Bader and D. A. Lee (2003). "Influence of external uniaxial cyclic strain on oriented fibroblast-seeded collagen gels." Tissue Eng **9**(4): 613-24.

Bilodeau, K. and D. Mantovani (2006). "Bioreactors for tissue engineering: focus on mechanical constraints. A comparative review." Tissue Eng **12**(8): 2367-83.

Boerboom, R. A., M. P. Rubbens, N. J. Driessen, C. V. Bouten and F. P. Baaijens (2008). "Effect of strain magnitude on the tissue properties of engineered cardiovascular constructs." Ann Biomed Eng **36**(2): 244-53.

Brown, R. A., R. Prajapati, D. A. McGrouther, I. V. Yannas and M. Eastwood (1998). "Tensional homeostasis in dermal fibroblasts: mechanical responses to

mechanical loading in three-dimensional substrates." Journal of Cellular Physiology **175**(3): 323-32.

Bujor, A. M., J. Pannu, S. Bu, E. A. Smith, R. C. Muise-Helmericks and M. Trojanowska (2008). "Akt blockade downregulates collagen and upregulates MMP1 in human dermal fibroblasts." J Invest Dermatol **128**(8): 1906-14.

Butler, D. L., S. A. Goldstein and F. Guilak (2000). "Functional tissue engineering: the role of biomechanics." J Biomech Eng **122**(6): 570-5.

Cataloglu, A., R. E. Clark and P. L. Gould (1977). "Stress analysis of aortic valve leaflets with smoothed geometrical data." J Biomech **10**(3): 153-8.

Chahine, N. O., M. A. Albro, E. G. Lima, V. I. Wei, C. R. Dubois, C. T. Hung and G. A. Ateshian (2007). "Effect of Dynamic Loading on the Transport of Solutes into Agarose Hydrogels." Biophysical Journal **inpress**.

Chambers, R. C., P. Leoni, N. Kaminski, G. J. Laurent and R. A. Heller (2003). "Global expression profiling of fibroblast responses to transforming growth factor-beta1 reveals the induction of inhibitor of differentiation-1 and provides evidence of smooth muscle cell phenotypic switching." Am J Pathol **162**(2): 533-46.

Chester, A. H. and P. M. Taylor (2007). "Molecular and functional characteristics of heart-valve interstitial cells." Philos Trans R Soc Lond B Biol Sci **362**(1484): 1437-43.

Christie, G. W. and B. G. Barratt-Boyes (1995). "Mechanical properties of porcine pulmonary valve leaflets: how do they differ from aortic leaflets?" Ann Thorac Surg **60**(2 Suppl): S195-9.

Clark, R. A., L. D. Nielsen, M. P. Welch and J. M. McPherson (1995). "Collagen matrices attenuate the collagen-synthetic response of cultured fibroblasts to TGF-beta." J Cell Sci **108 (Pt 3)**: 1251-61.

Cobanoglu, A., C. L. Fessler, L. Guvendik, G. Grunkemeier and A. Starr (1988). "Aortic valve replacement with the Starr-Edwards prosthesis: a comparison of the first and second decades of follow-up." Ann Thorac Surg **45**(3): 248-52.

Cummings, C. L., D. Gawlitta, R. M. Nerem and J. P. Stegemann (2004). "Properties of engineered vascular constructs made from collagen, fibrin, and collagen-fibrin mixtures." Biomaterials **25**(17): 3699-706.

Dayan, D., Y. Hiss, A. Hirshberg, J. J. Bubis and M. Wolman (1989). "Are the polarization colors of picrosirius red-stained collagen determined only by the diameter of the fibers?" Histochemistry **93**(1): 27-9.

Davidson, J. M., P. A. LuValle, O. Zoia, D. Quaglino, Jr. and M. Giro (1997). "Ascorbate differentially regulates elastin and collagen biosynthesis in vascular smooth muscle cells and skin fibroblasts by pretranslational mechanisms." J Biol Chem **272**(1): 345-52.

De Hart, J., G. W. Peters, P. J. Schreurs and F. P. Baaijens (2004). "Collagen fibers reduce stresses and stabilize motion of aortic valve leaflets during systole." J Biomech **37**(3): 303-11.

Driessen, N. J., A. Mol, C. V. Bouten and F. P. Baaijens (2007). "Modeling the mechanics of tissue-engineered human heart valve leaflets." J Biomech **40**(2): 325-34.

Dumont, K., J. Yperman, E. Verbeken, P. Segers, B. Meuris, S. Vandenberghe, W. Flameng and P. R. Verdonck (2002). "Design of a new pulsatile bioreactor for tissue engineered aortic heart valve formation." Artif Organs **26**(8): 710-4.

Elkins, R. C., P. E. Dawson, S. Goldstein, S. P. Walsh and K. S. Black (2001). "Decellularized human valve allografts." Ann Thorac Surg **71**(5 Suppl): S428-32.

Elvin, C. M., A. G. Brownlee, M. G. Huson, T. A. Tebb, M. Kim, R. E. Lyons, T. Vuocolo, N. E. Liyou, T. C. Hughes, J. A. Ramshaw and J. A. Werkmeister (2009). "The development of photochemically crosslinked native fibrinogen as a rapidly formed and mechanically strong surgical tissue sealant." Biomaterials **30**(11): 2059-65.

Engelmayr, G. C., Jr., E. Rabkin, F. W. Sutherland, F. J. Schoen, J. E. Mayer, Jr. and M. S. Sacks (2005). "The independent role of cyclic flexure in the early in vitro development of an engineered heart valve tissue." Biomaterials **26**(2): 175-87.

Fancy, D. A. and T. Kodadek (1999). "Chemistry for the analysis of protein-protein interactions: rapid and efficient cross-linking triggered by long wavelength light." Proc Natl Acad Sci U S A **96**(11): 6020-4.

Falanga, V., *et al.* (1993) Low oxygen tension increases mRNA levels of alpha 1 (I) procollagen in human dermal fibroblasts. *J Cell Physiol* **157,** 408-412.

Flanagan, T. C., C. Cornelissen, S. Koch, B. Tschoeke, J. S. Sachweh, T. Schmitz-Rode and S. Jockenhoevel (2007). "The in vitro development of autologous fibrin-based tissue-engineered heart valves through optimised dynamic conditioning." Biomaterials **28**(23): 3388-97.

Freed, L. E., F. Guilak, X. E. Guo, M. L. Gray, R. Tranquillo, J. W. Holmes, M. Radisic, M. V. Sefton, D. Kaplan and G. Vunjak-Novakovic (2006). "Advanced tools for tissue engineering: scaffolds, bioreactors, and signaling." Tissue Eng **12**(12): 3285-305.

Gao, Z. B., S. Pandya, N. Hosein, M. S. Sacks and N. H. Hwang (2000). "Bioprosthetic heart valve leaflet motion monitored by dual camera stereo photogrammetry." J Biomech **33**(2): 199-207.

Grassl, E. D., T. R. Oegema and R. T. Tranquillo (2002). "Fibrin as an alternative biopolymer to type-I collagen for the fabrication of a media equivalent." J Biomed Mater Res **60**(4): 607-12.

Grassl, E. D., T. R. Oegema and R. T. Tranquillo (2003). "A fibrin-based arterial media equivalent." J Biomed Mater Res A **66**(3): 550-61.

Grinnell, F. and C. H. Ho (2002). "Transforming growth factor beta stimulates fibroblast-collagen matrix contraction by different mechanisms in mechanically loaded and unloaded matrices." Exp Cell Res **273**(2): 248-55.

Grouf, J. L., A. M. Throm, J. L. Balestrini, K. A. Bush and K. L. Billiar (2007). "Differential effects of EGF and TGF-beta1 on fibroblast activity in fibrin-based tissue equivalents." Tissue Eng **13**(4): 799-807

Hahn, M. S., M. K. McHale, E. Wang, R. H. Schmedlen and J. L. West (2007). "Physiologic pulsatile flow bioreactor conditioning of poly(ethylene glycol)-based tissue engineered vascular grafts." Ann Biomed Eng **35**(2): 190-200.

He, Z., J. Ritchie, J. S. Grashow, M. S. Sacks and A. P. Yoganathan (2005). "In vitro dynamic strain behavior of the mitral valve posterior leaflet." J Biomech Eng **127**(3): 504-11.

Hildebrand, D. K., Z. J. Wu, J. E. Mayer, Jr. and M. S. Sacks (2004). "Design and hydrodynamic evaluation of a novel pulsatile bioreactor for biologically active heart valves." Ann Biomed Eng **32**(8): 1039-49.

Ho, W., B. Tawil, J. C. Dunn and B. M. Wu (2006). "The behavior of human mesenchymal stem cells in 3D fibrin clots: dependence on fibrinogen concentration and clot structure." Tissue Eng **12**(6): 1587-95.

Hoerstrup, S. P., R. Sodian, S. Daebritz, J. Wang, E. A. Bacha, D. P. Martin, A. M. Moran, K. J. Guleserian, J. S. Sperling, S. Kaushal, J. P. Vacanti, F. J. Schoen and J. E. Mayer, Jr. (2000). "Functional living trileaflet heart valves grown in vitro." Circulation **102**(19 Suppl 3): III44-9.

Hoerstrup, S. P., R. Sodian, J. S. Sperling, J. P. Vacanti and J. E. Mayer, Jr. (2000). "New pulsatile bioreactor for in vitro formation of tissue engineered heart valves." Tissue Eng **6**(1): 75-9.

Hoerstrup SP, S. R., Daebritz S, Wang J, Bacha EA, Martin DP, Moran AM, Guleserian KJ, Sperling JS, Kaushal S, Vacanti JP, Schoen FJ, Mayer JE Jr, (2000). "Functional living trileaflet heart valves grown in vitro." Circulation **102**(19 Suppl 3): III44-49.

Huang-Lee, L. L., D. T. Cheung and M. E. Nimni (1990). "Biochemical changes and cytotoxicity associated with the degradation of polymeric glutaraldehyde derived crosslinks." J Biomed Mater Res **24**(9): 1185-201.

Isenberg, B. C. and R. T. Tranquillo (2003). "Long-term cyclic distention enhances the mechanical properties of collagen-based media-equivalents." Ann Biomed Eng **31**(8): 937-49.

Isenberg, B. C., C. Williams and R. T. Tranquillo (2006). "Endothelialization and Flow Conditioning of Fibrin-Based Media-Equivalents." Ann Biomed Eng.

Isenberg, B. C., C. Williams and R. T. Tranquillo (2006). "Small-diameter artificial arteries engineered in vitro." Circ Res **98**(1): 25-35.

Ishizaki, T., M. Uehata, I. Tamechika, J. Keel, K. Nonomura, M. Maekawa and S. Narumiya (2000). "Pharmacological properties of Y-27632, a specific inhibitor of rho-associated kinases." Mol Pharmacol **57**(5): 976-83.

Jeong, S. I., J. H. Kwon, J. I. Lim, S. W. Cho, Y. Jung, W. J. Sung, S. H. Kim, Y. H. Kim, Y. M. Lee, B. S. Kim, C. Y. Choi and S. J. Kim (2005). "Mechano-active tissue engineering of vascular smooth muscle using pulsatile perfusion bioreactors and elastic PLCL scaffolds." Biomaterials **26**(12): 1405-11.

Junqueira, L. C., G. S. Montes and E. M. Sanchez (1982). "The influence of tissue section thickness on the study of collagen by the Picrosirius-polarization method." Histochemistry **74**(1): 153-6.

Kalath, S., P. Tsipouras and F. H. Silver (1986). "Non-invasive assessment of aortic mechanical properties." Ann Biomed Eng **14**(6): 513-24.

Karamichos, D., R. A. Brown and V. Mudera (2007). "Collagen stiffness regulates cellular contraction and matrix remodeling gene expression." J Biomed Mater Res A **83**(3): 887-94.

Kim, A., N. Lakshman and W. M. Petroll (2006). "Quantitative assessment of local collagen matrix remodeling in 3-D culture: the role of Rho kinase." Exp Cell Res **312**(18): 3683-92.

Kim, B. S., J. Nikolovski, J. Bonadio and D. J. Mooney (1999). "Cyclic mechanical strain regulates the development of engineered smooth muscle tissue." Nat Biotechnol **17**(10): 979-83.

Kim, C. H., E. Takai, H. Zhou, D. von Stechow, R. Muller, D. W. Dempster and X. E. Guo (2003). "Trabecular bone response to mechanical and parathyroid hormone stimulation: the role of mechanical microenvironment." J Bone Miner Res **18**(12): 2116-25.

Kortsmit, J., N. J. Driessen, M. C. Rutten and F. P. Baaijens (2008). "Nondestructive and Noninvasive Assessment of Mechanical Properties in Heart Valve Tissue Engineering." Tissue Eng Part A.

Ku, C. H., P. H. Johnson, P. Batten, P. Sarathchandra, R. C. Chambers, P. M. Taylor, M. H. Yacoub and A. H. Chester (2006). "Collagen synthesis by mesenchymal stem cells and aortic valve interstitial cells in response to mechanical stretch." Cardiovasc Res **71**(3): 548-56.

Knight, R. L., C. Booth, H. E. Wilcox, J. Fisher and E. Ingham (2005). "Tissue engineering of cardiac valves: re-seeding of acellular porcine aortic valve matrices with human mesenchymal progenitor cells." J Heart Valve Dis **14**(6): 806-13.

Kuang, P. P. and R. H. Goldstein (2005). "Regulation of elastin gene transcription by proteasome dysfunction." Am J Physiol Cell Physiol **289**(3): C766-73.

Kuang, P. P., X. H. Zhang, C. B. Rich, J. A. Foster, M. Subramanian and R. H. Goldstein (2007). "Activation of elastin transcription by transforming growth factor-beta in human lung fibroblasts." Am J Physiol Lung Cell Mol Physiol **292**(4): L944-52.

Kucich, U., J. C. Rosenbloom, W. R. Abrams and J. Rosenbloom (2002). "Transforming growth factor-beta stabilizes elastin mRNA by a pathway requiring active Smads, protein kinase C-delta, and p38." Am J Respir Cell Mol Biol **26**(2): 183-8.

Lee, T. C., R. J. Midura, V. C. Hascall and I. Vesely (2001). "The effect of elastin damage on the mechanics of the aortic valve." J Biomech **34**(2): 203-10.

L'Heureux, N.*, et al.* (2006) Human tissue-engineered blood vessels for adult arterial revascularization. *Nat Med* **12,** 361-365.

L'Heureux, N., N. Dusserre, A. Marini, S. Garrido, L. de la Fuente and T. McAllister (2007). "Technology insight: the evolution of tissue-engineered vascular grafts--from research to clinical practice." Nat Clin Pract Cardiovasc Med **4**(7): 389-95.

Li, J., X. Y. Luo and Z. B. Kuang (2001). "A nonlinear anisotropic model for porcine aortic heart valves." J Biomech **34**(10): 1279-89.

Li, Y. S., J. H. Haga and S. Chien (2005). "Molecular basis of the effects of shear stress on vascular endothelial cells." J Biomech **38**(10): 1949-71.

Lima, E. G., L. Bian, K. W. Ng, R. L. Mauck, B. A. Byers, R. S. Tuan, G. A. Ateshian and C. T. Hung (2007). "The beneficial effect of delayed compressive loading on tissue-engineered cartilage constructs cultured with TGF-beta3." Osteoarthritis Cartilage **15**(9): 1025-33.

Lindahl, G. E., R. C. Chambers, J. Papakrivopoulou, S. J. Dawson, M. C. Jacobsen, J. E. Bishop and G. J. Laurent (2002). "Activation of fibroblast procollagen alpha 1(I) transcription by mechanical strain is transforming growth factor-beta-dependent and involves increased binding of CCAAT-binding factor (CBF/NF-Y) at the proximal promoter." J Biol Chem **277**(8): 6153-61.

Lo, D. and I. Vesely (1995). "Biaxial strain analysis of the porcine aortic valve." Ann Thorac Surg **60**(2 Suppl): S374-8.

Long, J. L. and R. T. Tranquillo (2003). "Elastic fiber production in cardiovascular tissue-equivalents." Matrix Biol **22**(4): 339-50.

Luo, X. Y., W. G. Li and J. Li (2003). "Geometrical stress-reducing factors in the anisotropic porcine heart valves." J Biomech Eng **125**(5): 735-44.

Massague, J. (2000). "How cells read TGF-beta signals." Nat Rev Mol Cell Biol **1**(3): 169-78.

Massague, J., J. Seoane and D. Wotton (2005). "Smad transcription factors." Genes Dev **19**(23): 2783-810.

Masters, K. S., D. N. Shah, G. Walker, L. A. Leinwand and K. S. Anseth (2004). "Designing scaffolds for valvular interstitial cells: cell adhesion and function on naturally derived materials." J Biomed Mater Res A **71**(1): 172-80.

Merryman, W. D., H. D. Lukoff, R. A. Long, G. C. Engelmayr, Jr., R. A. Hopkins and M. S. Sacks (2007). "Synergistic effects of cyclic tension and transforming growth factor-beta1 on the aortic valve myofibroblast." Cardiovasc Pathol **16**(5): 268-76.

Mol, A., N. J. Driessen, M. C. Rutten, S. P. Hoerstrup, C. V. Bouten and F. P. Baaijens (2005). "Tissue engineering of human heart valve leaflets: a novel bioreactor for a strain-based conditioning approach." Ann Biomed Eng **33**(12): 1778-88.

Mol, A., M. I. van Lieshout, C. G. Dam-de Veen, S. Neuenschwander, S. P. Hoerstrup, F. P. Baaijens and C. V. Bouten (2005). "Fibrin as a cell carrier in cardiovascular tissue engineering applications." Biomaterials **26**(16): 3113-21.

Moons, P., T. Sluysmans, D. De Wolf, M. Massin, B. Suys, A. Benatar and M. Gewillig (2009). "Congenital heart disease in 111 225 births in Belgium: birth prevalence, treatment and survival in the 21st century." Acta Paediatr **98**(3): 472-7.

Nakatani, T., T. Marui, T. Hitora, M. Doita, K. Nishida and M. Kurosaka (2002). "Mechanical stretching force promotes collagen synthesis by cultured cells from human ligamentum flavum via transforming growth factor-beta1." J Orthop Res **20**(6): 1380-6.

Naughton, G. K. (2002). "From lab bench to market: critical issues in tissue engineering." Ann N Y Acad Sci **961**: 372-85.

Neidert, M. R., E. S. Lee, T. R. Oegema and R. T. Tranquillo (2002). "Enhanced fibrin remodeling in vitro with TGF-beta1, insulin and plasmin for improved tissue-equivalents." Biomaterials **23**(17): 3717-31.

Neuenschwander, S. and S. P. Hoerstrup (2004). "Heart valve tissue engineering." Transpl Immunol **12**(3-4): 359-65.

Niklason, L. E., J. Gao, W. M. Abbott, K. K. Hirschi, S. Houser, R. Marini and R. Langer (1999). "Functional arteries grown in vitro." Science **284**(5413): 489-93.

Papakrivopoulou, J., G. E. Lindahl, J. E. Bishop and G. J. Laurent (2004). "Differential roles of extracellular signal-regulated kinase 1/2 and p38MAPK in mechanical

load-induced procollagen alpha1(I) gene expression in cardiac fibroblasts." Cardiovasc Res **61**(4): 736-44.

Pedersen, J. A. and M. A. Swartz (2005). "Mechanobiology in the third dimension." Ann Biomed Eng **33**(11): 1469-90.

Poh, M., M. Boyer, A. Solan, S. L. Dahl, D. Pedrotty, S. S. Banik, J. A. McKee, R. Y. Klinger, C. M. Counter and L. E. Niklason (2005). "Blood vessels engineered from human cells." Lancet **365**(9477): 2122-4.

Poobalarahi, F., C. F. Baicu and A. D. Bradshaw (2006). "Cardiac myofibroblasts differentiated in 3D culture exhibit distinct changes in collagen I production, processing, and matrix deposition." Am J Physiol Heart Circ Physiol **291**(6): H2924-32

Purinya, B., V. Kasyanov, J. Volkolakov, R. Latsis and G. Tetere (1994). "Biomechanical and structural properties of the explanted bioprosthetic valve leaflets." J Biomech **27**(1): 1-11.

Robinson, P. S., S. L. Johnson, M. C. Evans, V. H. Barocas and R. T. Tranquillo (2008). "Functional tissue-engineered valves from cell-remodeled fibrin with commissural alignment of cell-produced collagen." Tissue Eng Part A **14**(1): 83-95.

Rosamond, W., K. Flegal, K. Furie, A. Go, K. Greenlund, N. Haase, S. M. Hailpern, M. Ho, V. Howard, B. Kissela, S. Kittner, D. Lloyd-Jones, M. McDermott, J. Meigs, C. Moy, G. Nichol, C. O'Donnell, V. Roger, P. Sorlie, J. Steinberger, T. Thom, M. Wilson and Y. Hong (2008). "Heart disease and stroke statistics--2008 update: a report from the American Heart Association Statistics Committee and Stroke Statistics Subcommittee." Circulation **117**(4): e25-146.

Ross, J. J. and R. T. Tranquillo (2003). "ECM gene expression correlates with in vitro tissue growth and development in fibrin gel remodeled by neonatal smooth muscle cells." Matrix Biol **22**(6): 477-90.

Rothenburger, M., P. Vischer, W. Volker, B. Glasmacher, E. Berendes, H. H. Scheld and M. Deiwick (2001). "In vitro modelling of tissue using isolated vascular cells on a synthetic collagen matrix as a substitute for heart valves." Thorac Cardiovasc Surg **49**(4): 204-9.

Rubbens, M. P., A. Mol, R. A. Boerboom, R. A. Bank, F. P. Baaijens and C. V. Bouten (2008). "Intermittent Straining Accelerates the Development of Tissue Properties in Engineered Heart Valve Tissue." Tissue Eng Part A.

Ruberti, J. W. and N. J. Hallab (2005). "Strain-controlled enzymatic cleavage of collagen in loaded matrix." Biochem Biophys Res Commun **336**(2): 483-9.

Ruel, J. and G. Lachance (2009). "A New Bioreactor for the Development of Tissue-Engineered Heart Valves." Ann Biomed Eng.

Samouillan, V., J. Dandurand-Lods, A. Lamure, E. Maurel, C. Lacabanne, G. Gerosa, A. Venturini, D. Casarotto, L. Gherardini and M. Spina (1999). "Thermal analysis characterization of aortic tissues for cardiac valve bioprostheses." J Biomed Mater Res **46**(4): 531-8.

Sato, M., D. Shegogue, E. A. Gore, E. A. Smith, P. J. McDermott and M. Trojanowska (2002). "Role of p38 MAPK in transforming growth factor beta stimulation of collagen production by scleroderma and healthy dermal fibroblasts." J Invest Dermatol **118**(4): 704-11.

Sauren, A. A., M. C. van Hout, A. A. van Steenhoven, F. E. Veldpaus and J. D. Janssen (1983). "The mechanical properties of porcine aortic valve tissues." J Biomech **16**(5): 327-37.

Schoen, F. J. and R. J. Levy (1999). "Founder's Award, 25th Annual Meeting of the Society for Biomaterials, perspectives. Providence, RI, April 28-May 2, 1999. Tissue heart valves: current challenges and future research perspectives." J Biomed Mater Res **47**(4): 439-65.

Schriefer, J. L., S. J. Warden, L. K. Saxon, A. G. Robling and C. H. Turner (2005). "Cellular accommodation and the response of bone to mechanical loading." J Biomech **38**(9): 1838-45.

Scott, M. and I. Vesely (1995). "Aortic valve cusp microstructure: the role of elastin." Ann Thorac Surg **60**(2 Suppl): S391-4.

Scott, M. J. and I. Vesely (1996). "Morphology of porcine aortic valve cusp elastin." J Heart Valve Dis **5**(5): 464-71.

Seliktar, D., R. A. Black, R. P. Vito and R. M. Nerem (2000). "Dynamic mechanical conditioning of collagen-gel blood vessel constructs induces remodeling in vitro." Ann Biomed Eng **28**(4): 351-62.

Seliktar, D., R. M. Nerem and Z. S. Galis (2003). "Mechanical strain-stimulated remodeling of tissue-engineered blood vessel constructs." Tissue Eng **9**(4): 657-66.

Senthilnathan, V., T. Treasure, G. Grunkemeier and A. Starr (1999). "Heart valves: which is the best choice?" Cardiovasc Surg **7**(4): 393-7.

Shinoka, T., P. X. Ma, D. Shum-Tim, C. K. Breuer, R. A. Cusick, G. Zund, R. Langer, J. P. Vacanti and J. E. Mayer, Jr. (1996). "Tissue-engineered heart valves. Autologous valve leaflet replacement study in a lamb model." Circulation **94**(9 Suppl): II164-8.

Siddiqui, A.*, et al.* (1996) Differential effects of oxygen on human dermal fibroblasts: acute versus chronic hypoxia. *Wound Repair Regen* **4,** 211-218.

Silver, F. H., L. M. Siperko and G. P. Seehra (2003). "Mechanobiology of force transduction in dermal tissue." Skin Res Technol **9**(1): 3-23.

Sodian, R., S. P. Hoerstrup, J. S. Sperling, S. H. Daebritz, D. P. Martin, F. J. Schoen, J. P. Vacanti and J. E. Mayer, Jr. (2000). "Tissue engineering of heart valves: in vitro experiences." Ann Thorac Surg **70**(1): 140-4.

Solan, A., S. Mitchell, M. Moses and L. Niklason (2003). "Effect of pulse rate on collagen deposition in the tissue-engineered blood vessel." Tissue Eng **9**(4): 579-86.

Solomon, N. A., S. K. Pranav, K. A. Jain, M. Kumar, C. B. Kulkarni and J. Akbari (2006). "In search of a pediatric cardiac surgeon's 'Holy Grail': the ideal pulmonary conduit." Expert Rev Cardiovasc Ther **4**(6): 861-70.

Stradins, P., R. Lacis, I. Ozolanta, B. Purina, V. Ose, L. Feldmane and V. Kasyanov (2004). "Comparison of biomechanical and structural properties between human aortic and pulmonary valve." Eur J Cardiothorac Surg **26**(3): 634-9.

Syedain, Z. H., J. S. Weinberg and R. T. Tranquillo (2008). "Cyclic distension of fibrin-based tissue constructs: evidence of adaptation during growth of engineered connective tissue." Proc Natl Acad Sci U S A **105**(18): 6537-42.

Tang, L. L., Y. L. Wang, J. Pan and S. X. Cai (2004). "The effect of step-wise increased stretching on rat calvarial osteoblast collagen production." J Biomech **37**(1): 157-61.

Takehara, K. (2000). "Growth regulation of skin fibroblasts." J Dermatol Sci **24 Suppl 1**: S70-7.

Taylor, P. M., S. P. Allen, S. A. Dreger and M. H. Yacoub (2002). "Human cardiac valve interstitial cells in collagen sponge: a biological three-dimensional matrix for tissue engineering." J Heart Valve Dis **11**(3): 298-306; discussion 306-7.

Thom, T., N. Haase, W. Rosamond, V. J. Howard, J. Rumsfeld, T. Manolio, Z. J. Zheng, K. Flegal, C. O'Donnell, S. Kittner, D. Lloyd-Jones, D. C. Goff, Jr., Y. Hong, R. Adams, G. Friday, K. Furie, P. Gorelick, B. Kissela, J. Marler, J. Meigs, V. Roger, S. Sidney, P. Sorlie, J. Steinberger, S. Wasserthiel-Smoller, M. Wilson and P. Wolf (2006). "Heart disease and stroke statistics--2006 update: a report from the American Heart Association Statistics Committee and Stroke Statistics Subcommittee." Circulation **113**(6): e85-151.

Thubrikar M (1990). The Aortic Valve. Boca Raton, CRC Press.

Thubrikar, M., W. C. Piepgrass, L. P. Bosher and S. P. Nolan (1980). "The elastic modulus of canine aortic valve leaflets in vivo and in vitro." Circ Res **47**(5): 792-800.

Thubrikar, M., W. C. Piepgrass, J. D. Deck and S. P. Nolan (1980). "Stresses of natural versus prosthetic aortic valve leaflets in vivo." Ann Thorac Surg **30**(3): 230-9.

Thubrikar, M. J., J. Aouad and S. P. Nolan (1986). "Comparison of the in vivo and in vitro mechanical properties of aortic valve leaflets." J Thorac Cardiovasc Surg **92**(1): 29-36.

Thubrikar, M. J., J. R. Skinner, R. T. Eppink and S. P. Nolan (1982). "Stress analysis of porcine bioprosthetic heart valves in vivo." J Biomed Mater Res **16**(6): 811-26.

Tower, T. T., M. R. Neidert and R. T. Tranquillo (2002). "Fiber alignment imaging during mechanical testing of soft tissues." Ann Biomed Eng **30**(10): 1221-33.

Tudorache, I., S. Cebotari, G. Sturz, L. Kirsch, C. Hurschler, A. Hilfiker, A. Haverich and A. Lichtenberg (2007). "Tissue engineering of heart valves: biomechanical and morphological properties of decellularized heart valves." J Heart Valve Dis **16**(5): 567-73; discussion 574.

Turner, C. H. (1998). "Three rules for bone adaptation to mechanical stimuli." Bone **23**(5): 399-407.

Turner, C. H., A. G. Robling, R. L. Duncan and D. B. Burr (2002). "Do bone cells behave like a neuronal network?" Calcified tissue international **70**(6): 435-42.

Vesely, I. (1998). "The role of elastin in aortic valve mechanics." J Biomech **31**(2): 115-23.

Vesely, I. and A. Lozon (1993). "Natural preload of aortic valve leaflet components during glutaraldehyde fixation: effects on tissue mechanics." J Biomech **26**(2): 121-31.

Vesely, I. and R. Noseworthy (1992). "Micromechanics of the fibrosa and the ventricularis in aortic valve leaflets." J Biomech **25**(1): 101-13.

Wang, J. H., B. P. Thampatty, J. S. Lin and H. J. Im (2007). "Mechanoregulation of gene expression in fibroblasts." Gene **391**(1-2): 1-15.

Warnock, J. N., S. Konduri, Z. He and A. P. Yoganathan (2005). "Design of a sterile organ culture system for the ex vivo study of aortic heart valves." J Biomech Eng **127**(5): 857-61.

Webb, G. D. (2002). Advances in adult congenital heart disease Philadelphia, W.B. Saunders Co, .

Williams, C., S. L. Johnson, P. S. Robinson and R. T. Tranquillo (2006). "Cell sourcing and culture conditions for fibrin-based valve constructs." Tissue Eng **12**(6): 1489-502.

Yacoub, M. and R. Nerem (2007). "Introduction. Bioengineering the heart." Philos Trans R Soc Lond B Biol Sci **362**(1484): 1253-5.

Yao, L., D. D. Swartz, S. F. Gugino, J. A. Russell and S. T. Andreadis (2005). "Fibrin-based tissue-engineered blood vessels: differential effects of biomaterial and culture parameters on mechanical strength and vascular reactivity." Tissue Eng **11**(7-8): 991-1003.

Ye, Q., G. Zund, P. Benedikt, S. Jockenhoevel, S. P. Hoerstrup, S. Sakyama, J. A. Hubbell and M. Turina (2000). "Fibrin gel as a three dimensional matrix in cardiovascular tissue engineering." Eur J Cardiothorac Surg **17**(5): 587-91.

Appendix

Appendix A: Tubular tissue construct and valve equivalent fabrication protocols

A1: Tubular Constructs

Note: may need to keep mixtures cool until mixed if having difficulties

To make the final fibrin gel at 6.66mg/ml

Fibrinogen Solution (9 mL total): (1:5 ratio for Fibrin (30mg/ml):HEPES)
- 3 mL Fibrinogen (~30 mg/mL)
- 6 mL 20mM HEPES in Saline

Thrombin Solution (2 mL total):
- 2 mL medium WITHOUT FBS
- 200 μL Thrombin
- 15 μL 2N $CaCl_2$

Cell Solution
6x concentration of final (final usually $0.5x10^6$ cells/mL => $3x10^6$ cells//mL)

Gels:
- 4 parts Fibrinogen Solution
- 1 part Thrombin Solution
- 1 part Cell Soluiton

(hemispheres use 100 μL for 30 min then add media 1 mL)
(MEs use approx 1.5 mL for 30-45 min then add media- may want lower cell conc.)

TC preparation
1. Autoclave mandrels, rubber ends end-caps (12cc/6cc syringe), 12 cc outer casings, and plungers.
2. Coat mandrels and outer shells with 5% pluronic in water for 3-4 hours
3. Mix fibrinogen solution, thrombin solution, and cell suspension in 4:1:1 ratios as needed (up to~ 20 mL at a time, inject all within 1 minute)
4. Inject mixture into molds, incubate mandrel vertically so cells don't settle non-uniformly in the mold, wrap in parafilm and put in incubator for 15-30 minutes.
5. Push mandrels out of molds with autoclaved plunger into incubation jars/tubes.
6. Detach tissue from edges at first feeding (if needed).

A2: Valve Equivalent (Developed originally by Paul Robinson):

1: VE Molds have three main parts, upper section, lower section and outer casing. Additional rubber spacer can be used to reduce lower root height.

2: Sonicate mold with detergent (not contrad) for 1 hr (heat on), rinse with tap DI and add enzyme detergent (Contrex) for 1hr and sonicate (heat on).

3: rinse with tap DI water and soak in DI water overnight.

4: Parts can be sterilize by autoclaving or soaking in EtOH for 30 min in autoclaved 1000ml beaker (can hold upto two molds). Teflon will warp in autoclave hence prefer to use EtOH unless contamination is an issue.

5: dry on sterile towel for 30min (evaporate all EtOH)

6: pluroic coat for 3-4 hrs or overnight with 2.5% pluronic solution
(2.5g pluronic in 100 ml DI water)
7: dry molds after pluronic for 30 min and put pieces together using sterile gloves.

8: Warp out sheel casing with Teflon tape to ensure all gaps are sealed. Add sterile hank's buffer solution to test for leaks. Seal leaks with more Teflon tape or sterile vacuum grease.

9: Using desired fibrin recipe, make about 20 ml of fibrin solution for each full valve and 16mls for reduced lower root height valve.

10: After mixing the fibrin solution using 25 ml pipette inject fibrin solution 1/3 through each of the opening in upper post. Inject slowly to avoid creating air bubbles in gel (1 min max).
Also make HM as control if need be

11: Let VE sit in laminar hood for 4 minutes to completely gel. Ensure to not cause any vibration. After 4 minutes, incubate the valves in 37C incubator for 26mins for it to completely gel.

12: Remove Teflon tape/vacuum grease and slowly remove the outer casing, with a finger on upper mold to ensure it doesn't come off with outer housing.

13: place valves sideways in the incubating jars with approx 250ml of media.

Appendix B: Protocols for mechanical and biochemical analysis of tissue properties

B1: Mechanical testing of strips

Setup:
Attach one C-supporting bar with the T-bar to the load cell (stationary).
Be careful not to push or pull on the load cell.
Attach the other C-supporting bar with the T-bar to the actuator arm (moves).
Place the plastic tub around the T-bars. Will need a lift under the tub to raise height.
Fill tub with PBS so that most of the T-bar is submerged.
Turn on the power. (The MTS power is linked to the computer).
(May need to turn on noisy black box on floor at far back of table)

MTS Initialization:
TestStarII->Configuration Folder->YOUR Config
username: MTS; password: MTS
Push reset on Control Panel (left of computer)
Push low
Push high
Turn on manual control (can move the dial)
Want to be able to put the bars next to each other but not touching.

Conditioning:
In Test Start II Window ->TestWare SX->File->Open Template->
Open YOUR Temp
Place the sample around the top of T-bars. Narrow and/or long samples can be difficult.
Put T-bars as close as they can be yet not be touching.
Use arrow keys to hightlight "Force", then press Auto Zero.
Stretch until sample is taut but not pulling. Try to find the point where the force jumps.
Leave some slack.
Record the starting length so that the strain can be calculated.
Open Display Scope (Graph)->Edit Scope
Want Force vs. Displacement
Trace time 300 sec
Move displacement bar so that it's in the range you want to look at
(look at the controller display)
Adjust Force Axis scale

SHUT MANUAL CONTROL OFF before you tell the program to run
Hit Run for the graph as well as the program
If it doesn't overlap the first time, you may need to rerun the conditioning
(reset Graph: Control->Reset->Run)

DO NOT DO ANYTHING TO THE SAMPLE. Leave it as it is at the end of conditioning for when you start tensile testing.

Tensile Testing:
Close the Conditioning window (where you clicked run)
New window will appear.
Select Tensile Template (File~Open Template ~Tensile)
Save new file (ie date_s#t)
Run test.
Will go to 2cm so stop when it breaks (RTT setting).

Turn back to manual control.
Go back to the Conditioning steps and test next sample.

B2: Picrosirius red staining of collagen

Reagents:
Picro-Sirius Red:
0.25 g Sirius red (direct red 80, Sigma #365548)
250 ml saturated picric acid (Sigma)

Acidified water:
5 ml glacial acetic acid
1 liter ddH_2O

Procedure:

1: Thaw OCT section for 10 min

2: Neutral buffer formalin for 30 min

3: Weigert's harmatoxlin for 30 min

4: In running tap water 10min (for proper bluing of nuclei)

5: Stain in picro-sirius red stain for 1 hr

6: wash in acidified water 2x
1^{st} – let stand/mix (agitate) until no more color coming off the slides
2^{nd} – No color coming off, wait for 30 sec.

7: 100% EtOH, tap and wipe slides to remove water.

8: 3 x 100% EtOH for 3 min

9: 3 x Xylene for 3 min.

10: Cover slip with permount.

Image using color CCD camera with cross-polarizer. One polarizer is fixed on Olympus microscope, while second film of polarizer is placed on top of lens. All comparative images have to be acquired in a single run with exact same settings. The microscope has no capability to record settings. The slides can be stored at room temperature for extended duration.

B3: Pepsin Acid digestion of Collagen in Fibrin construct

1: After collection, freeze samples of un-fixed tissue at -80C

2: Thaw tissue samples, measure dimension or weight.

3: Add 1mg of pepsin (Sigma) in 1ml of Acetic acid (0.5M) for each sample.
The pH should be between 2-4

Note: Digestion activity depends on sample size, pepsin activity, pH, temperature, incubation time. All of which need to be determined. For now, we will use Billiar's parameters except for actual size of sample and g force in centrifuge (translate to 14000 rpm).

4: Incubate samples at room temperature (20C) with rotation overnight.

5: Centrifuge at 4C for 1hr at 14000 rpm

6: Remove supernatant and save for soluble collagen assay. Freeze pellet for insoluble Collagen assay by HPro.

B4: Western blotting protocol

1. Lysis protein in lysis buffer
    a. For 1/3 ME use 100ul of lysis buffer per piece
2. Sonicate sample for 30 sec with sonicator setting at 4 in cold room. Keep samples on ice the entire time. After sonication incubate sample on rocker for 15min in cold room.
3. Spin the sample at 13k rpm for 5min, take supernatant for western blotting.
4. Prepare gel at appropriate %
    a. For pERK/ERK use 10% gel
    b. For SMAD use 7.5% gel
5. dilute protein solution in ddH2O, add sample buffer +DTT (60ul of sampler buffer plus 20ul of DTT) gives samples buffer with 4x concentration
6. Load 20-40ug of protein per lane with max volume of 20mls.
    a. Run gel in SDS running buffer
        i. Dilute 10x SDS by adding 85ml to ddH2O to make 850ml
7. Run for 60min with 0.06A (for 2 gels, half for 1) constant current or until gel start running from bottom (blue color coming out)
8. Sandwich gel in transfer casket with cellulose paper
9. Transfer for 45min at 75volts (for 1 or 2 gels)
    a. CAPS buffer by adding 80ml CAPS, 80ml ethanol and ddH2O to 800mls
10. Block gel in blocking buffer for 1hr
    a. For pERK/ERK use milk at 5%
        i. (in 100ml water add 5g milk powder and 1ml TWEEN)
    b. For pSMAD/SMAD use BSA at 3%
        i. (in 40ml TBS add 1.2g BSA and 400ul TWEEN)
11. Add primary antibody with blocking buffer overnight (5ml solution)
    a. For pERK/ERK (cell signaling technology) use 1:1000 dilution
    b. For pSMAD/SMAD (cell signaling technology) use 1:1000 dilution
12. Rinse 3x for 5min each
    a. Use 1/2x milk if milk is blocking buffer, for BSA use TBS with 0.1% TWEEN (1ml TWEEN in 100ml TBS)
13. Add secondary antibody HRP linked at 1:10000 dilution (10ml solution) for 60 min
    a. In 10ml at 1ul of antibody
14. Rinse 3x for 5min each
    a. For milk blocking, use 1/2x milk for two rinse followed by PBS rinse
    b. For BSA blocking, use TBS with TWEEN for 2 rinse followed by TBS rinse
15. Rinse in dH2O several times (quick wash)
16. Mix glowing solution 1 and 2 right before adding (1.3ml per block)
17. Lay down cellulose on plastic wrap and pour solution over it for 1 min.

B5: Endothelial cells staining protocol

For non-fixed OCT frozen Native or Engineered tissue

1. On sectioned slide, mark the boundary with Pep-Pen.
2. Cover section with 4% PFA for 10 min
3. Rinse with PBS 2x for 5 min each
4. Permeabilize with 0.1% Triton-X for 5 min
5. Rinse with PBS 2x for 5 min each
6. **Serum Blocking**: incubate sections with normal donkey serum blocking solution for **30 minutes** to block non-specific binding of immunoglobulin.
7. **Primary Antibody**: for **1 hour** at room temperature.
    a. **vWF antibody**: 1:400 dilution in 5% Donkey serum
    b. **Anti PECAM-1 antibody**: 1:200 dilution in 5% Donkey Serum
8. Rinse in PBS 4x5 min with 1ml on the slide followed by 1X in stirred glass jar.
9. **Secondary Antibody**: diluted in PBS for **1 hr**.
    a. for vWF: 1:200 dilution of Cy3 donkey anti-rabbit
    b. for anti-PECAM-1: 1:200 dilution of Cy2 donkey anti-mouse
10. Rinse in PBS 4x5 min with 1ml on the slide followed by 1X in stirred glass jar.
11. Cover with DAPI counter-stain and seal edges of slide with nail-polish

Antibody Information

- ☐ vWF antbody: **rabbit** anti-mouse
- ☐ anti-PECAM 1 antibody (CD31): Chemicon MAB2148 **mouse** anti-human

B6: Photo-chemical crosslinking of thrombin-crosslinked fibrin gels

Solutions

All solution should be 72hr old or less (3days) and protected from light during storage

Ru solution (10x)

Add 0.15mg of Ru(II)Bpy_3^{2+} (Sigma 224758) in 10ml of ddH_2O
Vortex the solution until dissolved. Some red particles may still stay suspended.
Sterile filter through 0.2μm filter.
Use aluminium foil to warp the vial from light.

Sodium persulfate (20x)

Add 0.95g of sodium persulfate (Sigma S6172) to 20mls of ddH_2O
Vortex the solution, it should dissolve fairly quickly
Sterile filter and store with aluminium foul warp

Protocol

1. Dilute solution to 1x using sterile PBS and mix Ru and Sodium persulfate in a glass vial
    a. For example to make total 20mls = add 17ml PBS with 1ml Sodium persulfate and 2ml Ru solution
2. Place fibrin based ME/VE inside the vial with Ru solution
3. Count to 10 min, can keep the vials on ice
4. Shine blue light for 20 sec
    a. RTT special blue spiral designed by JBjork
5. Rinse ME/VE in PBS for 3 minutes, can use lactate ringer solution
6. Rinse second in DMEM media for 5 min/ or lactate ringer solution
7. Place back in culture media for further incubation
    a. The yellow color won't fully come off, the goal of rinse is to remove any sodium persulfate which is toxic to cells.

Appendix C: VE mold and bioreactor designs and schematics

C1: Bi-leaflet VE drawing

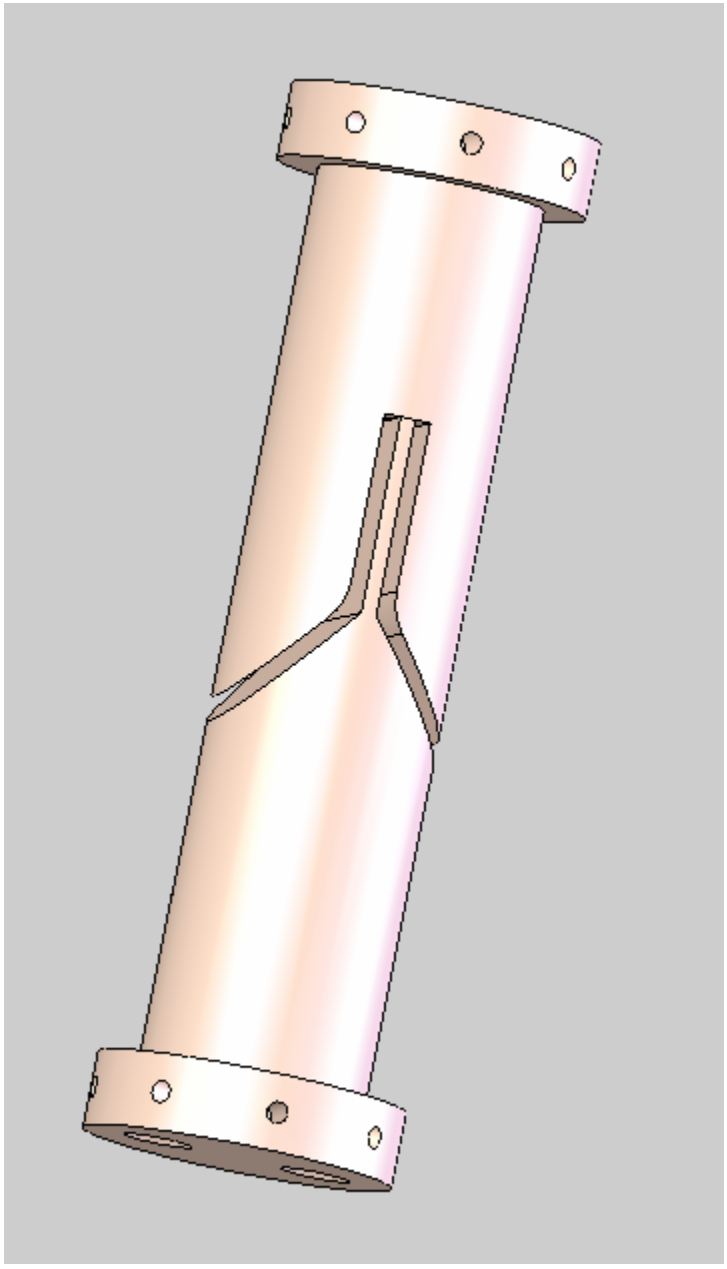

C2: VE mold dimensions and specs

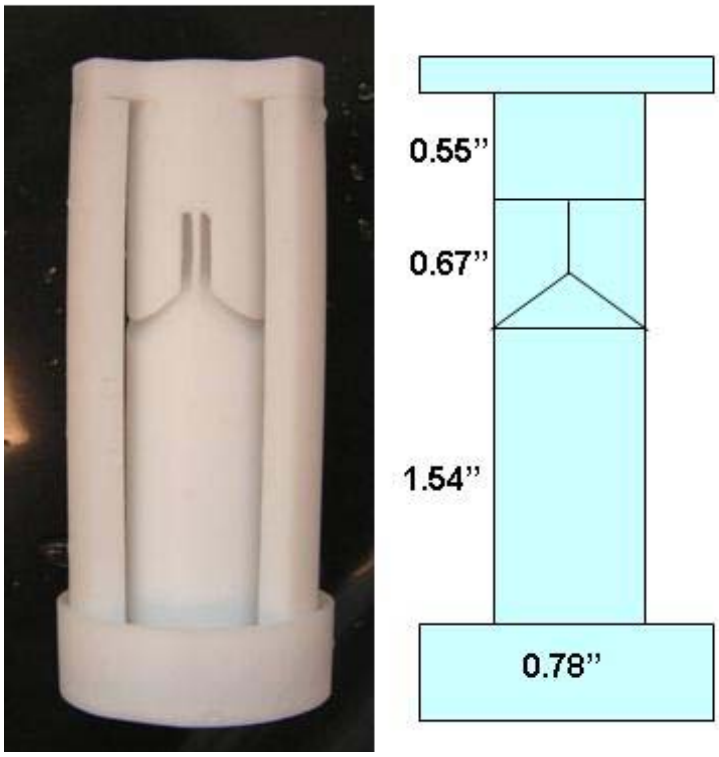

C3: CD bioreactor schematics

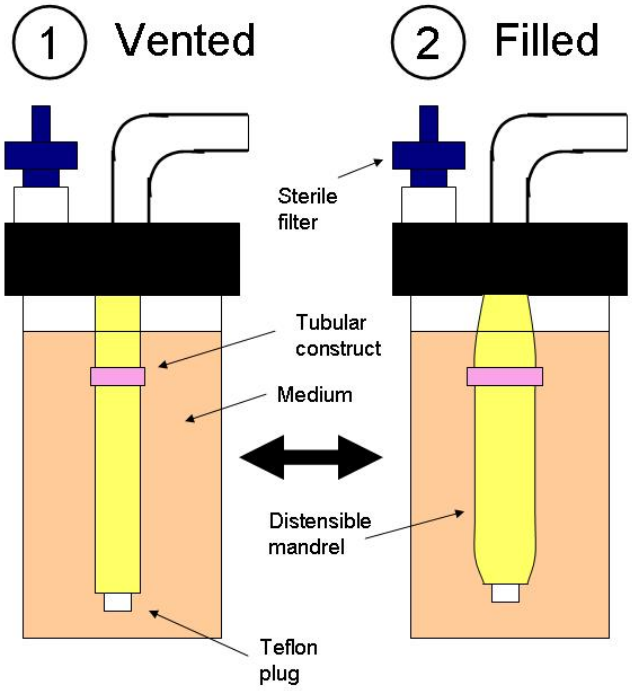

C4: Valve bioreactor (CS Bioreactor) design

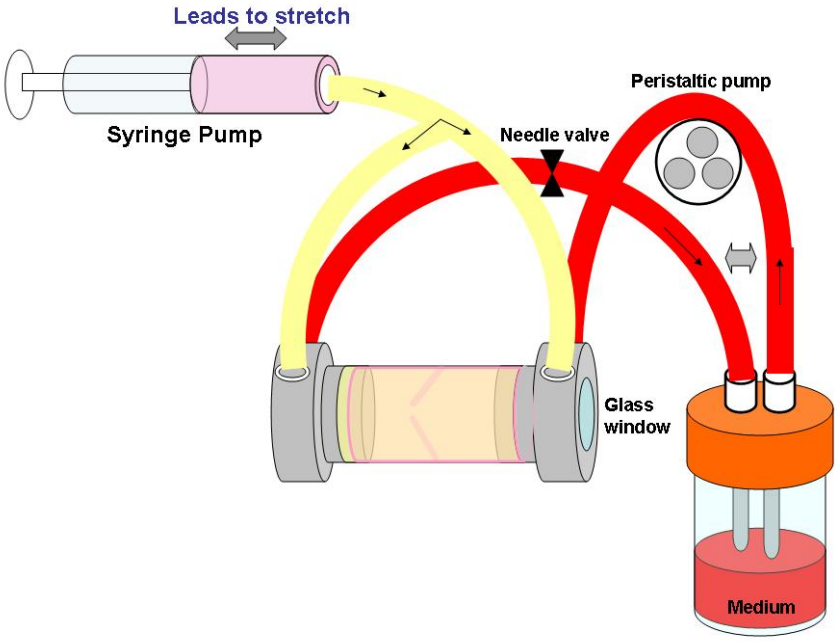

C5: Valve bioreactor end-piece design I

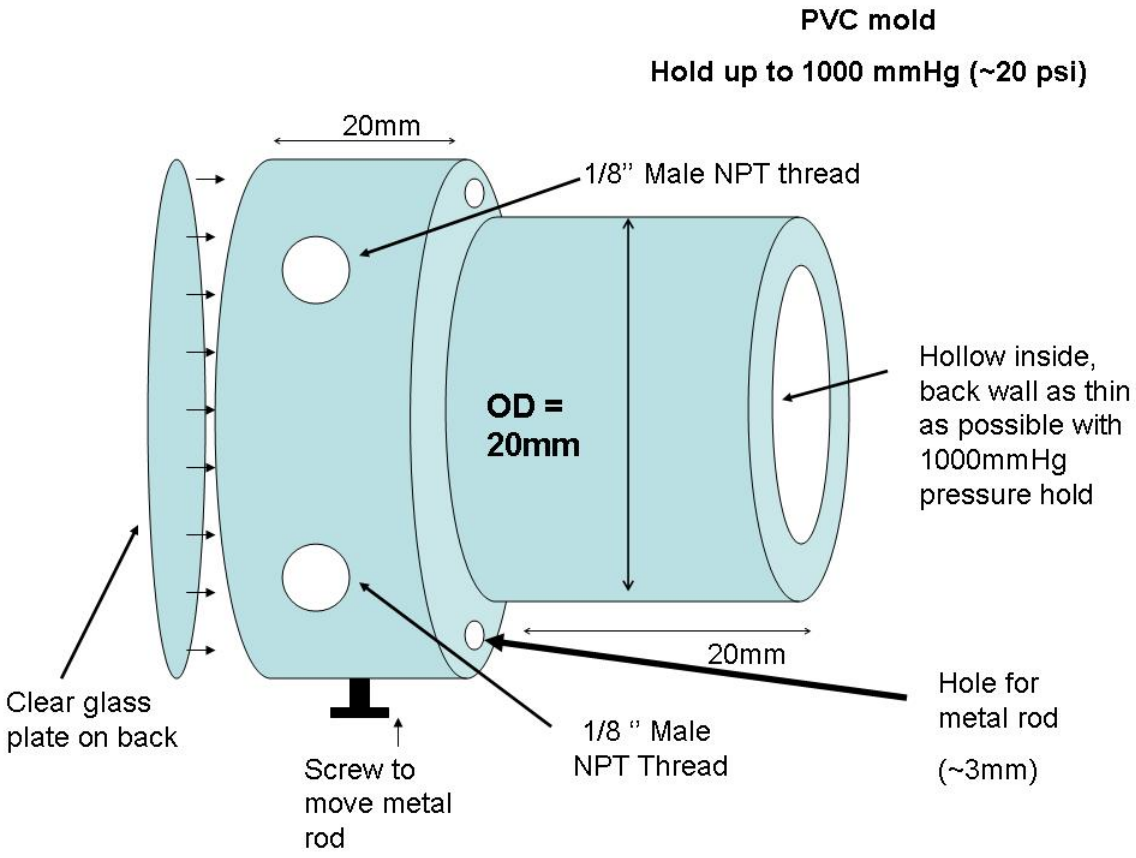

C6: Valve bioreactor end-piece design II